PEOPLE'S DEMOCRATIC REPUBLIC OF ALGERIA

MINISTRY OF HIGHER EDUCATION

AND SCIENTIFIC RESEARCH

University of Echahid Hamma Lakhdar - El Oued

Faculty of Technology, Department of Processes

Engineering and Petrochemicals

Thesis Submitted in Partial Fulfilment of the Requirement for the Degree of Doctor of Philosophy

LMD

Option: Environmental Engineering

Advanced Nanocomposite Hydrogels for Photocatalysis and Antibacterial Activity Applications: Synthesis, Characterization, and Performance Evaluation

Submitted by

BOUTALBI Abdelhakim

Before the jury composed of

KHELEF Abdelhamid	**Pr**	**University of El-Oued**	**President**
CHENNOUF Nasreddine	**Pr**	**University of Ouargla**	**Examiner**
SEKIRIFA Mohamed Lamine	**Pr**	**University of Ouargla**	**Examiner**
BELGHIT Mohamed Yazid	**MCA**	**University of El-Oued**	**Examiner**
MENECEUR Souhaila	**MCA**	**University of El-Oued**	**Supervisor**
LAOUINI Salah Eddine	**Pr**	**University of El-Oued**	**Co-Supervisor**

2023-2024

Acknowledgement

First and foremost, Praise be to Allah who granted me the strength and guidance to undertake this research endeavor.

I would like to extend my deepest appreciation to my supervisor, Dr. **Meneceur Souhaila**, and my co-supervisor, Prof. **Laouini Salah Eddine**, for their unwavering encouragement, invaluable guidance, dedicated support, patience, and understanding throughout the entirety of my doctoral journey.

I am sincerely thankful to the esteemed members of the jury who graciously accepted the responsibility of evaluating this thesis, dedicating their time and expertise to this endeavor.

My heartfelt thanks go to Prof. **Omar Ben Mya** for his constant encouragement, unwavering support, and insightful advice that guided me from the inception of this research to its completion.

I wish to express my profound appreciation to all my professors in the *Department of Process Engineering and Petrochemicals at the University of El Oued* for imparting invaluable knowledge and for their tireless efforts in shaping my academic path.

Special gratitude is extended to Mrs. **LAOUINI** and her assistants as well as Mr. **Ali TLIBA** for their invaluable assistance and unwavering support in the laboratory whenever I required it.

I would also like to acknowledge my colleagues, namely **Hamdi Ali Mohammed** and **Gamil Gamal Hasan**, as well as all the members of the *Laboratory of Biotechnology, Biomaterial, and Condensed Matter* for their collaborative efforts and support.

I take this opportunity to express my sincere thanks to PhD. **Bouafia Abderrhmane** for his exceptional assistance and friendship throughout this journey.

Last but not least, I extend my heartfelt appreciation to the entire scientific community at the University of El Oued.

Abstract

ملخص

Résumé

ملخص

الهلاميات المائية النانوية (NCHs) هي عبارة عن دمج عنصر نانوني في بنية هيدروجيل، ينتج عن هذا الدمج فئة متقدمة من المواد ذات خصائص فريدة من نوعها، مما يجعلها مناسبة لمختلف التطبيقات. والتي من بينها، الحفز والطب الحيوي. في هذه الدراسة، تم تحضير الهلاميات المائية النانوية (NCHs) عن طريق عملية "الإرجاع في الموقع". حيث استُخدم هيدروجيل متعدد أكريلات البوتاسيوم (PPAH) لتحميل جزيئات الفضة وأكسيد الزنك النانوية. تم تحليل العينات المحضرة PPAH/Agx وPPAH/Ag@ZnO NCHs بدقة من خلال تقنيات تحليلية مختلفة بما في ذلك UV-Vis وFTIR وXRD وSEM وEDX. وقد قدرت طاقات فجوة النطاق غير المباشرة بـ 2.5 و1.75 ev لـ PPAH /Ag وPPAH/Ag@ZnO، على التوالي، أظهرت صور المسح المجهري الإلكتروني SEM شكلًا مكعبًا لـجزيئات الفضة الناونية Ag NPs ، كما كشف التحليل الكمي EDX أن عينة PPAH/Ag تحتوي على 60.48% من عنصر الفضة بينما تحتوي عينة PPAH/Ag@ZnO على 58.77. 28.05، و13.18% من عناصر الفضة والزنك والأكسجين على التوالي. خلال هذا العمل، تم أيضا دراسة نشاط التحفيز الضوئي لـ NCHs المحضرة تحت إشعاع ضوء الشمس، وأظهرت النتائج إزالة 95٪ من صبغة البنغال الوردية على PPAH/Agوإزالة 98.77، و98.05٪من الصبغين أورتو أزرق التولويدين و4-بروموفينول، على التوالي، باستعمال PPAH/Ag@ZnO. علاوة على ذلك، تم إخضاع PPAH/Ag@ZnOلاختبار قابلية إعادة الاستخدام على مدار 5 دورات متتالية في تحلل الصبغين أورتو أزرق التولويدين و4-بروموفينول، وأظهرت النتائج فعاليته واستقراره الاستثنائيين، وأخيرًا، أظهر إختبار مضادات البيكتريا فاعلية قوية لعينات PPAH/Agx ضد مختلف أنواع السلالات البيكتيريا وهي *Pseudomonas aeruginosa ATCC 27853*، *Escherichia coli ATCC 25922*، و *Staphylococcus aureus ATCC 25923*. حسب النتائج المتحصل عليها من هذا الإختبار، قد لُوحظ أن كبح عينات PPAH/Agx للبيكتيريا أكثر فعالية مقارنة بغالبية المضادات الحيوية المختلفة التي أعتمدت في هذا الإختبار. بشكل عام، بناءً على كل النتائج، تتمتع هذه المواد المحضرة بإمكانيات واعدة لتطبيقها بنجاح في مجال الحفز الكيميائي ومجال الطب الحيوي.

الكلمات المفتاحية: الجسيمات النانوية؛ هيدروجيل. الإرجاع في الموقع؛ نشاط التحفيز الضوئي. قابلية إعادة الاستخدام؛ مضاد للبكتيريا.

Abstract

Nanocomposite hydrogels (NCHs) are a combination of two components nanofiller and hydrogel, this combination results in an advanced class of material known for its unique properties, making it suitable for various applications. Among them, are catalysis and biomedical. Herein, the preparation of nanocomposite hydrogels (NCHs) via the *in-situ* reduction approach was investigated. Potassium polyacrylate hydrogel (PPAH) was utilized to load silver (Ag) and Zinc oxide (ZnO) nanoparticles. The as-prepared samples PPAH/Agx and PPAH/Ag@ZnO NCHs were thoroughly characterized by different analytical techniques including UV-Vis, FTIR, XRD, SEM, and EDX. The indirect band gap energies were estimated to be 2.5 and 1.75 eV for PPAH/Ag and PPAH/Ag@ZnO, respectively, SEM images showed cubic shape for Ag NPs, The EDX

quantitative analysis revealed that PPAH/Ag contains 60.48% of silver while PPAH/Ag@ZnO contains 58.77, 28.05, and 13.18% of Silver, Zinc, and Oxygen elements. during this work, the photocatalytic activity of the as-prepared NCHs was studied under sunlight irradiation, the outcomes presented 95% elimination of Rose Bengal dye over PPAH/Ag. Also, 98.77, and 98.05% elimination of *o*-Toluidine blue and 4-Bromophenol dyes, respectively, over PPAH/Ag@ZnO. Besides, PPAH/Ag@ZnO was subjected to a reusability test over 5 consecutive cycles in the degradation of *o*-Toluidine blue and 4-bromophenol dyes, the findings demonstrated its exceptional effectiveness and stability, Finally, PPAH/Agx samples exhibited better antibacterial effect against different types of microorganisms, namely *Pseudomonas aeruginosa ATCC 27853, Escherichia coli ATCC 25922*, and *Staphylococcus aureus ATCC 25923* compared to most antibiotics used in this test. Overall, based on these results, these materials have promising potential for successful applications in catalysis and biomedical fields.

Keywords: Nanoparticles; Hydrogel; *In-situ* reduction; Photocatalytic activity; Reusablity; Antibacterial.

Résumé

Les hydrogels nanocomposites (NCH) sont une combinaison de deux composants: nanocharge et hydrogel. Cette combinaison donne naissance à une classe avancée de matériaux connus pour leurs propriétés uniques, ce qui les rend adaptés à diverses applications. Parmi eux, figurent la catalyse et le biomédical. Dans cette étude, la préparation d'hydrogels nanocomposites (NCH) via l'approche de reduction sur place *(in-situ)* a été étudiée. Un hydrogel de polyacrylate de potassium (PPAH) a été utilisé pour charger des nanoparticules d'argent et d'oxide de zinc ZnO. Les échantillons tels que préparés PPAH/Agx et PPAH/Ag@ZnO ont été caractérisés par différentes techniques analytiques, notamment UV-Vis, FTIR, DRX, MEB et EDX. Les énergies de bande interdite indirecte ont été estimées à 2,5 et 1,75 eV pour PPAH. /Ag et PPAH/Ag@ZnO, respectivement, les images de MEB ont montré une forme cubique pour les NPs Ag. L'analyse quantitative EDX a révélé que PPAH/Ag NCH contient 60,48 % d'argent tandis que PPAH/Ag@ZnO en contient 58,77, 28,05 et 13,18 % d'éléments Argent, Zinc et Oxygène. Au cours de ce travail, l'activité photo catalytique des NCH_s tels que préparés a été étudiée sous irradiation solaire, les résultats ont présenté une élimination de 95 % du colorant Rose Bengale sur

PPAH/Ag et une élimination de 98,77 et 98,05 % pour les colorants *o*-Toluidine bleu et 4-bromophénol, respectivement, sur PPAH/Ag@ZnO. En outre, PPAH/Ag@ZnO a été soumis au test de réutilisabilité sur 5 cycles consécutifs dans la dégradation des colorants *o*-toluidine bleu et 4-bromophénol, les résultats ont démontré son efficacité et sa stabilité exceptionnelles. Enfin, Les PPAH/Agx ont présenté un meilleur effet antibactérien contre différents types de micro-organismes, à savoir *Pseudomonas aeruginosa ATCC 27853*, *Escherichia coli ATCC 25922* et *Staphylococcus aureus ATCC 25923*, par rapport à la plupart des antibiotiques utilisés dans ce test. Généralement, d'après ces résultats, des matériaux présentent un potentiel prometteur pour des applications réussies dans les domaines de la catalyse et du biomédical.

Mots clés: Nanoparticules; Hydrogel; Réduction sur place (in-situ); Activité photocatalytique; Réutilisabilité; Antibactérien.

Index of figures

Index of tables

List of abbreviations

NPs	Nanoparticles
NCHs	Nanocomposite Hydrogels
PPAH	Potassium Polyacrylate Hydrogel
Fig	Figure
Eq	Equation
UV-Vis	Ultraviolet–visible spectroscopy
FTIR	Transform Infrared spectroscopy
XRD	X-Ray Diffraction
SEM	Scanning Electron Microscopy
EDX	Energy Dispersive X-ray analysis
eV	Electron Volt
R.B	Rose Bengal dye
4-Bph	4-Bromophenole dye
***o*-TB**	Ortho-Toluidine blue dye
R^2	Coefficient of determination
M	Molar
D%	Degradation efficiency
CFM	Cefixime
OFX	Ofloxacin

Table of Contents

Chapter I. Nanoparticles Overview

Chapter II. Hydrogels-Fundamentals

Chapter V. Results, Analysis, and Discussion

Introduction

Introduction

Nanotechnology is a multidisciplinary field of science, engineering, and technology that deals with materials, structures, and systems at the nanoscale. It involves the manipulation and control of matter at the nanometer level, typically in the range of 1 to 100 nanometers [1, 2]. Nanoparticulate materials have a long history of practical use spanning several centuries, particularly for their ability to impart unique properties such as fine luster to items like jewelry and pottery. One of the most renowned examples of this ancient nanotechnology is the Lycurgus cup from the Roman era, which is currently housed in the British Museum. The Lycurgus cup is famous for its remarkable color-changing properties. It appears green when illuminated from the front but transforms to a bright red when lit from behind. This striking effect is caused by the presence of finely dispersed particles of gold, probably alloyed with silver [3], which interact with light in a way that creates this visually stunning transformation. This ancient masterpiece serves as a testament to the early use of nanomaterials in craftsmanship and artistry. Nanoscience has experienced significant and continuous growth and development over the past few decades, evolving into one of the most dynamic and vibrant research areas within the broader field of materials science.

In the realm of materials science, nanoparticles recently offer an array of distinctive properties (e.g., enhanced mechanical strength and altered electrical and optical characteristics) that cannot be found in the same material in bulk [4]. These exceptional features open the door to an expansive range of applications across diverse fields, including medicine [5], electronics [6], etc. Catalysis is one of the famous fields in which nanoparticles are applied [7, 8]. Nanoparticles, particularly metal and metal oxide nanoparticles like silver (AgNPs), Palladium (PdNPs), Copper (CuNPs), Titanium Dioxide (TiO2NPs), and Zinc Oxide (ZnONPs) have been used as catalysts because of their high surface area and effective catalytic activity. In addition, their outstanding antibacterial properties make them effectively used in biomedical as antibacterial agents [9].

Despite metal nanoparticles providing different exceptional properties, their utilization is accompanied by certain limitations. Precisely, there is a challenge in the efficient separation of nanoparticles from solutions, which remains a crucial requirement for many applications [10]. Additionally, due to their high active surface area, nanoparticles have a natural tendency to aggregate in solution over time. Furthermore, it's worth noting that metal nanoparticles have a

disadvantage in that they are often inherently unstable materials, which can affect their long-term performance and behavior in various environments. Thus, a smart idea can overcome the challenges often encountered in nanoparticle applications, which is the integration of nanoparticles into hydrogels which generates new class of materials (known as nanocomposite hydrogels) [11]. Hydrogels serve as a stable and supportive environment for nanoparticles, effectively preventing their aggregation and ensuring the preservation of their properties over extended periods. Additionally, the unique structure of hydrogels enables the even distribution of nanoparticles throughout the material. Besides, this incorporation of nanoparticles into hydrogels enhances the mechanical strength of the hydrogels themselves. This expands the range of potential applications for hydrogels, making them more robust and adaptable materials in various fields.

Hydrogels are formed through the crosslinking of polymer chains, which can occur via either physical or chemical processes. Due to their soft, rubbery, and high swelling nature in aqueous media, they resemble tissues and exhibit stimuli-responsive behavior in changes in physical/chemical conditions of surrounding fluid such as pH [12], temperature [13], pressure [14], etc. Hydrogels can be embedded with organic nanoparticles or inorganic nanoparticles (such as clay, hydroxyapatite, graphene, and metallic nanoparticles). The ultimate physicochemical characteristics of the end product can result from either the combined effects of nanoparticles and the hydrogel network or from the mutually reinforcing interactions between them [12].

The purpose of this study is to synthesize nanocomposite hydrogels and to investigate their activity in organic dye remediation and antimicrobial, in particular, two distinct types of NCH were synthesized i) nanocomposite hydrogel incorporating silver nanoparticles (AgNPs) and ii) nanocomposite hydrogel incorporating both silver-zinc oxide nanoparticles (Ag-ZnONPs).To achieve the goals of this work, potassium polyacrylate hydrogel (PPAH) was employed as the base material for loading these nanoparticles. The integration of nanoparticles into the hydrogel matrix was accomplished using the *in-situ* reduction technique.

This thesis comprises five comprehensive chapters, each delving into specific aspects of the research:

Chapter 1: Nanoparticles Overview

In the opening chapter, we provide an in-depth introduction to nanoparticles. This includes discussions on their characteristics, and various applications, setting the foundation for the subsequent chapters.

Chapter 2: Hydrogels - Fundamentals

Chapter two offers a detailed exploration of hydrogels, covering essential concepts such as their polymerization techniques, classifications, and other key attributes. This chapter serves as a comprehensive reference for understanding hydrogels, a vital component in this research.

Chapter 3: Nanocomposite Hydrogels, Synthesis, Properties, and Application

In the third chapter, we dive into the intricate process of synthesizing nanocomposite hydrogels. We also discuss the distinctive properties of these materials and their broad spectrum of applications. This section sheds light on the core of our research, emphasizing the significance of nanocomposite hydrogels in various fields.

Chapter 4: Experimental Methodology and Testing Protocols

Chapter four provides an extensive explanation of our experimental methodology. We detail the procedures employed in synthesizing diverse nanocomposite hydrogel samples. Furthermore, we delve into the characterization techniques instrumental in identifying the as-prepared nanocomposite hydrogels. Additionally, this chapter encompasses comprehensive descriptions of the tests conducted in this research, including photocatalytic degradation assessments for different organic dyes, reusability studies, and antibacterial activity evaluations against three distinct microorganisms.

Chapter 5: Results, Analysis, and Discussion

The fifth chapter presents the outcomes derived from our diverse analytical techniques and conducted tests. We offer an accurate analysis of the as-prepared nanocomposite hydrogel samples and a comprehensive discussion of the obtained results to elucidate their implications and significance. This chapter serves as the heart of our research findings.

Conclusion and Future Recommendations

At the culmination of this thesis, we provide a conclusive summary, encapsulating the major findings and contributions of this research. Moreover, we outline future prospects and potential areas for further exploration in the field.

References

1. Nasrollahzadeh, M., et al., *An introduction to nanotechnology*, in *Interface science and technology*. 2019, Elsevier. p. 1-27.
2. Omran, B.A. and B.A. Omran, *Fundamentals of nanotechnology and nanobiotechnology.* Nanobiotechnology: A Multidisciplinary Field of Science, 2020: p. 1-36.
3. Barber, D.J. and I.C. Freestone, *An investigation of the origin of the colour of the Lycurgus Cup by analytical transmission electron microscopy.* Archaeometry, 1990. **32**(1): p. 33-45.
4. Kaniewska, K., M. Karbarz, and E. Katz, *Nanocomposite hydrogel films and coatings–Features and applications.* Applied Materials Today, 2020. **20**: p. 100776.
5. Aguilar, Z., *Nanomaterials for medical applications*. 2012: Newnes.
6. Poizot, P., et al., *Nano-sized transition-metal oxides as negative-electrode materials for lithium-ion batteries.* Nature, 2000. **407**(6803): p. 496-499.
7. Ohde, H., et al., *Hydrogenation of olefins in supercritical CO2 catalyzed by palladium nanoparticles in a water-in-CO2 microemulsion.* Journal of the American Chemical Society, 2002. **124**(17): p. 4540-4541.
8. Zohra, R., et al., *Biosynthesis and Characterization of MnO2 and Zn/Mn2O4 NPs Using Ziziphus Spina-Christi Aqueous Leaves Extract: Effect of Decoration on Photodegradation Activity against various organic Dyes.* Inorganic Chemistry Communications, 2023: p. 111304.
9. Terea, H., et al., *Preparation and characterization of cellulose/ZnO nanoparticles extracted from peanut shells: Effects on antibacterial and antifungal activities.* Biomass Conversion and Biorefinery, 2023: p. 1-12.
10. Ali, F., et al., *Bactericidal and catalytic performance of green nanocomposite based-on chitosan/carbon black fiber supported monometallic and bimetallic nanoparticles.* Chemosphere, 2017. **188**: p. 588-598.
11. Dannert, C., B.T. Stokke, and R.S. Dias, *Nanoparticle-hydrogel composites: from molecular interactions to macroscopic behavior.* Polymers, 2019. **11**(2): p. 275.
12. Piantanida, E., et al., *Design of nanocomposite injectable hydrogels for minimally invasive surgery.* Accounts of chemical research, 2019. **52**(8): p. 2101-2112.
13. Sershen, S. and J. West, *Implantable, polymeric systems for modulated drug delivery.* Advanced drug delivery reviews, 2002. **54**(9): p. 1225-1235.
14. van der Linden, H., et al., *Development of stimulus-sensitive hydrogels suitable for actuators and sensors in microanalytical devices.* Sens. Mater, 2002. **14**(3): p. 129-139.

Chapter 1

Nanoparticles

Overview

Chapter I. Nanoparticles Overview

Preface

Particles can be categorized based on their size into three groups: coarse particles, which measure between 10,000 and 2,500 nanometers, fine particles, spanning from 2,500 to 100 nanometers, and ultrafine nanoparticles, which range from just 1 to 100 nanometers in size. This chapter delves into the processes of preparing, modifying, and utilizing a wide range of ultrafine nanoparticles. It explores how these nanoparticles are synthesized and how they can be functionalized to enhance their properties for diverse applications. From their inception in the laboratory to their practical use in fields such as medicine, electronics, and materials science. This chapter also provides an in-depth examination of silver and zinc oxide nanoparticles preparation, their properties, and real-world applications.

I. Generalities

The term 'nanoparticle' was derived from the Greek word 'nano,' signifying 'small' or 'dwarf.' When employed as a prefix, it denotes a size of 10^{-9}, which is equivalent to one billionth of a meter, or 1 nm [15]. Nanoparticles are minute particles or structures with dimensions typically in the nanometer scale, typically ranging from 1 to 100 nanometers in size. These particles consist of carbon, metals, metal oxides, or organic substances [16]. Due to their exceptionally small size, nanoparticles often exhibit unique and novel properties that differ from their bulk counterparts. This phenomenon arises from a comparatively greater surface area relative to volume, resulting in heightened reactivity or stability in chemical processes, as well as improved mechanical strength, and so on.[17]. Nanoparticles play a pivotal role in various scientific, industrial, and technological applications, including sensing and detection [18, 19], nanotechnology [20], energy materials [21, 22], medicine [23, 24], catalysis [25, 26], computing [27], and electronics [28, 29], Although nanoscience has garnered substantial attention from the scientific community. Yet its commercial application still faces some limitations. Nevertheless, the exceptional properties exhibited by nanoparticles persistently hold substantial appeal for potential commercialization.

Nanoparticles exhibit variations not only in their material composition but also in their dimensions and shapes [30]. Nanoparticles can be classified into different dimensional categories: zero-dimensional, which have their length, breadth, and height concentrated at a single point, as

seen in nano dots; one-dimensional, where only one parameter varies, as exemplified by graphene; two-dimensional, characterized by length and breadth variations, as seen in carbon nanotubes; and three-dimensional, which possess variations in all three parameters of length, breadth, and height, as observed in gold nanoparticles.

I.1 Nanoparticles shapes

Nanoparticles come in a variety of shapes, each with unique properties and applications. However, some nanoparticles can take on irregular or complex shapes, depending on the synthesis method. including triangles, hexagons, or more intricate structures. Nanoparticles can exist in either a crystalline or amorphous state, and they may comprise single or multiple crystal solids, either in a dispersed form or as agglomerates [31]. The common nanoparticle shapes are:

- **Spheres:** Nanoparticles with a spherical shape are often referred to as nanospheres. They have a high degree of symmetry
- **Rods:** Nanorods have an elongated, rod-like shape. Their aspect ratio (length-to-width ratio) can be tailored for specific applications.
- **Tubes:** Nanotubes are hollow cylindrical structures with nanoscale dimensions. Carbon nanotubes, in particular, have gained significant attention for their exceptional electrical and mechanical properties.
- **Wires:** Nanowires are one-dimensional nanostructures with a thin, wire-like shape.
- **Plates:** Nanoplates have a flat, plate-like shape and can be used in various applications, including in the development of advanced materials.
- **Polyhedral:** Nanoparticles with polyhedral shapes, such as cubes or octahedra, offer unique optical and catalytic properties.
- **Janus Particles:** Janus nanoparticles have two distinct halves with different properties or surface chemistries.

I.2. Classification of nanoparticles

Nanoparticles are commonly categorized into three broad groups based on their composition: carbon-based nanoparticles, organic, and inorganic nanoparticles. This classification serves as a foundational framework for understanding and exploring the diverse world of nanomaterials, each group offering unique characteristics and applications.

I.2.1. Carbon-based nanoparticles

Carbon-based nanoparticles are tiny structures primarily composed of carbon atoms, often arranged in unique configurations at the nanoscale. These nanoparticles can take various forms and have garnered significant attention due to their exceptional properties and versatile applications. Common types of carbon-based nanoparticles include:

I.2.1.1. Carbon nanotubes (CNT)

These are cylindrical carbon structures with remarkable mechanical, electrical, and thermal properties. Carbon nanotubes come in single-walled (SWCNTs) and multi-walled (MWCNTs) varieties and are used in nanocomposites, electronics, and as drug delivery carriers.

I.2.1.2. Graphene

Graphene is a single layer of carbon atoms arranged in a two-dimensional honeycomb lattice. Typically, the graphene sheet has a thickness of approximately 1 nanometer. It is known for its exceptional electrical conductivity, mechanical strength, and flexibility. Graphene has applications in electronics, energy storage, and as a reinforcement material.

I.2.1.3. Fullerenes

Fullerenes are spherical carbon molecules, with C_{60} (buckminsterfullerene) being the most well-known. fullerenes are formed by approximately 28 to 1500 carbon atoms. For a single layer, the diameter can reach up to 8.2 nm, while multi-layered fullerenes exhibit diameters ranging from 4 to 36 nm. They have unique cage-like structures and find applications in drug delivery, superconductors, and as antioxidants.

I.2.1.4. Carbon Dots

Carbon dots are small carbon nanoparticles with quantum dot-like properties. They are often used in bioimaging, sensing, and as fluorescent labels.

I.2.1.5. Nanodiamonds

Nanodiamonds are small diamond particles at the nanoscale. They have excellent hardness and are used in biomedical applications, as well as for drug delivery and imaging.

I.2.1.6. Carbon nanoparticles from biomass

These are carbon nanoparticles derived from renewable biomass sources like wood, plants, or algae. They are environmentally friendly and can be used in various applications, including energy storage and environmental remediation.

Carbon-based nanoparticles are of great interest due to their unique combination of properties, including high surface area, electrical conductivity, and chemical stability. These properties make them valuable in a wide range of fields, such as nanotechnology, materials science, energy storage, and medicine.

I.3. Organic nanoparticles

This class of nanoparticles is primarily composed of organic compounds, such as polymers, lipids, proteins, etc. These nanoparticles possess biodegradable properties and are non-toxic. Some of them, like micelles and liposomes, have a hollow core, which is often referred to as nano capsules. Moreover, they exhibit sensitivity to thermal and electromagnetic radiation, including heat and light [32]. Organic nanoparticles are often used in drug delivery systems, where the encapsulation of pharmaceuticals within biocompatible organic carriers can enhance drug solubility, stability, and targeted delivery. They also find applications in areas like cosmetics, where nano-sized organic particles are employed in skincare products for improved penetration and effectiveness.

I.4. Inorganic nanoparticles

Inorganic nanoparticles are constructed from non-carbon-based materials, including metals (like gold, silver, and iron), metal oxides (such as titanium dioxide or iron oxide), and semiconductors (like silicon or quantum dots). These nanoparticles exhibit unique physical and chemical properties due to their inorganic nature. They are widely used in fields like catalysis, electronics, optics, and imaging technologies.

I.4.1. Metal nanoparticles

Metal or metallic nanoparticles consist of various metallic elements such as gold, silver, platinum, and copper, among others. They exhibit unique properties at the nanoscale, including enhanced electrical conductivity, catalytic activity, and plasmonic effects, depending on their size and shape. Metal nanoparticles find applications in a wide range of fields. For example, gold

nanoparticles are used in diagnostics and drug delivery due to their biocompatibility, while silver nanoparticles are employed for their antimicrobial properties in healthcare and consumer products.

I.4.2. Metal oxide nanoparticles

Metal oxide nanoparticles are composed of metal atoms bonded to oxygen atoms. Common metal oxides include titanium dioxide (TiO2), zinc oxide (ZnO), and iron oxide (Fe3O4). Metal oxide nanoparticles possess a variety of properties such as semiconductivity, catalytic activity, and magnetic behavior, making them versatile materials. They are used extensively in electronics, catalysis, environmental remediation, and as pigments in paints and sunscreens. For example, titanium dioxide nanoparticles are employed in sunscreen formulations for their ability to scatter and absorb UV radiation.

Generally, metal and metal oxide nanoparticles are engineered to have specific sizes and shapes to optimize their properties for various applications. Their nanoscale dimensions give them distinct advantages, such as large surface areas and quantum effects, making them invaluable in modern technology and science. Among divers metal and metal oxide nanoparticles, silver nanoparticles and zinc oxide nanoparticles have witnessed great attention

I.5. Silver nanoparticles (Ag NPs)

Historical records show that ancient civilizations, including the Greeks and Romans, used silver containers to store liquids to prevent spoilage and bacterial growth. Silver coins were also sometimes placed in drinking water containers to help purify the water. Prior to the 1980s, the scientific and practical fascination surrounding silver nanoparticles was primarily driven by the potential they held as finely dispersed substrates capable of amplifying signals generated by organic molecules in the realm of Raman spectroscopy [33]. During the 17th and 18th centuries, silver nitrite gained prominence as a therapeutic agent used in the treatment of ulcers [34]. In the 1800s, silver nitrate solutions were commonly used as disinfectants and antiseptics in medical practice. This marked an early form of using silver for its antimicrobial properties in modern medicine.

Nano-silver was first reported by M. C. Lea in 1889, M. C. Lea did indeed report on the synthesis of a citrate-stabilized silver colloid [35]. This work is an early example of colloidal chemistry and the stabilization of silver particles in a colloid using citrate. The particles generated through this approach typically have an average diameter falling within the range of 7 to 9 nm

[36]. This nanoscale size and the citrate-mediated stabilization closely resemble recent findings on the formation of nano-silver using silver nitrate and citrate, as reported in contemporary studies. During that period, the term “nano” was not formally coined or registered as it is today. However, historical literature indicates that silver colloids had been employed in the field of medicine for well over a century, dating back to 1897 when they were known by the name “Collargol”[37]. Collargol, with a mean particle size of approximately 10 nm [38], was recognized as having a diameter within the nanoscale range [39], as early as 1907. This early understanding of its nanosized particles highlights the historical appreciation of nanoscale materials, even before the formal terminology and advanced characterization techniques of modern nanotechnology were established. With advancements in nanotechnology, researchers began developing silver nanoparticles in the late 20th century. This allowed for better control of particle size and shape. Over the past three decades, fundamental research has revealed that silver nanoparticles possess a remarkable blend of valuable properties. Particularly, their unique optical characteristics linked to surface plasmon resonance (SPR), well-defined and highly reactive surfaces, catalytic activity, and a high electrical double-layer capacitance, among others [40]. These diverse properties have opened up new avenues for the introduction of silver nanoparticles into various applications. As nanotechnology continued to advance, silver nanoparticles gained significant attention in the 21st century. They were increasingly incorporated into consumer products such as textiles, cosmetics, and household items for their antimicrobial benefits. This widespread use led to concerns about potential environmental and health impacts. Currently, there has been a significant rise in the number of scientific publications dedicated to silver nanoparticle synthesis methods, gaining an understanding of their toxicological effects, and establishing guidelines for their safe utilization in various applications.

I.5.1. Synthesis of silver nanoparticles

The synthesis of nanoparticles, with the goal of achieving improved control over particle size, distribution, morphology, purity, quantity, and quality, while utilizing environmentally friendly and cost-effective processes, has consistently posed a challenge for researchers [41]. Silver nanoparticles can be synthesized through a variety of methods (e.g., chemical reduction, physical methods, green synthesis, photochemical synthesis, Sol-Gel method, etc.) each with its own set of advantages and disadvantages. Among these methods, chemical reduction stands out as the most commonly employed approach for producing stable, colloidal dispersions of silver

nanoparticles in both water and organic solvents [42, 43]. Chemical reduction is favored in the synthesis of silver nanoparticles Because it is considered a relatively straightforward procedure. It involves the reduction of silver ions (Ag^{+}) in aqueous solution by a reducing agent. Sodium borohydride, Sodium citrate, ascorbate, and elemental hydrogen are frequently used reductants in this method [44]. The choice of reducing agent and stabilizing agent, as well as the reaction conditions, allows for fine-tuning the properties of the resulting nanoparticles. This reduction process leads to the formation of colloidal silver nanoparticles with controlled properties such as size, shape, and dispersity. When colloidal particles are significantly smaller than the wavelength of visible light, the formed solutions appear with a yellow-brown color, and a distinct and intense band is observed in the range of 380 to 400 (nm) in their absorption spectrum. Additionally, there may be other, smaller absorption bands detected at longer wavelengths in the spectrum [45, 46].

One of the key advantages of chemical reduction is its adaptability to various scales of production, from laboratory-scale to industrial-scale. Additionally, it allows for precise control over the particle size and morphology by adjusting factors such as reactant concentrations, reaction temperature, and reaction time. This method often yields high-quality silver nanoparticles with a narrow size distribution. Previous research has indicated that when strong reductants like borohydride are used, they tend to produce relatively small particles that are somewhat uniform in size. However, controlling the formation of larger particles under these conditions has proven to be challenging. On the other hand, when a weaker reductant such as citrate is employed, it results in a slower reduction process, but the size distribution of the produced particles is far from being narrow.

To achieve controlled synthesis of silver nanoparticles (Ag NPs), a two-step reduction process has been reported [47]. In this method, a strong reducing agent is initially used to produce small silver particles. These small particles are then enlarged in a subsequent step through further reduction, utilizing a weaker reducing agent [33]. This two-step approach allows for better control over the size and distribution of the resulting silver nanoparticles.

I.5.2 Applications of silver nanoparticles

Silver nanoparticles have unique properties, including their antimicrobial activity, high surface area, excellent electrical and thermal conductivity, and relatively low contact resistance, makes it an ideal choice in:

I.5.2.1 Medical and Healthcare Applications

a/ Antimicrobial

Silver, an inorganic antibacterial agent with a long history of safe and non-toxic use spanning centuries, possesses the remarkable capability to eliminate approximately 650 disease-causing microorganisms [48, 49]. Even at minimal concentrations, it demonstrates potent bactericidal (antibacterial) effects. These attributes underscore its considerable potential for diverse biological applications, including countering antibiotic-resistant bacteria [50], infection prevention [51], bandages [52], medical coatings [53], wound healing [54], and anti-inflammatory purposes [55].

b/ Drug Delivery

AgNPs can be used as carriers for drug delivery systems [56]. Their small size allows for targeted delivery to specific cells or tissues, and they can be functionalized to release drugs in a controlled manner.

c/ Diagnostics

AgNPs are employed in various diagnostic assays, including colorimetric, electrochemical [57], and surface-enhanced Raman Scattering (SERS) assays, for the detection of biomolecules [58], pathogens [59], and diseases. It has been reported that silver nanoparticles (AgNPs) can significantly boost the efficiencies of Surface-Enhanced Raman Scattering (SERS) by an astonishing magnitude [60], ranging from 10^{14} to 10^{15} fold. This remarkable enhancement enables the detection and identification of individual molecules.

d/ Electronics and Optoelectronics

Silver nanoparticles are used in conductive inks for printing electronic circuits on flexible substrates [61]. They enable the production of flexible and lightweight electronics. They have also found application in the production of electrodes for thin-film transistors [62], as well as in data storage devices, and materials for battery-based intercalation [63]. Furthermore, they are employed in a range of sensor types, including those designed for gas detection [64], biosensing [65], and environmental monitoring.

e/ Catalysis

Due to their exceptionally minute dimensions, silver nanoparticles (AgNPs) boast a wide surface area. This attribute grants them substantial surface energy and a multitude of potential reactive sites. These unique features establish AgNPs as highly promising materials in the field of catalysis.

f/ Other fields

Silver nanoparticles find applications across many other domains. In food packaging, they contribute to extended shelf life by inhibiting the proliferation of spoilage microorganisms and pathogens and preserving perishable products. In photovoltaics, these nanoparticles enhance light absorption and electron transport within solar cells, thereby increasing the efficiency of photovoltaic devices. Additionally, in environmental monitoring, silver nanoparticles are employed in water quality testing systems to detect and eliminate pollutants, ensuring the safety of drinking water supplies.

I.6. Zinc oxide nanoparticles (ZnO NPs)

Zinc oxide nanoparticles (ZnO NPs) are nanoscale particles of zinc oxide, a compound made up of zinc and oxygen atoms. These nanoparticles exhibit unique physical, chemical, and optical properties due to their small size and high surface area-to-volume ratio. Zinc oxide has been a prominent subject of study in semiconductor research for over seven decades, with references appearing in publications dating as far back as 1945 [66]. It experienced periods of heightened interest, particularly during the 1950s and 1970s, focusing on aspects like growth, doping, transport, band structure, and luminescence [67]. In the 1990s and early 2000s, ZnO nanoparticles gained prominence in semiconductor research. They were investigated for their potential as a wide-band gap semiconductor material, which could be used in electronic and optoelectronic devices. Presently, significant attention in the realm of ZnO research has pivoted towards biosensing and optoelectronic applications that make use of nanostructures. Notably, the past two decades have witnessed a substantial increase in the volume of publications dedicated to ZnO nanostructures, with a particular emphasis on ZnO nanowires [67]. From the 2000s until now, the methods employed in the synthesis of ZnO nanoparticles have witnessed continuous development, allowing better control over particle size, shape, and purity.

I.6.1 Synthesis of zinc oxide nanoparticles

ZnO nanoparticles can be synthesized using various methods, including chemical precipitation, sol-gel processes, hydrothermal methods, and vapor-phase deposition. The choice of synthesis method can influence the size, shape, and properties of the nanoparticles. The chemical precipitation method is mostly used for synthesizing zinc oxide nanoparticles [68]. This method involves mixing solutions of zinc salts (typically zinc nitrate, zinc chloride, or zinc acetate) with a suitable alkaline solution (such as sodium hydroxide or ammonium hydroxide), leading to the precipitation of ZnO nanoparticles. Precipitation is controlled by adjusting the pH of the reaction mixture, and maintaining a specific pH range is crucial for controlling the size and morphology of the resulting nanoparticles. Following precipitation, the ZnO nanoparticles are usually separated by centrifugation or filtration to remove impurities, and they are subsequently washed and dried to yield the final ZnO nanopowder. This method is preferred due to its simplicity, cost-effectiveness [68], and the ability to produce ZnO nanoparticles with a wide range of sizes and shapes by adjusting reaction conditions such as temperature, pH, and precursor concentrations.

I.6.2. Applications of zinc oxide nanoparticles (ZnO NPs)

Zinc oxide (ZnO) stands out as a semiconductor boasting a wide band gap of 3.3 eV at typical room temperatures. This material holds immense technological significance, finding versatile applications across various fields, in electronics, ZnO NPs are indispensable in a wide array of electronic devices, including sensors [69], transistors [70], and light-emitting diodes (LEDs) [71], owing to their remarkable semiconductor properties and electrical conductivity. In catalysis [72], their catalytic activity facilitates chemical reactions, including the degradation of organic pollutants, contributing to environmental sustainability. In the field of environmental monitoring, they are deployed in gas sensors [73] that enable the accurate detection and measurement of specific gases in the environment. Besides, they have potential applications in the biomedical field as drug delivery systems [74]. ZnO nanoparticles also play a big role in optics because they are transparent and scatter light. This makes them really useful for making coatings and devices that reduce reflections and make optical systems work better [75]. In addition, zinc oxide nanoparticles have gained huge interest in renewable energy, especially in solar cells [76], due to their semiconductor properties that can boost energy conversion efficiency, promoting the shift towards sustainable energy sources.

Summary

The utilization of silver nanoparticles (Ag NPs) and zinc oxide nanoparticles (ZnO NPs) presents a wide array of advantages across numerous fields. Ag NPs offer powerful antimicrobial properties, fostering applications in healthcare, water purification, and consumer products. Meanwhile, ZnO NPs excel in UV protection, photocatalysis, and advanced technologies, including electronics and biomedical applications. The versatility, efficiency, and potential for innovation associated with these nanoparticles underscore their significance in addressing contemporary challenges and shaping future advancements in science, technology, and sustainability. Despite the synthesis of both Ag NPs and ZnO NPs is not new, the ongoing and spirited research into their synthesis techniques and diverse applications remains imperative.

References

1. You, H., et al., *Synthesis of colloidal metal and metal alloy nanoparticles for electrochemical energy applications.* Chemical Society Reviews, 2013. **42**(7): p. 2880-2904.
2. Hasan, S., *A review on nanoparticles: their synthesis and types.* Res. J. Recent Sci, 2015. **2277**: p. 2502.
3. Ealia, S.A.M. and M.P. Saravanakumar. *A review on the classification, characterisation, synthesis of nanoparticles and their application*. in *IOP conference series: materials science and engineering*. 2017. IOP Publishing.
4. Shomura, R., et al., *Gold nanoparticles with cyclic phenylazomethines: one-pot synthesis and metal ion sensing.* Langmuir, 2011. **27**(13): p. 7972-7975.
5. Hazarika, P., S.M. Jickells, and D.A. Russell, *Rapid detection of drug metabolites in latent fingermarks.* Analyst, 2009. **134**(1): p. 93-96.
6. Bouafia, A., et al., *Removal of hydrocarbons and heavy metals from petroleum water by modern green nanotechnology methods.* Scientific Reports, 2023. **13**(1): p. 5637.
7. Kim, G.H., et al., *Inverted colloidal quantum dot solar cells.* Advanced Materials, 2014. **26**(20): p. 3321-3327.
8. Pichaandi, J. and F.C. van Veggel, *Near-infrared emitting quantum dots: Recent progress on their synthesis and characterization.* Coordination Chemistry Reviews, 2014. **263**: p. 138-150.
9. Noske, A.B. and B.J. Marsh, *Mapping the ß-Cell in 3D at the nanoscale using novel cellular electron tomography and computational approaches.* BetaSys: Systems Biology of Regulated Exocytosis in Pancreatic ß-Cells, 2011: p. 147-183.
10. Bogart, L.K., et al., *Nanoparticles for imaging, sensing, and therapeutic intervention.* ACS nano, 2014. **8**(4): p. 3107-3122.
11. Hasan, G.G., et al., *Synergistic effect of novel biosynthesis SnO2@ Fe3O4 nanocomposite: A comprehensive study of its photocatalytic of Dyes & antibiotics, antibacterial, and antimutagenic activities.* Journal of Photochemistry and Photobiology A: Chemistry, 2023. **443**: p. 114874.
12. Zohra, R., et al., *Enhanced photocatalytic degradation of dyes and antibiotics with biosynthesized FeMn2O4 nanocomposite under sunlight irradiation: isotherm and kinetic study.* Biomass Conversion and Biorefinery, 2023: p. 1-12.
13. Terris, B. and T. Thomson, *Nanofabricated and self-assembled magnetic structures as data storage media.* Journal of physics D: Applied physics, 2005. **38**(12): p. R199.
14. Bouafia, A., et al., *The recent progress on silver nanoparticles: Synthesis and electronic applications.* Nanomaterials, 2021. **11**(9): p. 2318.
15. Ahmad, S., et al., *Development of conductive fabrics by using silver nanoparticles for electronic applications.* Journal of Electronic Materials, 2020. **49**: p. 1330-1337.
16. Cho, E.J., et al., *Nanoparticle characterization: state of the art, challenges, and emerging technologies.* Molecular pharmaceutics, 2013. **10**(6): p. 2093-2110.
17. Machado, S., et al., *Characterization of green zero-valent iron nanoparticles produced with tree leaf extracts.* Science of the total environment, 2015. **533**: p. 76-81.
18. Tiwari, D.K., J. Behari, and P. Sen, *Application of nanoparticles in waste water treatment.* World Appl Sci J, 2008. **3**(3): p. 417-433.

19. Lee, P. and D. Meisel, *Adsorption and surface-enhanced Raman of dyes on silver and gold sols.* The Journal of Physical Chemistry, 1982. **86**(17): p. 3391-3395.
20. Klasen, H., *Historical review of the use of silver in the treatment of burns. I. Early uses.* Burns, 2000. **26**(2): p. 117-130.
21. Lea, M.C., *Allotropic forms of silver.* American Journal of science, 1889. **3**(222): p. 476-491.
22. Frens, G. and J.T.G. Overbeek, *Carey Lea's colloidal silver.* Kolloid-Zeitschrift und Zeitschrift für Polymere, 1969. **233**: p. 922-929.
23. Yu, S.-j., Y.-g. Yin, and J.-f. Liu, *Silver nanoparticles in the environment.* Environmental Science: Processes & Impacts, 2013. **15**(1): p. 78-92.
24. Bogdanchikova, N., et al., *Activity of colloidal silver preparations towards smallpox virus.* Pharmaceutical Chemistry Journal, 1992. **26**(9-10): p. 778-779.
25. Bechhold, H., *Die Gallertfiltration.* Zeitschrift für Chemie und Industrie der Kolloide, 1907. **2**(1): p. 3-9.
26. Henglein, A., *Small-particle research: physicochemical properties of extremely small colloidal metal and semiconductor particles.* Chemical reviews, 1989. **89**(8): p. 1861-1873.
27. Hahn, H., *Unique features and properties of nanostructured materials.* Nanomaterials by Severe Plastic Deformation, 2004: p. 2-17.
28. Kim, M., et al., *Spontaneous formation of silver nanoparticles on polymeric supports.* Materials Research Bulletin, 2009. **44**(2): p. 334-338.
29. Khan, Z., et al., *Preparation and characterization of silver nanoparticles by chemical reduction method.* Colloids and Surfaces B: Biointerfaces, 2011. **82**(2): p. 513-517.
30. Qurbat, Z., et al., *A mini review on the synthesis of ag-nanoparticles by chemical reduction method and their biomedical applications.* 2016.
31. Tessier, P.M., et al., *Assembly of gold nanostructured films templated by colloidal crystals and use in surface-enhanced Raman spectroscopy.* Journal of the American Chemical Society, 2000. **122**(39): p. 9554-9555.
32. Rosi, N.L. and C.A. Mirkin, *Nanostructures in biodiagnostics.* Chemical reviews, 2005. **105**(4): p. 1547-1562.
33. Steinigeweg, D. and S. Schluecker, *Monodispersity and size control in the synthesis of 20–100 nm quasi-spherical silver nanoparticles by citrate and ascorbic acid reduction in glycerol–water mixtures.* Chemical Communications, 2012. **48**(69): p. 8682-8684.
34. Abdulrahaman, M. and H.Z. Hussein, *Antifungal effect of silver nanoparticles (AgNPs) against Aspergillus flavus.* EC Microbiol, 2017. **6**: p. 63-66.
35. Widatalla, H.A., et al., *Green synthesis of silver nanoparticles using green tea leaf extract, characterization and evaluation of antimicrobial activity.* Nanoscale Advances, 2022. **4**(3): p. 911-915.
36. Kotakadi, V.S., et al., *New generation of bactericidal silver nanoparticles against different antibiotic resistant Escherichia coli strains.* Applied Nanoscience, 2015. **5**: p. 847-855.
37. Wang, J., et al., *Silver nanoparticles coated poly (L-lactide) electrospun membrane for implant associated infections prevention.* Frontiers in Pharmacology, 2020. **11**: p. 431.
38. Senthamarai Kannan, M., et al., *Fabrication of anti-bacterial cotton bandage using biologically synthesized nanoparticles for medical applications.* Progress in Biomaterials, 2022. **11**(2): p. 229-241.

39. Vigneswari, S., et al., *Transformation of biowaste for medical applications: incorporation of biologically derived silver nanoparticles as antimicrobial coating.* Antibiotics, 2021. **10**(3): p. 229.
40. Kithiyon, M., et al., *Efficacy of mycosynthesised AgNPs from Earliella scabrosa as an in vitro antibacterial and wound healing agent.* IET nanobiotechnology, 2019. **13**(3): p. 339-344.
41. Hebeish, A., et al., *Antimicrobial wound dressing and anti-inflammatory efficacy of silver nanoparticles.* International journal of biological macromolecules, 2014. **65**: p. 509-515.
42. KJ, P., *Multi-functional silver nanoparticles for drug delivery: A review.* Int. J. Curr. Pharm. Rev. Res, 2017. **9**: p. 1-5.
43. Van Cleve, T., E. Gibara, and S. Linic, *Electrochemical oxygen reduction reaction on Ag nanoparticles of different shapes.* ChemCatChem, 2016. **8**(1): p. 256-261.
44. Mughal, S.S., *Role of silver nanoparticles in colorimetric detection of biomolecules.* Authorea Preprints, 2022.
45. Wahab, M.A., et al., *Silver nanoparticle-based nanocomposites for combating infectious pathogens: Recent advances and future prospects.* Nanomaterials, 2021. **11**(3): p. 581.
46. Qian, X.-M. and S.M. Nie, *Single-molecule and single-nanoparticle SERS: from fundamental mechanisms to biomedical applications.* Chemical Society Reviews, 2008. **37**(5): p. 912-920.
47. Li, Y., Y. Wu, and B.S. Ong, *Facile synthesis of silver nanoparticles useful for fabrication of high-conductivity elements for printed electronics.* Journal of the American Chemical Society, 2005. **127**(10): p. 3266-3267.
48. Tate, J., et al., *Anodization and microcontact printing on electroless silver: Solution-based fabrication procedures for low-voltage electronic systems with organic active components.* Langmuir, 2000. **16**(14): p. 6054-6060.
49. Tolaymat, T.M., et al., *An evidence-based environmental perspective of manufactured silver nanoparticle in syntheses and applications: a systematic review and critical appraisal of peer-reviewed scientific papers.* Science of the total environment, 2010. **408**(5): p. 999-1006.
50. Jin, H., et al., *Selective and sensitive electrochemical sensing of gastrodin based on nickel foam modified with reduced graphene oxide/silver nanoparticles complex-encapsulated molecularly imprinted polymers.* Sensors and Actuators B: Chemical, 2018. **277**: p. 14-21.
51. Wang, N., et al., *A novel surface plasmon resonance biosensor based on the PDA-AgNPs-PDA-Au film sensing platform for horse IgG detection.* Spectrochimica Acta Part A: Molecular and Biomolecular Spectroscopy, 2018. **191**: p. 290-295.
52. Brubaker, D. and M. Fuller, *The electrical charging of electron diffraction specimens.* Journal of Applied Physics, 1945. **16**(3): p. 128-130.
53. Gomez, J.L. and O. Tigli, *Zinc oxide nanostructures: from growth to application.* Journal of Materials Science, 2013. **48**: p. 612-624.
54. Jay Chithra, M., M. Sathya, and K. Pushpanathan, *Effect of pH on crystal size and photoluminescence property of ZnO nanoparticles prepared by chemical precipitation method.* Acta Metallurgica Sinica (English Letters), 2015. **28**: p. 394-404.
55. Maruthupandy, M., et al., *Synthesis of metal oxide nanoparticles (CuO and ZnO NPs) via biological template and their optical sensor applications.* Applied Surface Science, 2017. **397**: p. 167-174.

56. Narayana, A., et al., *Green and low-cost synthesis of zinc oxide nanoparticles and their application in transistor-based carbon monoxide sensing.* RSC advances, 2020. **10**(23): p. 13532-13542.
57. Son, D.I., et al., *Emissive ZnO–graphene quantum dots for white-light-emitting diodes.* Nature nanotechnology, 2012. **7**(7): p. 465-471.
58. Sun, Y., et al., *The applications of morphology controlled ZnO in catalysis.* Catalysts, 2016. **6**(12): p. 188.
59. Franco, M.A., et al., *A review on chemiresistive ZnO gas sensors.* Sensors and Actuators Reports, 2022. **4**: p. 100100.
60. Nigam, A. and S. Pawar, *Synthesis and characterization of ZnO nanoparticles to optimize drug loading and release profile for drug delivery applications.* Materials Today: Proceedings, 2020. **26**: p. 2625-2628.
61. Vaseem, M., A. Umar, and Y.-B. Hahn, *ZnO nanoparticles: growth, properties, and applications.* Metal oxide nanostructures and their applications, 2010. **5**(1): p. 10-20.
62. Han, J., et al., *ZnO nanotube-based dye-sensitized solar cell and its application in self-powered devices.* Nanotechnology, 2010. **21**(40): p. 405203.

Chapter II

Hydrogels-Fundamentals

Chapter II. Hydrogels-Fundamentals

Preface

The following chapter highlights the generalities of hydrogels, an examination of their classifications, and wide-ranging applications. Moreover, comprehensive of the various methodologies employed in the preparation of hydrogels are also well-detailed in this chapter along with their fundamental properties.

II.1. Definition of hydrogel

The most common definition of hydrogel in the literature is that hydrogel is a three-dimensional network of crosslinked polymer chains that has the ability to absorb and retain a significant amount of water or other aqueous solutions while maintaining its structural integrity. These materials are highly water-absorbent and can hold water content ranging from a few times to several hundred times their dry weight.

The presence of hydrophilic chemical groups including hydroxylic (-OH), carboxylic (-COOH), sulfonic (-SO3H), imide (–CONH), amide (-$CONH_2$), and amine (–NH_2) groups allow hydrogels to absorb water in wide range, whereas their ability to remain significant amount of water without dissolving in it is due to the interconnections formed among the chains within the network.

Hydrogels can be synthesized using a variety of traditional chemical methods. These methods include both single-step processes such as polymerization and simultaneous cross-linking of multifunctional monomers, as well as multi-step procedures involving the creation of polymer molecules containing reactive groups followed by their subsequent cross-linking. In some cases, polymers can also be cross-linked by reacting them with appropriate cross-linking agents. In the process of hydrogels' preparation, it is possible to meticulously engineer and synthesize polymer networks with precise control at the molecular level. This allows for the fine-tuning of essential characteristics like cross-linking density and specific properties such as biodegradability, mechanical resilience, and the ability to respond to various chemical and biological stimuli [77].

II.2. Hydrogels classifications

Hydrogels can originate from natural polymers, synthetic polymers, or a blend of both. The classification of hydrogels can be established using various criteria, which include their source polymers, polymerization methods, ionic charges, physical attributes, stimuli-responsive properties, or the types of cross-linking agents employed.

II.2.1. Classification based on source

Based on their origins, hydrogels can be divided into two groups, natural hydrogels or synthetic hydrogels [78].

a/ Natural Hydrogels: These hydrogels are derived from naturally occurring polymers found in living organisms or extracted from natural sources. The common natural polymers used for hydrogel production are:

- Alginate: Derived from brown seaweed.
- Collagen: Obtained from animal connective tissues.
- Hyaluronic Acid: Found in the human body.
- Chitosan: Derived from chitin, a substance in the exoskeleton of crustaceans.

Although natural hydrogels are recognized for their limited mechanical strength, and could potentially contain pathogens or trigger immune and inflammatory reactions, they do possess numerous beneficial characteristics. These include inherent compatibility with biological systems, the ability to biodegrade, and the presence of biologically recognizable components that facilitate cellular functions.

b/ Synthetic Hydrogels: These hydrogels are produced through chemical synthesis, where engineers design and control the polymerization process to achieve specific properties. Synthetic hydrogels offer advantages like long life-to-failure duration, exceptional water-absorbing capacity, precise control over chemical composition, reproducibility, and improved mechanical properties as the structure can be tailored to its functionality [79]. The most common synthetic hydrogels include those made from acrylates, polyethylene glycol (PEG), and N-isopropyl acrylamide (NIPAAm).

The choice between natural and synthetic hydrogels depends on the intended application, as each type offers unique advantages and limitations. Natural hydrogels are often favored in

biological and medical applications due to their biocompatibility and resemblance to native tissues. In contrast, synthetic hydrogels provide versatility in tailoring properties for various purposes, including drug delivery, wound healing, and tissue engineering.

Table II.1 Natural polymers and synthetic monomers used in hydrogel synthesizing [80-82]

Natural polymers	Synthetic monomer
Chitosan	Hydroxyethyl methacrylate (HEMA)
Alginate	N-(2-hydroxypropyl) methacrylate (HPMA)
Fibrin	N-vinyl-2-pyrrolidone (NVP)
Collagen	N-isopropyl acrylamide (NIPAAm)
Gelatin	Vinyl acetate (VAc)
Hyaluronic acid	Acrylic acid (AA)
Dextran	Methacrylic acid (MAA)
	Polyethylene glycol acrylate/methacrylate (PEGA/PEGMA)
	Polyethylene glycol diacrylate/dimethacrylate (PEGDA/PEGDMA)

II.2.2. Classification based on the polymeric composition

The preparation method results in the creation of significant categories of hydrogels. These can be further explained below:

a/ Homopolymeric hydrogels: this class of hydrogels is formed from a single type of polymer chain. In these hydrogels, the entire three-dimensional network consists of identical polymer chains, typically derived from a single monomer [83]. The presence of a cross-linked skeletal structure in homopolymers depends on the specific monomer used and the method of polymerization employed. Their simplicity in composition allows for precise control over their physical and chemical properties, making them suitable for specific biomedical and industrial purposes.

b/ Copolymeric hydrogels: this class of hydrogels is composed of two or more distinct monomer species, with at least one hydrophilic component, these monomers are chemically linked together

to form a polymer network structure. The key characteristic of copolymeric hydrogels is the arrangement of these different monomer units along the polymer chain. The arrangement of the monomer units can have various configurations, which include random, block, or alternating configuration [84]:

- Random Copolymers: In this configuration, the different monomer species are distributed randomly along the polymer chain. There is no specific order or pattern to their placement.
- Block Copolymers: Block copolymers consist of distinct blocks of monomers arranged in a specific sequence along the polymer chain. For hydrogels, this means that blocks of one monomer type alternate with blocks of another monomer type.
- Alternating Copolymers: In alternating copolymers, the different monomers alternate regularly along the polymer chain, creating a highly ordered and predictable sequence of monomer units.

The inclusion of multiple monomer species in copolymeric hydrogels allows for the combination of different chemical properties, which can be advantageous for achieving a wide range of properties and functionalities. Also, the specific arrangement of monomer units can be tailored to meet desired performance characteristics.

Multipolymer Interpenetrating Polymeric Hydrogel (Multipolymer IPN Hydrogel) is a class of hydrogel that is composed of multiple independent polymer networks interwoven within each other. In other words, it's a hydrogel structure where two or more distinct polymers (natural and/or synthetic) are present in a complex, intertwined arrangement. This configuration can offer several advantages, including enhanced mechanical strength, improved stability, and the ability to tailor the properties of the hydrogel to specific applications. By combining different polymers, each with its unique characteristics, it is possible to create hydrogels with a wide range of properties, making them suitable for various uses in many fields.

The interpenetrating polymer networks (IPN) within these hydrogels can be formed through various methods, including simultaneous polymerization of different monomers or sequential polymerization of different polymers. This versatility allows for precise control over the hydrogel's properties.

II.2.3. Classification based on type of cross-linking

Hydrogels can be categorized into two groups depending on the type of cross-linking they employ, which can be either chemical or physical in nature. In chemically cross-linked networks, the junctions are permanent and stable. On the other hand, physical networks feature junctions that are transient and can change over time due to factors like polymer chain entanglements or physical interactions, such as ionic attractions, hydrogen bonding, or hydrophobic interactions [85].

Chemically cross-linked hydrogels are characterized by covalent bonds that firmly hold the polymer chains together. These bonds create a strong and durable network, making the hydrogel less susceptible to degradation or changes in its structure. Consequently, hydrogels with chemical cross-links tend to have long-lasting and consistent properties, which can be advantageous in applications requiring stability and reliability, such as in medical implants or contact lenses.

In contrast, physically cross-linked hydrogels rely on non-covalent interactions, such as hydrogen bonds or ionic attractions, to form their network structure. These interactions are weaker than covalent bonds and can be influenced by external factors like temperature, pH, or the presence of specific ions. As a result, physically cross-linked hydrogels can be more responsive to environmental changes, which makes them suitable for applications such as drug delivery systems that need controlled release in response to specific triggers or stimuli.

II.2.4. Classification based on configuration

The classification of hydrogels is based on their physical structure and chemical composition, which can be grouped into three main categories:

a/ Amorphous (non-crystalline): Amorphous hydrogels lack a well-defined, ordered structure at the molecular level. Instead, their polymer chains are randomly arranged, resulting in a disordered and non-crystalline structure. This lack of crystallinity gives amorphous hydrogels their unique properties, such as high water-absorbing capacity and flexibility. They are often used in applications where high-water content and conformability are important.

b/ Semicrystalline: Semicrystalline hydrogels exhibit a more complex structure that combines both amorphous and crystalline phases. In these hydrogels, some parts of the polymer chains are arranged in an ordered, crystalline fashion, while other regions remain disordered and amorphous. This dual-phase structure can provide a balance of properties, including improved mechanical

strength, while retaining good water-absorbing capabilities. Semicrystalline hydrogels are commonly used in applications that require a combination of strength and flexibility.

c/ Crystalline: Crystalline hydrogels have a highly ordered and structured molecular arrangement throughout their polymer chains. This results in a well-defined crystalline structure with repeating patterns. Crystalline hydrogels are relatively rare and are often used in specialized applications where precise control over properties is essential, such as in certain types of biomaterials or advanced drug delivery systems.

I.2.5. Classification based on physical appearance

This classification categorizes hydrogels into different forms, such as matrix, film, or microsphere. The appearance of hydrogels in these various forms is determined by the specific polymerization techniques used during the preparation process.

a/ Matrix Hydrogels: Matrix hydrogels are typically three-dimensional, bulk structures. They form a continuous network throughout their volume, resembling a gel-like matrix. These hydrogels are commonly used in applications where a three-dimensional structure is needed. The polymerization process for matrix hydrogels involves cross-linking polymer chains in a way that creates a cohesive, gel-like structure.

b/ Film Hydrogels: Film hydrogels are thin, flat sheets or films of hydrogel material. The polymerization process for film hydrogels involves spreading the hydrogel precursor solution into a thin, even layer and allowing it to solidify or cross-link.

c/ Microsphere Hydrogels: Microsphere hydrogels consist of tiny, spherical particles of hydrogel material. These microspheres can vary in size and are used in drug delivery systems, where they can encapsulate and release drugs over time. The polymerization process for microsphere hydrogels involves forming small droplets of the hydrogel precursor solution, which are then solidified into microspheres.

I.2.6. Classification based on network electrical charge

The presence or absence of electrical charge in hydrogels significantly influences their properties and functions. Hydrogels might be divided into four distinct groups, depending on whether or not electrical charges are present on the crosslinked polymer chains:

a/ Nonionic Hydrogels: Nonionic hydrogels are composed of polymer chains that do not contain charged groups. These hydrogels lack electrical charges and are often used in applications where minimal interaction with ions or biomolecules is required.

b/ Anionic Hydrogels: Anionic hydrogels have polymer chains with negatively charged groups, such as carboxylate or sulfate groups. These charged groups can interact with positively charged ions or molecules.

c/ Cationic Hydrogels: Cationic hydrogels contain polymer chains with positively charged groups, such as amino groups. These charged groups can interact with negatively charged species.

d/ Ampholytic Hydrogels: Ampholytic hydrogels possess a mixture of both positively and negatively charged groups on their polymer chains. This balanced charge distribution allows them to interact with a wide range of ions and biomolecules.

II.3. Hydrogels applications

Since their initial discovery by Wichterle and Lim in 1954 [86], The use of hydrogels was limited because their modest properties did not allow them to be introduced into multiple fields. Over the years, they have garnered significant attention, resulting in an extensive body of patents, research papers, and scientific investigations dedicated to synthetic hydrogels. This research effort has been focused on their preparation, thorough characterization, and diverse applications [87]. Consequently, this concerted effort has led to the development of hydrogels properties and made them applicable in a wide range of applications across various fields due to their unique properties, including high water absorption capacity, biocompatibility, biodegradability, non-toxicity, and tunable mechanical properties. Some of the major applications of hydrogels include:

a/ Biomedical and Healthcare [88]

- Wound Dressings [89]: Hydrogels are used as wound dressings due to their ability to maintain a moist wound environment, promote healing, and provide comfort to patients.
- Contact Lenses [90]: Soft contact lenses are often made from hydrogel materials, as they are comfortable to wear and allow oxygen to pass through to the eye.
- Drug Delivery: Hydrogels can be used as drug delivery systems, providing a controlled release of medications over time [91]. They are especially useful for delivering sensitive drugs or treating localized conditions.

- Tissue Engineering [92]: Hydrogels are used as scaffolds for growing artificial tissues and organs. They provide a three-dimensional environment that supports cell growth and differentiation [93].

b/ Pharmaceuticals [94]

- Topical and Transdermal Formulations: Hydrogels are used in topical medications, creams, and transdermal patches for drug delivery through the skin.
- Oral Drug Delivery: Some hydrogel-based formulations are used to improve the solubility and bioavailability of poorly water-soluble drugs.

c/ Agriculture [95, 96]

- Soil Conditioning: Super absorbent hydrogels are employed to enhance soil water retention and improve crop growth, particularly in arid and semi-arid regions.

d/ Environmental Applications: Hydrogels can remove pollutants, heavy metals, and contaminants from water in wastewater treatment and purification processes [97].

e/ Consumer Products

- Hygiene Products [98]: Hydrogels are a key component of disposable diapers and adult incontinence products, as they can absorb and retain large amounts of liquid.

e/ Food Industry [99]: Hydrogels can also be used as food packaging materials to prolong the shelf life of perishable goods.

f/ Electronics and Sensors [100, 101]

- Hydrogel-Based Sensors: Hydrogels can be incorporated into sensors to detect changes in environmental conditions, such as pH, humidity, or specific ions.

II.4. Hydrogel preparation

The preparation of hydrogels involves a series of steps to create a three-dimensional network of polymer chains that can absorb and retain water or aqueous meadia. The specific method of preparation may vary depending on the type of hydrogel (e.g., natural or synthetic) and its intended use.

Hydrogels can generally be formulated using either synthetic polymers or natural polymers. Synthetic polymers, by their nature, exhibit hydrophobic tendencies and offer greater chemical resilience in comparison to natural polymers. This heightened mechanical strength leads to a decelerated degradation rate, although it also contributes to their prolonged durability. Achieving a harmonious equilibrium between these contrasting properties is crucial, as indicated by optimal design considerations [102]. Furthermore, this methodology can be extended to create hydrogels from natural polymers provided that these polymers possess suitable functional groups or have been modified with radically polymerizable groups [103]. The basic employed steps in hydrogel preparation are detailed as follow:

1/ Monomer Selection: In the case of synthetic hydrogels, the monomers that will form the polymer chains need to be selected. In general, Hydrogels are known by their hydrophilicity and are typically synthesized using hydrophilic monomers. However, in certain instances, hydrophobic monomers have been selected to enhance the characteristics of hydrogels for various applications.

2/ Selection of Polymer: The first step is to choose the appropriate polymer or combination of polymers based on the desired properties and application of the hydrogel. Natural polymers like alginate, collagen, or synthetic polymers like polyacrylamide, polyacrylate, or polyethylene glycol (PEG) are commonly selected.

3/ Cross-Linking Agent: Various cross-linking methods are employed in the preparation of hydrogels, including chemical cross-linking and physical cross-linking. Chemical cross-linking relies on primary forces to create the crosslinks, while physical cross-linking relies on secondary effects like hydrogen bonding and ionic interactions temperature, pH, or radiation [104, 105].

4/ Cross-Linking Process: The cross-linking process can occur during polymerization, either in situ or through post-polymerization methods. For chemically cross-linked hydrogels, cross-linking agents are typically added during the polymerization process, while physically cross-linked hydrogels may form through cooling, pH adjustment, or other external triggers.

5/ Polymerization: The polymerization process is initiated by adding initiators, catalysts, or other chemicals as needed. This step results in the formation of polymer chains and the creation of the hydrogel network.

6/ Solvent or Water Addition: Water or an aqueous solution is added to the polymer or monomer mixture to control the temperature of polymerization and to induce swelling and create the hydrogel's three-dimensional structure. The hydrogel absorbs and retains water due to its hydrophilic nature.

7/ Washing and Purification: The hydrogel is often washed or purified to remove any unreacted monomers, initiators, or impurities that could affect its properties or biocompatibility.

II.5. Hydrogels preparation techniques

It should be worth mentioning that there are several polymerization techniques that can be used to create the three-dimensional network of polymer chains. These techniques vary depending on the type of hydrogel and its intended application which provide excellent mechanical strength and stable hydrogels [106]. The commonly used techniques are explained below:

II.5.1. Free Radical Polymerization

In this technique, the cross-linking rate can be adjusted or altered by various variables, including temperature, crosslinker type, concentration, and the choice of initiator and catalyst. This method is applicable for producing both degradable and non-degradable polymers and is particularly well-suited for generating substantial cross-linking, a critical feature for biomedical applications. Typically, acrylate and acrylic acid monomers are synthesized using this technique [107].

II.5.2. Ionic Cross-Linking

Ionic cross-linking relies on the interaction between oppositely charged ions to form ionic bonds that link polymer chains. Common ionic cross-linking agents include multivalent metal ions like calcium or zinc, which can bind with negatively charged groups on polymers.

II.5.3. Bulk polymerization

Bulk hydrogels can be generated utilizing single or multiple monomer types. The extensive range of available monomers offers the flexibility to tailor hydrogel physical properties to meet specific application requirements. Typically, a minor quantity of cross-linking agent is incorporated into hydrogel formulations. Polymerization reactions are commonly initiated through radiation, ultraviolet light, or chemical catalysts.

Bulk polymerization considered as the most straightforward method, relies solely on the monomer and initiators that can dissolve in the monomer. This approach results in a rapid and extensive polymerization due to the elevated monomer concentration. However, as the reaction progresses, the viscosity of the mixture significantly rises, leading to the generation of heat during polymerization. To overcome these issues, the reaction should be operated at lower conversion rates [108].

Bulk polymerization of monomers, aimed at creating a uniform hydrogel, results in the formation of a rigid, transparent polymer matrix with a glassy texture. When this matrix is submerged in water, it undergoes a swelling process, transitioning into a soft and pliable material. The polymerized hydrogel can be crafted into a diverse array of configurations, including films and membranes, rods, particles, and emulsions.

II.5.4. Thermal Polymerization

Thermal polymerization utilizes heat as an initiator to drive polymerization reactions. It is a common method for creating hydrogels, especially those used in drug delivery applications.

II.5.5. Electro-Polymerization

Electro-polymerization involves the application of an electric current to induce the formation of polymer chains on an electrode surface. It is often used to create thin hydrogel coatings or films.

II.5.6. Grafting to a support

Typically, hydrogels synthesized through bulk polymerization exhibit a relatively weak structure. To enhance the mechanical characteristics of a hydrogel, it can be attached to or grafted onto the surface of a more robust support material. This polymerization technique is used to attach or graft polymer chains onto a pre-existing support or substrate. This method involves chemically bonding monomers or polymer chains to the surface of a solid support material, such as a particle, membrane, or surface, to modify its properties or impart new functionalities. Numerous polymeric substrates have been employed in grafting techniques for hydrogel synthesis [109].

Grafting to a support is a commonly used technique in materials science, surface modification, and various industrial applications. It allows for the customization of surfaces to achieve desired properties, such as improved adhesion, enhanced functionality, or controlled

release of substances, making it valuable in fields like biomaterials, catalysis, and advanced coatings.

II.5.7. Polymerization by irradiation

This technique refers to the process of initiating and driving polymerization reactions using radiation as a stimulus. In this technique, high-energy radiation sources, such as ultraviolet (UV) light, gamma rays [110], or electron beams [111], are utilized to initiate chemical reactions that lead to the formation of polymer chains and the formation of a polymer matrix.

Irradiating an aqueous polymer solution generates radicals along the polymer chains. Additionally, the radiolysis of water molecules produces hydroxyl radicals, which also interact with the polymer chains, leading to the creation of macro-radicals. When these macro-radicals from different chains recombine, covalent bonds are formed, resulting in the ultimate development of a cross-linked structure. Examples of polymers that undergo cross-linking through radiation include poly(vinyl alcohol), poly(ethylene glycol), and poly(acrylic acid). One major advantage of using radiation as the initiation method, as opposed to chemical initiation, is the production of hydrogels that are relatively pure and free from initiators.

II.5.8. Self-assembly polymerization

Finally, this fascinating phenomenon in the formation of hydrogels, where certain molecules or polymers have the remarkable ability to spontaneously organize themselves into a hydrogel structure without the requirement of external initiators or cross-linking agents. This process relies on the inherent molecular interactions and properties of the components involved. Self-assembly in hydrogels is driven by molecular interactions, such as hydrogen bonding, van der Waals forces, hydrophobic interactions, and electrostatic forces. These interactions cause the individual molecules or polymer chains to organize themselves in a specific way.

II.6. Properties of hydrogel

Hydrogels are unique materials with a wide range of properties that make them valuable for various applications, The most interesting properties of hydrogels are discussed as follows:

1/High Water Content: Hydrogels are primarily composed of water (typically more than 90% water by weight), giving them the ability to absorb and retain large quantities of water or aqueous solutions.

2/ Biocompatibility: Hydrogels are often biocompatible materials, which means that they are well-tolerated by biological systems.

3/ Soft and Flexible: Hydrogels are soft and flexible, which allows them to conform to irregular shapes and provides comfort when they come into contact with biological tissues.

4/ Tunable Mechanical Properties: The mechanical properties of hydrogels, such as elasticity and stiffness, can be adjusted to match specific requirements by varying the polymer composition, cross-linking density, or other factors.

5/ Environmental Responsiveness: Some hydrogels exhibit changes in properties (e.g., swelling or mechanical behavior) in response to environmental factors like pH, temperature, or ion concentration.

6/ Biodegradability: Depending on their composition, hydrogels can be designed to be biodegradable, meaning they can break down into non-toxic byproducts over time.

7/ Non-Toxicity: Hydrogels are generally non-toxic and do not elicit adverse immune responses when properly designed and used.

8/ Ease of Fabrication: Hydrogels can be synthesized through various methods, including polymerization, cross-linking, and self-assembly, allowing for versatile fabrication processes.

9/ Tensile strength and elasticity: Tensile strength and elasticity are important mechanical properties of hydrogels. These properties are essential for understanding the material's behavior and suitability for various applications, and they are influenced by the concentration of the crosslinking agent. Therefore, optimizing the crosslinking degree is necessary for the synthesis of hydrogels with appropriate mechanical strength and elasticity [112].

- Tensile strength is the maximum stress a material can withstand while being stretched or pulled before it fails or breaks, it is typically measured in units of pressure, such as Pascals (Pa). Hydrogels generally have low tensile strength compared to many other materials. Their structure is composed of water-swollen polymer chains, which makes them inherently weak in terms of resisting stretching or pulling forces. The tensile strength of hydrogels is mostly affected by the crosslinking density. Higher crosslinking density often results in increased tensile strength.

- Elasticity refers to a material's ability to deform when subjected to a force and return to its original shape when the force is removed, it is often described by the material's Young's Modulus, which quantifies its stiffness or how much it resists deformation under load. Hydrogels are known for their high elasticity, which is a result of the polymer network's ability to face reversible deformation as water is taken up or released. When a force is applied, hydrogels can deform but will return to their original shape when the force is removed. The elasticity of hydrogels depends on factors like the polymer's chain length, crosslinking density, and the degree of swelling. More highly crosslinked hydrogels tend to be stiffer and less elastic, while less crosslinked hydrogels are more elastic.

10/ Rheological properties: Rheological properties refer to the flow and deformation behavior of materials in response to applied forces or stresses. Rheological characterization is essential for understanding how hydrogels respond to mechanical forces, which is crucial in various applications. There exist several rheological properties, including but not limited to:

- Viscosity: Viscosity measures a fluid's resistance to flow. In the case of hydrogels, it determines how easily the gel flows when subjected to shear forces.
- Thixotropy: Thixotropy describes the property of a material to become less viscous when subjected to shear stress and return to its higher-viscosity state when at rest. Thixotropic hydrogels are useful in applications where controlled flow is required.
- Creep and Stress Relaxation: Creep measures how a material deforms over time under a constant applied stress. While Stress relaxation measures how the stress in a material decreases over time under constant strain.

11/ Swelling Behavior: Hydrogels swell when in contact with water or aqueous fluids. The swelling ratio of hydrogels is influenced by various factors, with porosity being a key parameter. Hydrogels fall into four categories based on porosity: non-porous, micro-porous, macro-porous, and super-porous. Non-porous hydrogels have closely packed polymer chains, leading to slower swelling and limited absorption [113, 114].

In contrast, porous hydrogels, especially macro-porous and super-porous ones with larger pores, promote cell growth, vascularization, and nutrient diffusion. These porous hydrogels facilitate faster swelling and improved absorption compared to non-porous hydrogels. Super-

porous hydrogels, with capillary-like interconnected pores, exhibit rapid water diffusion, making them exceptionally efficient in swelling and water absorption compared to other absorption mechanisms [115].

II.7. swelling ratio estimation

The following equation defines the swelling ratio (Rs) in hydrogels

$$R_s = \frac{W_s - W_d}{W_d} \times 100 \qquad (II.1)$$

Where W_s is the weight of the hydrogel after immersing in water (swelling form), and W_d is the weight of the hydrogel at its dry form [116]. The measurement of the swelling characteristics of hydrogels is very important. To do this, the hydrogel is immersed in water at room temperature, and the alterations in its mass are tracked over various time intervals. The water retention Wr can be calculate by the following equation:

$$W_r = \frac{W_t - W_d}{W_s} \times 100 \qquad (II.2)$$

Where Wt represents the overall mass of the hydrogels, measured at specific time intervals, while Ws and Wd correspond to the weight of the hydrogels when they are in their swollen and dried states, respectively.

The degree of swelling in hydrogels is a complex interplay of factors related to the nature of the solvent, the structure of the polymer network, and the interactions between the polymer and the solvent. Understanding and controlling these factors is essential for tailoring hydrogel properties to specific applications [117, 118].

1/ Solvent Nature: The type of solvent in which the hydrogel is placed plays a significant role in its swelling behavior. Some solvents are more compatible with the hydrogel's polymer structure and promote greater swelling, while others may cause minimal swelling or even shrinkage.

2/ Network Density: The density of the polymer network within the hydrogel is another critical factor. A more densely cross-linked network tends to limit the ability of the hydrogel to swell because there are fewer spaces available for solvent molecules to penetrate and interact with the polymer chains.

Interaction of Polymer-Solvent Parameters: The interactions between the polymer and the solvent also influence swelling. Parameters such as the polymer-solvent compatibility, chemical composition of the polymer, and the presence of functional groups on the polymer chains can affect the affinity between the polymer and the solvent. Some polymers may exhibit a strong attraction to the solvent, leading to increased swelling, while others may repel the solvent and resist swelling.

Summary

hydrogels are versatile materials with a remarkable capacity to swell and retain water and respond to environmental conditions. The facile preparation of hydrogels and their unique properties allow them to be used in a wide array of applications, including drug delivery, tissue engineering, wound care, and environmental sensing. Ongoing research and innovations continue to expand the boundaries of what hydrogels can achieve, promising even more exciting developments in the future.

References

1. Burkert, S., et al., *Cross-linking of poly (N-vinyl pyrrolidone) films by electron beam irradiation.* Radiation Physics and Chemistry, 2007. **76**(8-9): p. 1324-1328.
2. Zhao, W., et al., *Degradable natural polymer hydrogels for articular cartilage tissue engineering.* Journal of Chemical Technology & Biotechnology, 2013. **88**(3): p. 327-339.
3. Sennakesavan, G., et al., *Acrylic acid/acrylamide based hydrogels and its properties-A review.* Polymer Degradation and Stability, 2020. **180**: p. 109308.
4. Peppas, N.A., et al., *Hydrogels in pharmaceutical formulations.* European journal of pharmaceutics and biopharmaceutics, 2000. **50**(1): p. 27-46.
5. Davis, K.A. and K.S. Anseth, *Controlled release from crosslinked degradable networks.* Critical Reviews™ in Therapeutic Drug Carrier Systems, 2002. **19**(4-5).
6. Lin, C.-C. and A.T. Metters, *Hydrogels in controlled release formulations: network design and mathematical modeling.* Advanced drug delivery reviews, 2006. **58**(12-13): p. 1379-1408.
7. Iizawa, T., et al., *Synthesis of porous poly (N-isopropylacrylamide) gel beads by sedimentation polymerization and their morphology.* Journal of applied polymer science, 2007. **104**(2): p. 842-850.
8. Yang, L., J.S. Chu, and J.A. Fix, *Colon-specific drug delivery: new approaches and in vitro/in vivo evaluation.* International journal of pharmaceutics, 2002. **235**(1-2): p. 1-15.
9. Ahmed, E.M., *Hydrogel: Preparation, characterization, and applications: A review.* Journal of advanced research, 2015. **6**(2): p. 105-121.
10. Wichterle, O. and D. Lim, *Hydrophilic gels for biological use.* Nature, 1960. **185**(4706): p. 117-118.
11. Abdullah, J.A.A., et al., *Biopolymer-Based Films Reinforced with FexOy-Nanoparticles.* Polymers, 2022. **14**(21): p. 4487.
12. Tavakoli, J. and Y. Tang, *Hydrogel based sensors for biomedical applications: An updated review.* Polymers, 2017. **9**(8): p. 364.
13. Tavakoli, S. and A.S. Klar, *Advanced hydrogels as wound dressings.* Biomolecules, 2020. **10**(8): p. 1169.
14. Kopecek, J., *Hydrogels: From soft contact lenses and implants to self-assembled nanomaterials.* Journal of Polymer Science Part A: Polymer Chemistry, 2009. **47**(22): p. 5929-5946.
15. Sun, Y., et al., *Recent advances of injectable hydrogels for drug delivery and tissue engineering applications.* Polymer Testing, 2020. **81**: p. 106283.
16. Jeong, K.-H., D. Park, and Y.-C. Lee, *Polymer-based hydrogel scaffolds for skin tissue engineering applications: a mini-review.* Journal of Polymer Research, 2017. **24**(7): p. 112.
17. Ahmadi, F., et al., *Chitosan based hydrogels: characteristics and pharmaceutical applications.* Research in pharmaceutical sciences, 2015. **10**(1): p. 1.
18. Parhi, R., *Cross-linked hydrogel for pharmaceutical applications: A review.* Advanced pharmaceutical bulletin, 2017. **7**(4): p. 515-530.
19. Ramli, R.A., *Slow release fertilizer hydrogels: a review.* Polymer Chemistry, 2019. **10**(45): p. 6073-6090.
20. Azeem, M.K., et al., *Eco-friendly three-dimensional hydrogels for sustainable agricultural applications: Current and future scenarios.* Polymers for Advanced Technologies, 2023. **34**(9): p. 3046-3062.

21. Zhang, Z., et al., *Hydrogel materials for sustainable water resources harvesting & treatment: Synthesis, mechanism and applications.* Chemical Engineering Journal, 2022. **439**: p. 135756.
22. Bachra, Y., et al., *Synthesis, characterization, and swelling properties of a new highly absorbent hydrogel based on carboxymethyl guar gum reinforced with bentonite and Silica particles for disposable hygiene products.* ACS omega, 2022. **7**(43): p. 39002-39018.
23. Shewan, H.M. and J.R. Stokes, *Review of techniques to manufacture micro-hydrogel particles for the food industry and their applications.* Journal of Food Engineering, 2013. **119**(4): p. 781-792.
24. Zhang, J., et al., *Flexible and wearable strain sensors based on conductive hydrogels.* Journal of Polymer Science, 2022. **60**(18): p. 2663-2678.
25. Guo, X., et al., *Application of conductive polymer hydrogels in flexible electronics.* Journal of Polymer Science, 2022. **60**(18): p. 2635-2662.
26. Tabata, Y., *Biomaterial technology for tissue engineering applications.* Journal of the Royal Society interface, 2009. **6**(suppl_3): p. S311-S324.
27. Shantha, K. and D. Harding, *Synthesis and evaluation of sucrose-containing polymeric hydrogels for oral drug delivery.* Journal of applied polymer science, 2002. **84**(14): p. 2597-2604.
28. Mane, S., S. Ponrathnam, and N. Chavan, *Effect of chemical cross-linking on properties of polymer microbeads: A review.* Can Chem Trans, 2015. **3**(4): p. 473-485.
29. Wang, H. and S.C. Heilshorn, *Adaptable hydrogel networks with reversible linkages for tissue engineering.* Advanced Materials, 2015. **27**(25): p. 3717-3736.
30. Kenawy, E.-R., et al., *Physically crosslinked poly (vinyl alcohol)-hydroxyethyl starch blend hydrogel membranes: Synthesis and characterization for biomedical applications.* Arabian Journal of Chemistry, 2014. **7**(3): p. 372-380.
31. de Santa Maria, L.C., et al., *Synthesis of crosslinked resin based on methacrylamide, styrene and divinylbenzene obtained from polymerization in aqueous suspension.* European polymer journal, 2003. **39**(2): p. 291-296.
32. Kiatkamjornwong, S., *Superabsorbent polymers and superabsorbent polymer composites.* ScienceAsia, 2007. **33**(1): p. 39-43.
33. Qunyi, T. and Z. Ganwei, *Rapid synthesis of a superabsorbent from a saponified starch and acrylonitrile/AMPS graft copolymers.* Carbohydrate polymers, 2005. **62**(1): p. 74-79.
34. Karadağ, E., D. Saraydın, and O. Güven, *Radiation induced superabsorbent hydrogels. Acrylamide/itaconic acid copolymers.* Macromolecular Materials and Engineering, 2001. **286**(1): p. 34-42.
35. Ajji, Z., et al., *Use of electron beam for the production of hydrogel dressings.* Radiation Physics and Chemistry, 2008. **77**(2): p. 200-202.
36. Ganji, F., F.S. Vasheghani, and F.E. Vasheghani, *Theoretical description of hydrogel swelling: a review.* 2010.
37. Lowman, A.M., *Smart pharmaceuticals.* Journal, 2008.
38. Dorkoosh, F., et al., *Intestinal absorption of human insulin in pigs using delivery systems based on superporous hydrogel polymers.* International journal of pharmaceutics, 2002. **247**(1-2): p. 47-55.
39. Mutar, M.A. and R.K. Kmal, *Preparation of copolymer of acrylamide and acrylic acid and its application for slow release sodium nitrate fertilizer.* Al-Qadisiyah Journal of Pure Science, 2012. **17**(4): p. 71-83.

40. Mun, G., et al., *Superabsorbent hydrogels.* Biomedical applications of hydrogels handbook, 2010: p. 375-391.
41. Yang, T., *Mechanical and swelling properties of hydrogels*. 2012, KTH Royal Institute of Technology.
42. Pal, K. and I. Banerjee, *Polymeric gels: characterization, properties and biomedical applications*. 2018: Woodhead Publishing.

Chapter III

Nanocomposite Hydrogels, Synthesis, Properties, and Application

Chapter III. Nanocomposite Hydrogels, Synthesis, Properties, and Applications

Preface

Developing technology requires the creation of novel materials, which can often result from the combination of unique components. Hence, the incorporation of nanostructures into hydrogel networks gives rise to a novel category of diverse materials known as nanocomposite hydrogels (NCHs). In reality, both components, the nanoparticles (metals, nonmetals, metal oxides, and polymeric moieties), and the hydrogel matrix, possess distinct properties (detailed in chapter 1, and chapter 2), and their combination yields NCHs with novel properties that are not found in each of them separately. Hence, the different preparation approaches of NCHs, their properties, and applications are well detailed within this chapter.

III.1. What is nanocomposite hydrogel (NCH)?

A "nanocomposite hydrogel" refers to a hydrogel material that incorporates nanoparticles or nanomaterials within its structure. This integration of nanoscale components augments the properties and functionality of the hydrogel. On the other hand, it overcomes the limitations associated with the use of nanoparticles, as previously mentioned in the introduction section.

III.2. Synthesis of nanocomposite hydrogels (NCHs)

The invention of NCHs (nanocomposite hydrogels) took place after continuous studies aimed at synthesizing polymer/metal or metal oxide nanocomposites. For instance, Hamdi A. M. et al. reported the preparation of a Polyethylene glycol/magnesium oxide (PEG/MgO) nanocomposite [119]. Other works, such as polyvinylpyrrolidone/manganese oxide (PVP/Mn_3O_4), and poly(vinyl alcohol)/silver (PVA/Ag) nanocomposites were also published [120, 121].

In the synthesis of nanocomposite hydrogels, the networks of the hydrogel act as a template for the synthesis of smaller sized nanoparticles with fair stability [122]. The free spaces (the open areas or voids within the hydrogel's structure that are not occupied by the polymer matrix) are typically created as a result of the crosslinking of polymer chains in the hydrogel network, can serve as "nanoreactors" for the nucleation and growth of nanoparticles [123]. In other words, they provide a confined environment where the formation and enlargement of nanoparticles can occur.

This is advantageous because it allows for precise control over the size, distribution, and characteristics of the nanoparticles within the hydrogel.

The use of these free spaces as nanoreactors is a strategy often employed in nanocomposite hydrogel synthesis to incorporate nanoparticles into the hydrogel matrix in a controlled manner, thereby tailoring the properties and functionalities of the resulting material for specific applications.

Metal nanoparticles have been successfully integrated within hydrogels based natural polymer chains or modified natural polymer chain such as gelatin [124], starch [125], chitosan [126] and hydrogels based synthetic polymer chain like poly[N-isopropylacrylamide-co-(sodium acrylate)] [127], and poly(sodium acrylate) [128].When it comes to constructing nanocomposite hydrogels, various methods and approaches have been created. These methods differ significantly in how they arrange the nanoparticles within the hydrogel structure and in their ability to seamlessly integrate either organic or inorganic nanoparticles into the three-dimensional hydrogel network [129].

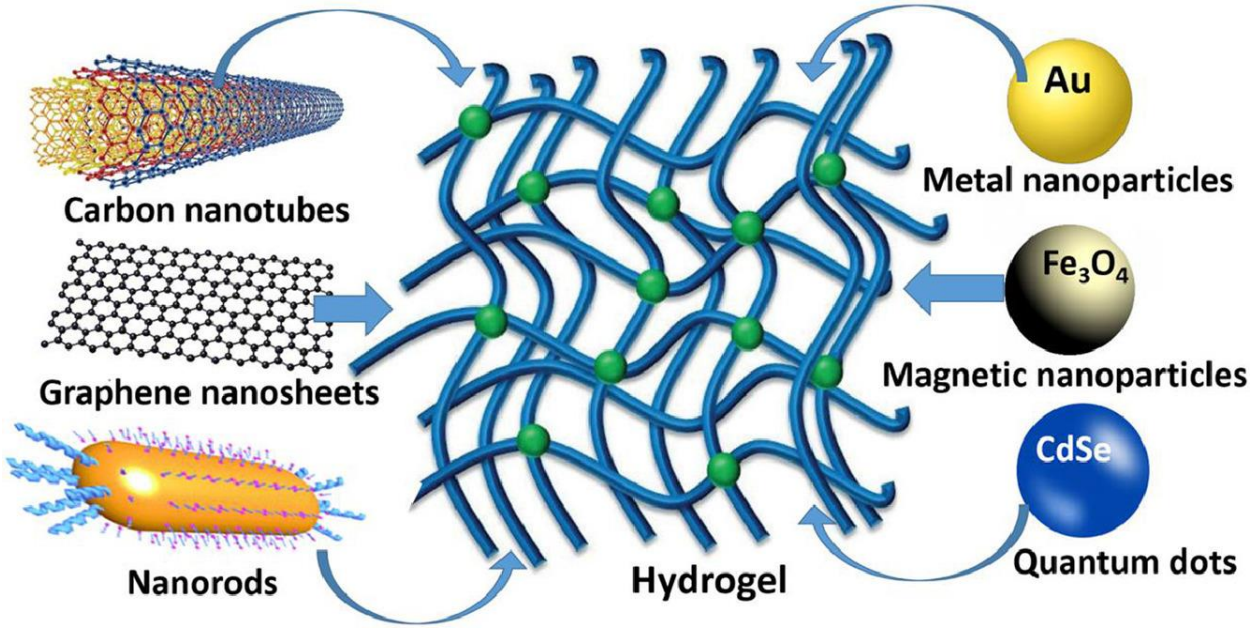

Fig.III.1 Different nano-species loaded hydrogels for preparing novel NCHs [4]

III.2.1. Methods used for the synthesis of NCHs

A wide array of nanocomposite hydrogels have been created, incorporating different types of nanoparticles into the structure of hydrogels. To achieve a uniform distribution of these nanoparticles, researchers have employed five primary approaches, each tailored to specific requirements and challenges.

III.2.1.1. Hydrogel crosslinking in nanoparticles suspension

One of the simplest and commonly used methods to create hybrid nanocomposite hydrogels involves mixing hydrogel precursors with colloidal nanoparticle suspensions before the hydrogel formation process begins. In this approach, the hydrogel precursors and the nanoparticles are combined, and they undergo a transformation together to form the final hydrogel structure. This method is favored because it tends to result in a relatively even distribution of nanoparticles within the hydrogel matrix, which is important for ensuring consistent properties and functionalities in the resulting nanocomposite material. One significant benefit of employing this method is its versatility in accommodating a diverse range of nanoparticles within the hydrogel matrix, due to the fact that the nanoparticles can be pre-formed before the hydrogel crosslinking process takes place.

This versatility empowers researchers to create intricate and advanced nanocarriers within the hydrogel framework, all while maintaining the integrity of the hydrogel formation process. It is important that the chemical reactions and conditions used for crosslinking the hydrogel do not have a significant adverse impact on the stability and essential characteristics of the nanoparticles. Conversely, the presence of the chosen nanomaterials should not hinder the crosslinking of the hydrogel matrix.

One other significant advantage of this approach is its adaptability for constructing nanocomposite hydrogels that contain living cells. This is achievable by using biocompatible materials and appropriate crosslinking conditions that will not harm the cells. In essence, it enables the development of hydrogels that not only incorporate nanoparticles but also support the growth and functionality of living cells when required, S. R. Sershen et al. [130] utilized this approach to prepare gold nanoparticle (Au-NP) hydrogel composites. Other research groups [131] have also embraced this straightforward method to produce hydrogels that incorporate gold (Au) or silicon (Si) nanoparticles (NPs).

III.2.1.2. Physical incorporation of nanoparticles into a hydrogel matrix after gelation

In this method, the nanoparticles are introduced into a pre-formed and already crosslinked hydrogel structure through physical means, where the hydrogel has already been solidified or gelled, and nanoparticles are added afterward. The nanoparticles do not chemically bond with the hydrogel but are distributed within its structure. This method is suitable when the primary goal is to introduce nanoparticles into the hydrogel without altering its crosslinked network.

The advantage of this approach is its simplicity and the ability to control the concentration and distribution of nanoparticles within the hydrogel post-gelation. It is often used when specific properties or functionalities offered by the nanoparticles are desired in the final nanocomposite hydrogel.

III.2.1.3. In situ generation of metallic nanoparticles in the hydrogel matrix

In this method, metal nanoparticles are formed directly within a hydrogel matrix. The hydrogel acts as a scaffold for the creation of these nanoparticles. Typically, the procedure begins with loading nanoparticle precursors into a swelling hydrogel, followed by exposure to a reducing agent. Sodium borohydride [132] and trisodium citrate [133] are often used as a reducing agents. Green reducing agents can be also used like mint leaf extract [134]. This process ultimately results in the development of metal nanoparticles within the hydrogel structure. This method was developed by Langer's group [135] and it is easy and facile in applied.

III.2.1.4. Nanoparticles as crosslinker for hydrogel formation

Also known in literature as “Co-Dependent Nanocomposite Hydrogels Leveraging Nanoparticles as Crosslinkers” [136], it is a technique In which nanoparticles are employed to facilitate the cross-linking or bonding of polymer chains to create hydrogels. This approach typically involves dispersing nanoparticles within a polymer precursor solution. These nanoparticles can serve as cross-linkers, helping to form a stable three-dimensional network as the polymer chains cross-link around them.

This method provides several advantages. First, it allows for the engineering of nanoparticles' surfaces with specific functional groups. These functional groups can enhance interactions with complementary molecules present in hydrogel precursors. This interaction leads to the creation of nanocomposite hydrogels through a cooperative assembly process. Furthermore,

the interactions between nanoparticles and the hydrogel are highly adaptable. Depending on the types of bonds formed (non-covalent, covalent, or dynamic covalent bonds), the resulting hybrid structure can be tailored for different applications. Additionally, adjusting the concentration of nanoparticles in these co-dependent nanocomposite hydrogels naturally affects the density of crosslinks within the hydrogel network. This, in turn, impacts the release profile of bioactive molecules encapsulated within the hydrogel or attached to the nanoparticles.

Nanoparticles can also have multiple binding sites on their surfaces, which is beneficial for enhancing the mechanical strength and responsiveness of nanocomposite hydrogel networks. These numerous binding sites enable multiple connections, contributing to the overall stability of the network. Additionally, they enhance the hydrogel's sensitivity to external stimuli due to the multitude of interconnected binding interactions.

This approach was employed to produce bacteriophage molecular networks by the spontaneous assembly of phage with Au-NPs. The resulting hydrogel network preserved the cell surface receptor binding and internalization attributes of the peptide [137]. Likewise, in a study by K. Zhang and his colleagues, they described a nanocomposite hydrogel based on hyaluronic acid and self-assembled bisphosphonate-magnesium (BP-Mg) nanoparticles [138].

III.2.1.5. Using nanoparticles, polymers, and distinct gelator molecules

This technique involves the combination of nanoparticles, polymers, and unique gelator molecules are combined to create a hydrogel with enhanced properties and functionalities. In this approach, nanoparticles are typically dispersed within a polymer matrix, and distinct gelator molecules are introduced to aid in the gelation process. These gelator molecules promote the formation of a stable hydrogel structure by encouraging the entanglement and crosslinking of polymer chains. This results in a nanocomposite hydrogel where the nanoparticles are uniformly distributed within the hydrogel matrix. Through this method, H. Wu et al [139]. documented the integration of a conductive polymer hydrogel into silicon-based anodes. This hydrogel is formed in situ through polymerization, creating an intricately interconnected three-dimensional framework composed of silicon nanoparticles that are uniformly coated with the conductive polymer.

In general, the method chosen for preparing nanocomposite hydrogels is influenced by several factors, including the type, size, and surface properties of the nanoparticles to be incorporated into the hydrogel play a crucial role in method selection. Different methods may be better suited for specific types of nanoparticles. Also, the intended properties of the nanocomposite hydrogel, such as mechanical strength, porosity, responsiveness to stimuli, and drug release kinetics, can influence the choice of method. The intended use of the nanocomposite hydrogel and the compatibility of the chosen method with the materials involved, including the hydrogel precursor, nanoparticles, and any additional components, should be taken in mind. The above demonstrated methods are represented in **Fig.III.2**.

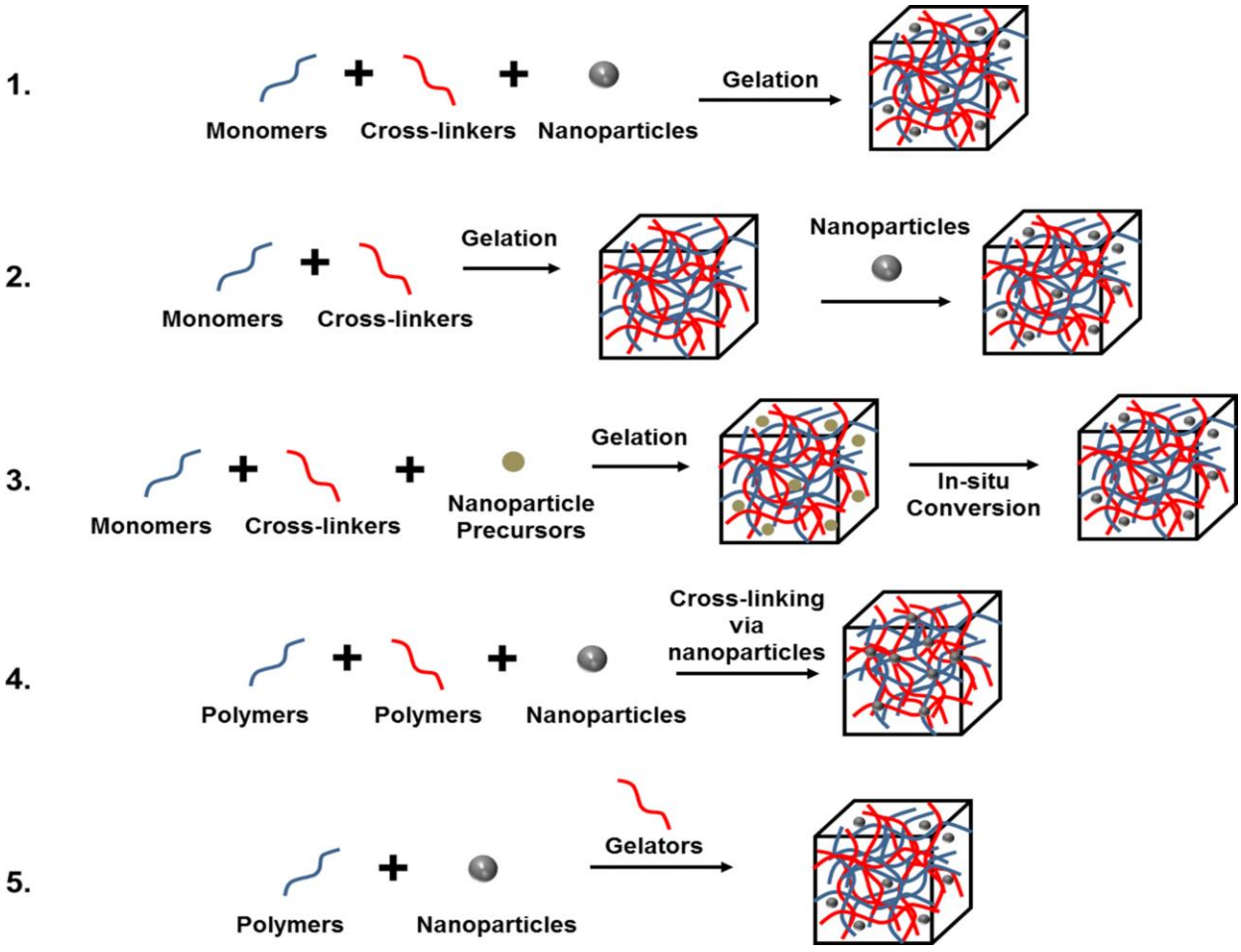

Fig.III.2 The major approaches employed in the synthesis of nanocomposite hydrogels: (1) Crosslinking hydrogel in a nanoparticle suspension (2) Physically incorporating nanoparticles into a hydrogel matrix after gelation, (3) In situ generation of metallic nanoparticles in the hydrogel matrix, (4) Nanoparticles as crosslinker for hydrogel formation, and (5) Using Nanoparticles, Polymers, and Distinct Gelator Molecules [129]

III.3. Properties of NCHs

III.3.1. swelling and deswelling

The exceptional porosity of nanocomposite hydrogels allows them to expand when exposed to water. This remarkable swelling capacity sets nanocomposite hydrogels apart from conventional hydrogels. Instead of dissolving, nanocomposite hydrogels absorb the surrounding solution during swelling. This property of swelling and deswelling yields favorable outcomes for controlled drug release in pharmaceutical applications. the swelling percentage (Ps), can be quantified as follows [140]:

$$P_S = \frac{W_S - W_d}{W_d} \times 100 \qquad \text{(III. 1)}$$

where W_s is the weight of the swelling NCH, and W_d is the weight of the dry NCH.

III.3.2. Improved Drug Delivery

Nanocomposite hydrogels can be designed to release drugs or bioactive molecules in a controlled and sustained manner, making them suitable for drug delivery systems. There are two methods for drug loading [140]:

In the first method, the monomer of the nanocomposite hydrogel is mixed with the drug and initiator without using a cross-linker. This mixture is then allowed to polymerize, trapping the drug within the matrix. In the second method, a nanocomposite hydrogel is immersed in a drug solution, causing it to swell.

III.3.3. Stimuli-Responsiveness

Nanocomposite hydrogels, composed of polymers, can undergo alterations in both shape and volume in response to various stimuli in their surroundings. These changes can be triggered by factors such as pH levels, light exposure, magnetic fields, or electric fields. However, because of the ease with which their characteristics can be adjusted, temperature-responsive nanocomposite hydrogels have garnered the most attention in research investigations.

III.3.4. Enhanced mechanical strength

The incorporation of nanoparticles can significantly enhance the mechanical properties of hydrogels, making them stronger. Mechanically robust nanocomposite hydrogels hold significant

promise for a wide range of applications, including biomedical engineering and electronic devices [141].

III.3.5 Tunable Porosity

The addition of nanoparticles allows for the control of hydrogel porosity, which can impact drug release rates, cell infiltration, and nutrient transport.

III.3.6. Electrical Conductivity

Certain types of nanoparticles can confer electrical conductivity to hydrogels, enabling their use in applications like biosensors and neural interfaces.

III.3.7. Tensile property

The tensile properties of nanocomposite hydrogels refer to their ability to withstand tensile or stretching forces. These properties are essential for understanding how the material behaves when subjected to tension. Tensile tests on nanocomposite hydrogels can measure parameters such as tensile strength (the maximum stress a material can endure before breaking), elongation at break (how much the material can stretch before breaking), and Young's modulus (a measure of stiffness). In general, nanocomposite hydrogels can be stretched more than 1000% from their original length [140].

III.4. Applications of nanocomposite hydrogels

Nano-Composite Hydrogels (NCHs) are a type of advanced material that brings together the best features of two other materials: hydrogels and nano-fillers. Hydrogels are known for being biocompatible (safe for the human body) and biodegradable, while nano-fillers have unique properties like strength, electrical conductivity, magnetism, and light interaction. By combining these two materials, NCHs gain exceptional abilities. They become materials with remarkable functions like enhanced strength, the ability to conduct electricity, respond to magnets, and interact with light, making NCHs useful in various fields

III.4.1. Biomedical applications

III.4.1.1. Drug delivery system

NCHs might serve as a suitable carrier to load and transport biomedical substances. The NCHs' physical properties, such as their ability to swell, the size of their mesh structure, and the quick diffuse of substances within them, could all influence how these biochemical factors are

released from the hydrogel matrix. Nanocomposite hydrogels have the capability to function as storage containers for drug molecules, and this interaction between the drug molecules and the nanofillers is significant. Alterations in external factors like magnetic fields, electric fields, temperature, and pH levels assist in the controlled release of drugs from the nanocomposite matrix [142]. Moreover, The incorporation of nanoparticles into NCHs reduces the burst release effect and provides stability of the drug as well as slower and continuous drug release [143].

III.4.1.2. Tissue Engineering

Because of their improved properties, nanocomposite hydrogels have been demonstrated to be excellent materials for scaffolding purposes (Kawaguchi et al., 2006; Sharma, 2017). Their enhanced characteristics, such as increased strength, greater stability, and enhanced biocompatibility, render them particularly effective for providing support and structure in fields like tissue engineering. In this context, scaffolds are necessary to facilitate the growth of cells and tissues. For instance, A. Sinha et al. reported the fabrication of hydroxyapatite-poly (vinyl alcohol) (HAp-PVA) nanocomposite hydrogels to fulfill the requirements of tissue engineering [144].

III.4.1.3. Wound dressing

Wound healing is a cellular and biochemical process which occurs in four different phases: inflammation, granulation tissue formation, matrix remodeling and re-epithelialization [145]. The process of wound healing is significantly influenced by the right amount of moisture in the wound area. This moisture creates an ideal biological environment that supports the intricate processes involved in wound healing. It enhances the metabolic activity of individual cells as well as the entire tissue, this cannot happen in dry tissues [146]. Nanocomposite hydrogels, which are typically employed as wound-dressing materials, are applied directly to wounds to stop bleeding, alleviate pain, and shield against infection. These wound-dressing materials, including foams, pastes, and films, possess exceptional characteristics like impressive swelling capacity, high tensile strength, and excellent biocompatibility [147], making them outstanding choices for wound care. Among different NCHs Poly(vinyl alcohol) and chitosan NCHs [148, 149] have excellent features that make them strong candidates for dressing applications.

III.4.1.4. Antibacterial activity

Nanocomposite hydrogels (NCHs) have garnered significant attention in the scientific community due to their outstanding antibacterial properties. The substantial research and

numerous publications dedicated to this topic serve as compelling evidence of their effectiveness in combating bacterial infections. For instance, M. Yadollahi et al synthesized carboxymethyl cellulose/ZnO nanocomposite hydrogels [150]. CMC/ZnO NCHs were tested against Escherichia coli and Staphylococcus aureus bacteria. In another study conducted by G. C. Porter et al. they have investigated the antibacterial effect of Ag NP/Alginate NCH against seven types of microorganisms using a static colony biofilm assay. The results from this study showed significant cell killing on biofilms of Gram positive and negative bacteria [151].

Overall, the extensive research underlines the importance of NCHs as a valuable tool in the fight against microbial threats and their role in enhancing the safety and efficacy of biomedical treatments.

III.4.2. Environmental applications of NCHs

III.4.2.1. Photocatalysis

Nanocomposite hydrogels have become the focus of increased interest, particularly in the context of wastewater treatment Li et al. in 2016. One of the key reasons for this attention is their ability to enhance photocatalytic activity, which is the process of using light to drive chemical reactions, and this enhancement is attributed to the presence of specific polar chemical groups within the polymeric matrix. These polar groups include hydroxyl, epoxide, ether, and carboxylate groups, which are chemically reactive and interact with light. When these polar groups are incorporated into the polymeric framework of the hydrogel, they create active sites that can participate in photocatalytic reactions.

Furthermore, the polymeric framework of the hydrogel acts as a stable and supportive platform for these catalytic centers. It not only enhances the stability and durability of the photocatalytic materials but also provides a structured environment for the chemical reactions to occur. This structured platform helps in achieving efficient solar energy conversion, where light energy is efficiently harnessed and converted into chemical reactions that can break down or oxidize contaminants in wastewater. As an example, for NCHs in photocatalysis, D. Pathania et al, used chitosan-g-poly(acrylamide)/ZnS (ChPA/ZS) nanocomposite hydrogel for the photocatalytic degradation of methyl orange and congo red dyes under simulated solar irradiation. In this study, after 2 hours of exposure to irradiation, 75% of Congo Red dye was decomposed, while 69% of

Methyl Orange was decomposed after 4 hours of simulated solar irradiation [152]. Similar works were performed using alginate/carboxymethyl cellulose (CMC)/TiO2-NPs [153], starch/poly(alginic acid-cl-acrylamide)/Fe/Zn NCH [154], etc., for degrading several pollutants.

III.4.2.2. Ion exchange

Ion exchange represents the simplest and most efficient approach for managing substantial quantities of wastewater containing hazardous metal ions [155]. Among different exchanger employed in this approach, nanocomposite hydrogel ion exchangers are specialized materials that combine the characteristics of nanocomposite hydrogels with ion exchange properties. These materials can selectively exchange ions with their surroundings, making them valuable in various applications, including water treatment, chemical separations, and industrial processes. The nanocomposite hydrogel component provides a three-dimensional, water-absorbing structure that can hold and release ions effectively. Meanwhile, the incorporation of nanomaterials or specific functional groups enhances the ion exchange capabilities of the hydrogel. This combination allows nanocomposite hydrogel ion exchangers to efficiently remove or replace ions from solutions.

These materials find use in scenarios such as softening hard water by removing calcium and magnesium ions, purifying drinking water by eliminating harmful contaminants like heavy metals, and facilitating chemical reactions by selectively binding and releasing ions to promote desired reactions. The pectin thorium tungstomolybdate, polyaniline zirconium selenotungstophosphate and polyacrylamide zirconium vanadophosphate are few of the polymeric nanocomposite ion exchange materials used for wastewater treatment [156-158].

III.4.2.3. Agriculture

Some nanocomposite hydrogels can be engineered to release growth-promoting substances like hormones or beneficial microorganisms, fostering healthier and more vigorous plant growth. In addition, nanocomposite hydrogels can be used to develop thin films that can be applied to fruits and vegetables. These films provide a protective barrier against physical damage, microbial contamination, and moisture loss, thus extending the shelf life of agricultural produce.

Due to their ability to absorb large amounts of water, hydrogels are used as soil conditioners. The incorporation of nanoparticles into hydrogel matrix may enhance their water absorption as Sayed et al., mentioned that after incorporating zinc oxide nanoparticles (nZnO) into

guar gum-pectin/polyacrylamide hydrogel composite (GG-PC/PAAm/ZnOx), the capacity of liquid absorption was increased, which could be due to the presence of nZnO [159]. Another research proved the benefits of NCHs in agriculture where chitosan-based hydrogel loaded with copper oxide nanoparticles (CuONPs) used for the treatment of lettuce seedlings. This treatment led to the suppression of disease caused by *Fusarium oxysporum f. sp. lactucae* [160].

Summary

Nanocomposite hydrogels are advanced materials that combine hydrogels (which are highly water-absorbent networks of polymers), with nanoparticles or nanomaterials. Compared to conventional hydrogels, nanocomposite hydrogels demonstrate enhanced properties, including high water retention, mechanical strength, and the ability to respond to external stimuli like temperature and pH. Nanocomposite hydrogels find applications in several fields such as drug delivery, tissue engineering, wound healing, and environmental remediation due to their versatility, biocompatibility, and customizable characteristics. They offer innovative solutions to various challenges in science, environment, medicine, and technology.

References

1. Mohammed Mohammed, H.A., et al., *A novel biosynthesis of MgO/PEG nanocomposite for organic pollutant removal from aqueous solutions under sunlight irradiation.* Environmental Science and Pollution Research, 2023. **30**(19): p. 57076-57085.
2. Salmi, C., et al., *Biosynthesis of Mn3O4/PVP nanocomposite for enhanced photocatalytic degradation of organic dyes under sunlight irradiation.* Journal of Cluster Science, 2023: p. 1-15.
3. Mbhele, Z., et al., *Fabrication and characterization of silver− polyvinyl alcohol nanocomposites.* Chemistry of Materials, 2003. **15**(26): p. 5019-5024.
4. Xu, S., et al., *From hybrid microgels to photonic crystals.* Advanced functional materials, 2003. **13**(6): p. 468-472.
5. Thomas, V., et al., *Review on polymer, hydrogel and microgel metal nanocomposites: A facile nanotechnological approach.* Journal of Macromolecular Science, Part A: Pure and Applied Chemistry, 2007. **45**(1): p. 107-119.
6. Kamal, T., et al., *Silver nanoparticles embedded in gelatin biopolymer hydrogel as catalyst for reductive degradation of pollutants.* Journal of Polymers and the Environment, 2020. **28**: p. 399-410.
7. Eid, M., *Gamma radiation synthesis and characterization of starch based polyelectrolyte hydrogels loaded silver nanoparticles.* Journal of Inorganic and Organometallic Polymers and Materials, 2011. **21**: p. 297-305.
8. Nguyen, N.T.-P., et al., *Stabilization of silver nanoparticles in chitosan and gelatin hydrogel and its applications.* Materials Letters, 2019. **248**: p. 241-245.
9. Mohan, Y.M., et al., *Fabrication of silver nanoparticles in hydrogel networks.* Macromolecular Rapid Communications, 2006. **27**(16): p. 1346-1354.
10. Loo, S.-L., et al., *Effect of synthesis routes on the properties and bactericidal activity of cryogels incorporated with silver nanoparticles.* RSC Advances, 2015. **5**(55): p. 44626-44635.
11. Thoniyot, P., et al., *Nanoparticle–hydrogel composites: Concept, design, and applications of these promising, multi-functional materials.* Advanced Science, 2015. **2**(1-2): p. 1400010.
12. Kaniewska, K., M. Karbarz, and E. Katz, *Nanocomposite hydrogel films and coatings–Features and applications.* Applied Materials Today, 2020. **20**: p. 100776.
13. Sershen, S., et al., *Independent optically addressable nanoparticle-polymer optomechanical composites.* Applied Physics Letters, 2002. **80**(24): p. 4609-4611.
14. Weissman, J.M., et al., *Thermally switchable periodicities and diffraction from mesoscopically ordered materials.* Science, 1996. **274**(5289): p. 959-963.
15. Mohan, Y.M., et al., *Controlling of silver nanoparticles structure by hydrogel networks.* Journal of Colloid and Interface Science, 2010. **342**(1): p. 73-82.
16. Saxena, S. and S. Bajpai, *Is a Cationic-Resin-Loaded Polymeric Gel a Better Antibacterial Material than a Nanosilver-Loaded Gel?* Designed Monomers and Polymers, 2010. **13**(2): p. 157-165.
17. Varaprasad, K., et al., *Development of microbial resistant Carbopol nanocomposite hydrogels via a green process.* Biomaterials science, 2014. **2**(2): p. 257-263.

18. Wang, C., N.T. Flynn, and R. Langer, *Controlled structure and properties of thermoresponsive nanoparticle–hydrogel composites.* Advanced Materials, 2004. **16**(13): p. 1074-1079.
19. Lavrador, P., et al., *Stimuli-responsive nanocomposite hydrogels for biomedical applications.* Advanced Functional Materials, 2021. **31**(8): p. 2005941.
20. Souza, G.R., et al., *Networks of gold nanoparticles and bacteriophage as biological sensors and cell-targeting agents.* Proceedings of the National Academy of Sciences, 2006. **103**(5): p. 1215-1220.
21. Zhang, K., et al., *Nanocomposite hydrogels stabilized by self-assembled multivalent bisphosphonate-magnesium nanoparticles mediate sustained release of magnesium ion and promote in-situ bone regeneration.* Acta biomaterialia, 2017. **64**: p. 389-400.
22. Wu, H., et al., *Stable Li-ion battery anodes by in-situ polymerization of conducting hydrogel to conformally coat silicon nanoparticles.* Nature communications, 2013. **4**(1): p. 1943.
23. Sharma, G., et al., *Applications of nanocomposite hydrogels for biomedical engineering and environmental protection.* Environmental chemistry letters, 2018. **16**: p. 113-146.
24. Haraguchi, K., K. Uyama, and H. Tanimoto, *Self-healing in nanocomposite hydrogels.* Macromolecular rapid communications, 2011. **32**(16): p. 1253-1258.
25. Zhang, J., Q. Wang, and A. Wang, *In situ generation of sodium alginate/hydroxyapatite nanocomposite beads as drug-controlled release matrices.* Acta Biomaterialia, 2010. **6**(2): p. 445-454.
26. Satarkar, N.S. and J.Z. Hilt, *Hydrogel nanocomposites as remote-controlled biomaterials.* Acta biomaterialia, 2008. **4**(1): p. 11-16.
27. Sinha, A., et al., *Poly (vinyl alcohol)–hydroxyapatite biomimetic scaffold for tissue regeneration.* Materials Science and Engineering: C, 2007. **27**(1): p. 70-74.
28. Baskovich, B., et al., *Wound dressing components degrade proteins detrimental to wound healing.* International wound journal, 2008. **5**(4): p. 543-551.
29. Hebeish, A. and S. Sharaf, *Novel nanocomposite hydrogel for wound dressing and other medical applications.* RSC advances, 2015. **5**(125): p. 103036-103046.
30. Varshney, L., *Role of natural polysaccharides in radiation formation of PVA–hydrogel wound dressing.* Nuclear Instruments and Methods in Physics Research Section B: Beam Interactions with Materials and Atoms, 2007. **255**(2): p. 343-349.
31. Chaturvedi, A., et al., *Evaluation of poly (vinyl alcohol) based cryogel–zinc oxide nanocomposites for possible applications as wound dressing materials.* Materials Science and Engineering: C, 2016. **65**: p. 408-418.
32. Mohandas, A., et al., *Chitosan based metallic nanocomposite scaffolds as antimicrobial wound dressings.* Bioactive materials, 2018. **3**(3): p. 267-277.
33. Yadollahi, M., et al., *Synthesis and characterization of antibacterial carboxymethyl cellulose/ZnO nanocomposite hydrogels.* International journal of biological macromolecules, 2015. **74**: p. 136-141.
34. Porter, G.C., et al., *AgNP/Alginate Nanocomposite hydrogel for antimicrobial and antibiofilm applications.* Carbohydrate Polymers, 2021. **251**: p. 117017.
35. Pathania, D., et al., *Photocatalytic degradation of highly toxic dyes using chitosan-g-poly (acrylamide)/ZnS in presence of solar irradiation.* Journal of Photochemistry and Photobiology A: Chemistry, 2016. **329**: p. 61-68.

36. Thomas, M., et al., *Effective photocatalytic degradation of Congo red dye using alginate/carboxymethyl cellulose/TiO2 nanocomposite hydrogel under direct sunlight irradiation.* Journal of Photochemistry and Photobiology A: Chemistry, 2016. **327**: p. 33-43.
37. Sharma, G., et al., *Fabrication and characterization of a nanocomposite hydrogel for combined photocatalytic degradation of a mixture of malachite green and fast green dye.* Nanotechnology for Environmental Engineering, 2017. **2**: p. 1-7.
38. Naushad, M., et al., *Efficient removal of toxic phosphate anions from aqueous environment using pectin based quaternary amino anion exchanger.* International Journal of Biological Macromolecules, 2018. **106**: p. 1-10.
39. Sharma, G., et al., *Fabrication, characterization and antimicrobial activity of polyaniline Th (IV) tungstomolybdophosphate nanocomposite material: efficient removal of toxic metal ions from water.* Chemical Engineering Journal, 2014. **251**: p. 413-421.
40. Sharma, G., et al., *Polyacrylamide@ Zr (IV) vanadophosphate nanocomposite: ion exchange properties, antibacterial activity, and photocatalytic behavior.* Journal of Industrial and Engineering Chemistry, 2016. **33**: p. 201-208.
41. Sharma, G., et al., *A multifunctional nanocomposite pectin thorium (IV) tungstomolybdate for heavy metal separation and photoremediation of malachite green.* Desalination and Water Treatment, 2016. **57**(41): p. 19443-19455.
42. Sayed, A., et al., *Radiation synthesis of green nanoarchitectonics of guar gum-pectin/polyacrylamide/zinc oxide superabsorbent hydrogel for sustainable agriculture.* Journal of Inorganic and Organometallic Polymers and Materials, 2022. **32**(12): p. 4589-4600.
43. Shang, H., et al., *Copper oxide nanoparticle-embedded hydrogels enhance nutrient supply and growth of lettuce (Lactuca sativa) infected with Fusarium oxysporum f. sp. lactucae.* Environmental science & technology, 2021. **55**(20): p. 13432-13442.

Chapter IV

Experimental Methodology and Testing Protocols

Chapter IV. Experimental Methodology and Testing Protocols

Preface

The methodologies and materials employed in the experimental work are detailed in this chapter, which includes detailed protocols for each synthetic method used, as well as details on the purity of all chemicals used. Furthermore, this chapter delves into the analytical techniques employed to characterize the synthesized samples, including scanning electron microscopy, energy dispersive X-ray spectroscopy, X-ray diffraction, Fourier transform infrared spectroscopy, and UV/Vis spectroscopy. Additionally, within this chapter, the photocatalytic degradation process of diver organic pollutants over the synthesized materials is outlined, along with an examination of their antimicrobial potential against three distinct human pathogenic bacteria.

IV.1. Materials and Methods

IV.1.1. Chemicals

Table IV. 1 Chemicals used in this study

Chemical	Manufacturer	Country
Silver nitrate ($AgNO_3$ 99.92%)	Biochem Chemophara	United Kingdom
Zinc nitrate hexahydrate ($Zn(NO_3)_2 \cdot 6H_2O$)	Biochem Chemophara	United Kingdom
Sodium borohydride ($NaBH_4$ 98%)	Biochem Chemophara	United Kingdom
o-toluidine blue ($C_{15}H_{16}ClN_3S$)	Biochem Chemophara	United Kingdom
4-bromophenol (C_6H_5BrO)	Biochem Chemophara	United Kingdom
Rose Bengal ($C_{20}H_2Cl_4I_4Na_2O_5$)	Biochem Chemophara	United Kingdom
Nutrient agar	Titan Biotech LTD	India
Mueller Hinton agar	Biokar diagnostics	France
AgroNanoGel Basic hydrogel	ARTAGRO POLSKA	Poland

IV.1.1.1 Potassium Polyacrylate hydrogel PPAH

For this study, AgroNanoGel Basic hydrogel, developed by ARTAGRO POLSKA, a dynamic and progressive company based in Poland, was utilized. ARTAGRO POLSKA is committed to the commercialization of research outcomes, technology innovation transfer, and the practical application of scientific advancements in the business domain. With a focus on bridging

the gap between scientific discoveries and market implementation, ARTAGRO POLSKA plays a crucial role in translating cutting-edge research into real-world applications.

Table IV. 2 Main properties of AgroNanoGel Basic Hydrogel

Properties	AgroNanoGel Basic Hydrogel
Absorbency	(450-600ml/g)
pH	neutral
Biodegradability	10 years
Toxicity	Non-toxic

IV.1.2. Synthesis of metal NPs loaded potassium polyacrylate hydrogel (PPAH)

This research is composed of two separate works. The first one aims to incorporate silver nanoparticles (Ag NPs) into PPAH networks, while the second focuses on integrating both silver nanoparticles (Ag NPs) and zinc oxide nanoparticles (ZnO NPs) into PPAH networks.

IV.1.2.1. Synthesis of Ag NPs loaded PPAH

The preparation of Ag NPs loaded potassium polyacrylate hydrogel (PPAH) involved a meticulous procedure to ensure the successful incorporation of silver nanoparticles. Each step was carefully executed to optimize the loading and reduction processes, leading to the formation of well-defined and stable Ag NPs within the PPAH matrix.

To initiate the process, a stock solution of silver nitrate was meticulously prepared, ensuring accurate concentration measurements. This solution served as the source of silver ions for loading into the hydrogel. The PPAH, which had been precisely weighed (50 mg), was immersed in beakers containing 30 ml of various concentrations (2, 5, 10, and 16 mM) of the silver nitrate solution and kept in it for 24 hours to allow the sufficient interaction between the hydrogel and silver ions. During this time, the silver ions diffused into the hydrogel structure, utilizing the available space within the hydrogel networks and forming chemical bonds with specific functional groups present in the hydrogel, such as hydroxylic (-OH), carboxylic (-COOH), imide (–CONH), amide (-$CONH_2$), and amine (–NH_2) groups [1, 2].

Following the loading of silver ions, the hydrogel was carefully removed from the silver nitrate solutions and moved to the reduction step. A stock solution of sodium borohydride was also meticulously prepared to achieve the desired concentrations. The Gels loaded with Ag^+ ions, were immersed in beakers containing 30 ml of different concentrations (4, 10, 20, and 32 mM) of the sodium borohydride solution for 24 hours. This reduction process facilitated the conversion of silver ions into silver nanoparticles within the hydrogel matrix. The successful reduction was indicated by the immediate dark brown coloration of the swollen hydrogel, signifying the formation of silver nanoparticles

To ensure the purity and stability of the synthesized PPAH/Ag NPs samples. A thorough washing step was performed several times with double distilled water. Afterward, the hydrogel was carefully dried in an oven at 60°C for 24 h to remove any remaining moisture, resulting in a stable and dry hydrogel matrix embedded with silver nanoparticles. The prepared samples with varying concentrations (2, 5, 10, and 16 mM) of $AgNO_3$ are denoted as PPAH/Ag1, PPAH/Ag2, PPAH/Ag3, and PPAH/Ag4, respectively, in the subsequent sections.

The final step involved the analysis of the prepared samples using multiple analytical characterization techniques. The PPAH/Agx NPs samples were subjected to various techniques such as spectroscopy, and elemental analysis to determine their structural, morphological, and chemical properties. This comprehensive analysis provided valuable insights into the size, distribution, and composition of the silver nanoparticles within the PPAH matrix.

IV.1.2.2. Synthesis of Ag@ZnO NPs loaded PPAH

The integration of Ag@ZnO NPs follows the similar approach as the integration of Ag NPs into PPAH. Briefly, in separate beakers, solution of silver nitrate and zinc nitrate hexahydrate was prepared (25 ml, 16 mM each) and subsequently mixed in a glass beaker. Dry PPAH was then accurately weighed (50 mg), immersed in a beaker containing 50 ml of the mixed solution, and kept in it for 24 hours, resulting in silver and zinc cations loaded gels. To reduce the silver and zinc cations into silver and zinc oxide nanoparticles, a solution of sodium borohydride (50 ml, 32 mM) was prepared. Thereafter, the Gels loaded with the metals' cations were removed from the mixture, placed in the sodium borohydride solution, and left for 24 hours. The formation of silver and zinc oxide nanoparticles within the PPAH, causing the swollen PPAH to transform from transparent to a dark brown color with a slight whiteness on the surface. Subsequently, the swollen PPAH loaded

with silver and zinc oxide nanoparticles was thoroughly washed with double distilled water, dried, and characterized. The resulting sample is referred to as PPAH/Ag@ZnO in the subsequent sections.

In summary, the preparation of metal and metal oxide NPs loaded potassium polyacrylate hydrogel involved a systematic procedure that ensured their successful incorporation. The optimized loading and reduction steps, coupled with thorough washing and comprehensive analytical characterization, resulted in well-defined and stable PPAH/Agx and PPAH/Ag@ZnO samples ready for further investigation and potential applications in various fields. The process used for the formation of these samples is well described in **(Fig. IV.1, and Fig. IV.2)**

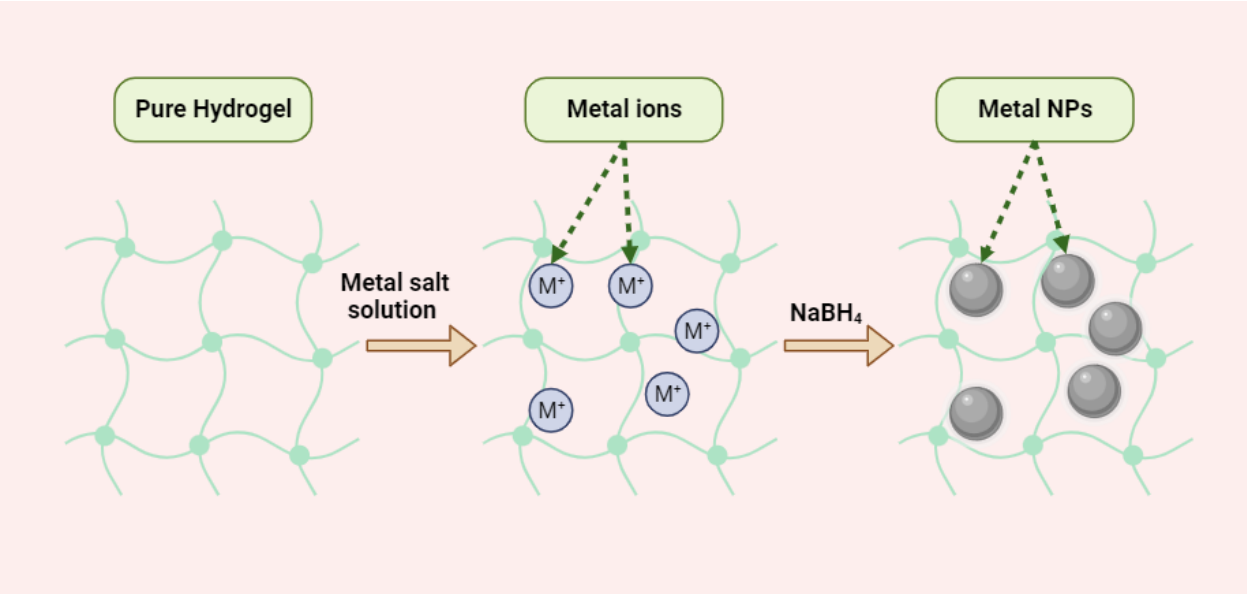

Fig. IV.1 Schematic representation for the metal nanoparticles integrations in the hydrogel network via the *in-situ* approach

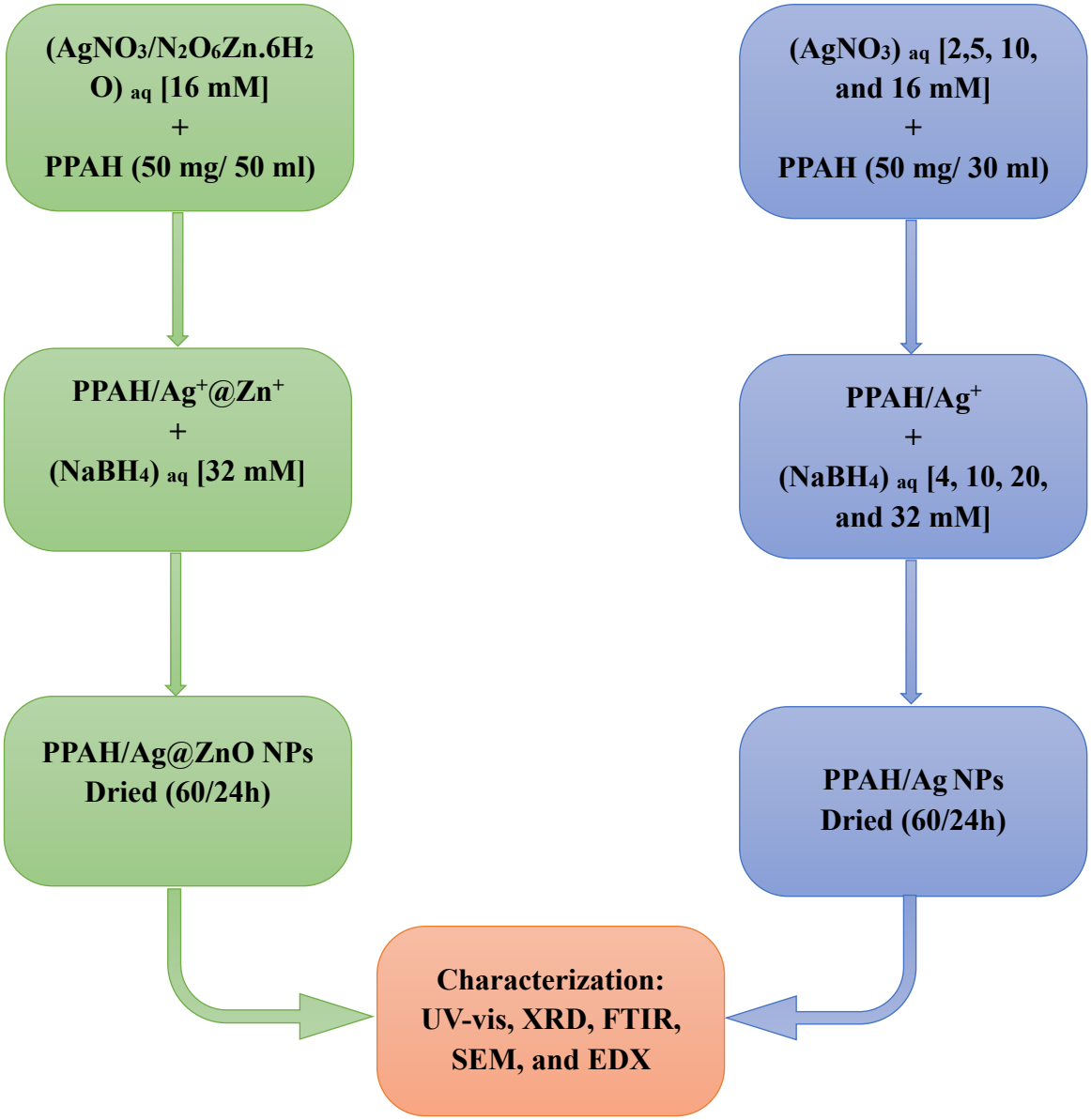

Fig. IV.2 Synthesis of Ag NPs and Ag@ZnO NPs loaded PPAH

IV.2. Characterization techniques

IV.2.1. Electron microscopy

IV.2.1.1. Scanning Electron Microscopy (SEM)

Scanning electron microscopy (SEM) is a rapid and precise technique used to investigate the surface morphology and microscopic features of materials, it enables the observation and analysis of the size, size distribution, and morphology of micro and nanoscale materials. This powerful technique provides a comprehensive and precise examination of the morphological and dimensional characteristics of the materials being studied.

An exceptional scanning electron microscope (SEM) can achieve a resolution finer than 1 nm. With this technique, it becomes possible to observe the intricate surface structures of a sample with exceptional precision, enabling the acquisition of highly accurate images that reveal the surface morphology and even topography of the material.

SEM technique is widely used in various scientific and industrial fields, including materials science, nanotechnology, biology, geology, and semiconductor analysis. It provides high-resolution images and valuable compositional information, making it an essential tool for understanding the microstructure and properties of diverse materials.

The basic operating principle of SEM is demonstrated bellow

a/ Sample Preparation: The specimen needs to be properly prepared before SEM analysis. It is typically dehydrated, dried, and coated with a thin conductive layer, such as gold or carbon. This coating helps prevent charging of the sample during imaging.

b/ Electron Beam Generation: In an SEM, a focused electron beam is generated using an electron source, usually a heated tungsten filament or a field emission gun (FEG). The beam is accelerated towards the sample using electromagnetic lenses.

c/ Interaction with the Sample: When the electron beam strikes the surface of the sample, several interactions occur. The primary interaction is known as elastic scattering or backscattering, where high-energy electrons bounce back, carrying information about the sample's composition. Additionally, secondary electrons, characteristic X-rays, and Auger electrons can also be emitted from the sample surface, providing additional information.

d/ Signal Detection: Different signals resulting from the electron-sample interactions are detected using various detectors. The two primary detectors used in SEM are the secondary electron (SE) detector and the backscattered electron (BSE) detector. The SE detector captures low-energy electrons emitted from the surface, providing information about topography and surface details. The BSE detector detects the high-energy backscattered electrons, which are sensitive to the sample's atomic number and density, allowing for compositional analysis.

e/ Image Formation: The detected signals are amplified and processed to generate an image [161]. SEM images are formed by scanning the electron beam across the sample surface in a raster pattern while continuously detecting the emitted signals. The intensity of the detected signals is used to create contrast and reveal surface features and compositional variations. In addition to imaging, SEM can be integrated with additional detectors and accessories to perform other analytical techniques. These include energy-dispersive X-ray spectroscopy (EDS) for elemental analysis, electron backscatter diffraction (EBSD) for crystallographic information, and focused ion beam (FIB) milling for sample preparation or cross-section imaging.

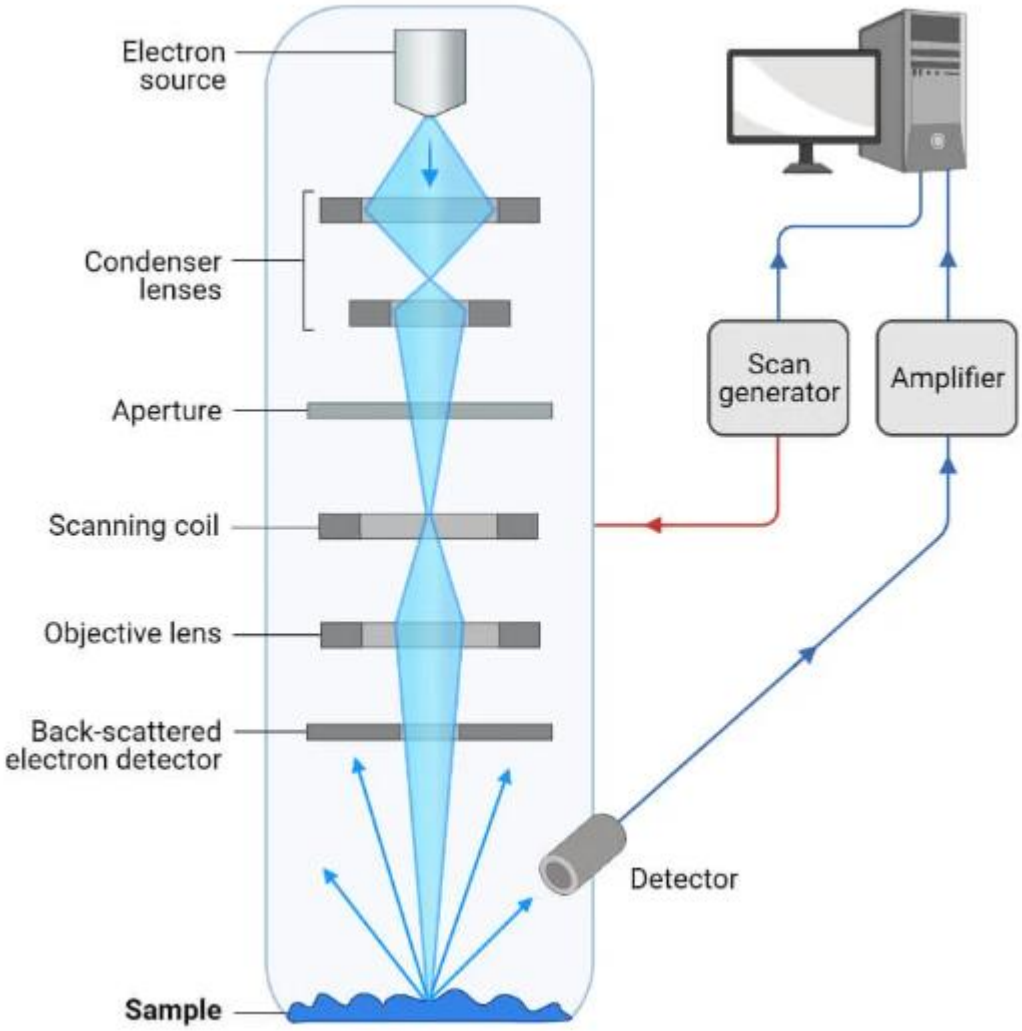

Fig. IV. 3 Schematic Diagram of Scanning Electron Microscope

IV.2.2. Optical properties

IV.2.2.1. UV-visible absorption spectroscopy

UV-visible absorption spectroscopy is a technique used to study the absorption of ultraviolet (UV) and visible light by molecules. It provides information about the electronic structure and transitions of molecules, which can be useful in various fields, including chemistry, biochemistry, and materials science.

The basic principle of UV-visible absorption spectroscopy involves passing a beam of UV or visible light through a sample and measuring the intensity of light that is absorbed by the sample at different wavelengths. The absorption of light occurs when a molecule absorbs energy from the

incident light and undergoes a transition from its ground state to an excited state. The energy absorbed corresponds to the energy difference between the two states, and this energy difference determines the wavelength or color of light that is absorbed. In more detail, when a substance is exposed to light, it absorbs a specific quantity of radiation while reflecting the rest. As the light traverses the sample, the absorption of radiation by the substance is determined by the disparity between the incident radiation (I_o) and the transmitted radiation (I). This absorption of radiation is referred to as absorbance (A), whereas transmittance (T) denotes the fraction (I/I_o), indicating the proportion of light that has successfully passed through the sample.

Transmittance, $T = I/ I_o$

Absorbance, $A = \log_{10}(I_o /I) = \log_{10} (1/T) = - \log_{10} (T)$

Beer-Lambert's law can be expressed by the following equation (Eq1) [162]:

$$A = \log_{10}\left(\frac{I_0}{I}\right) = \epsilon c l \qquad (IV.1)$$

Where:

A: is the absorbance of the solution.

ϵ: (epsilon) is the molar absorptivity or molar absorption coefficient, which is a constant specific to the solute and the wavelength of light being used.

c: is the concentration of the solute in moles per liter (M).

l: is the path length that the light travels through the solution in centimeters.

Beer-Lambert's Law is a principle in spectroscopy that describes the relationship between the absorbance of light by a solution and the concentration of the absorbing substance, as well as the path length of the light through the solution. According to this law, the absorbance is directly proportional to both the concentration of the absorbing species and the path length. In other words, as the concentration of the absorbing substance or the path length increases, the absorbance also increases. This law is widely used to quantitatively analyze the concentration of substances in solution based on their absorbance of light at specific wavelengths.

UV-visible absorption spectroscopy is typically performed using a spectrophotometer, which consists of a light source, a sample holder, a monochromator, and a detector. The light source emits a broad spectrum of UV or visible light, which is then passed through the sample cell containing the sample solution or solid. The monochromator selects a specific wavelength of light, and the detector measures the intensity of light that passes through the sample. By scanning the wavelength, a spectrum of absorption versus wavelength can be obtained.

The resulting absorption spectrum provides valuable information about the molecule's electronic structure, such as the presence of certain functional groups, the extent of conjugation, or the presence of specific chromophores. Each compound has a unique absorption spectrum, allowing for the identification and characterization of substances. Additionally, the intensity of absorption at a particular wavelength can provide quantitative information about the concentration of the absorbing species in a solution, allowing for quantitative analysis.

UV-visible absorption spectroscopy is widely used in many applications. In chemistry, it is used for the identification and quantification of compounds, the study of reaction kinetics, and the determination of molecular structure. In biochemistry, it is used for the analysis of biomolecules, such as proteins and nucleic acids. In materials science, it is used for the characterization of dyes, pigments, and semiconductor materials.

Overall, UV-visible absorption spectroscopy is a powerful and versatile technique that provides valuable insights into the electronic properties of molecules and is widely used in various scientific disciplines.

IV.2.2.2. Band gap energy theory

The band gap represents the distance between the valence band and the conduction band. Basically, is the lowest energy level needed for an electron to escape from its bound state. Once the energy level of the band gap is reached, the electron is excited into a free state and can engage in conduction.

The band gap of a semiconductor (eg: metal and metal nanoparticles) is the minimum energy needed to excite an electron that is stuck in its bound state into a free state, enabling its engagement in conduction. Semiconductors consist of two bands: The valence band (E_V) refers to the lower energy level, and the conduction band (E_C) represents the higher energy level at which

an electron is considered free. The gap energy between the valence band (E_V) and conduction band (E_C), is known as the band gap (E_G). When an electron excites to the conduction band, it leaves behind an empty space enable to create a hole in the valence band.

The optical band gap energy can be obtained from Tauc equation (Eq2):

$$(\alpha hv) = C(hv - E_g)^n \qquad (IV.2)$$

Where α is molar absorption coefficient, C is a constant, h is Planck's constant, v is the photon's frequency, E_g is the average band gap of the material and n is determined by the type of transition, n = ½, and n = 2 for direct allowed and indirect allowed transitions, respectively.

Therefore, the fundamental process of conducting a Tauc analysis involves obtaining optical absorbance measurements for the given sample across a spectrum of energies, encompassing both the energy range below and above the band gap transition. Creating a plot of $(\alpha\ h\ v)^{1/n}$ against $(h\ v)$ entails experimenting with two values for n, n = 1/2 and n = 2, in order to determine which value yields a more accurate fit. This comparison enables the identification of the appropriate type of transition.

IV.2.3. Chemical properties

IV.2.3.1. Fourier Transform Infrared (FTIR) spectroscopy

Fourier Transform Infrared (FTIR) spectroscopy is a powerful analytical technique used to investigate the interaction between molecules and infrared radiation. It provides information about the functional groups present in a sample and allows for the identification and characterization of various chemical compounds.

In FTIR spectroscopy, a beam of infrared light is passed through a sample, and the amount of light absorbed at different wavelengths is measured. The sample can be a solid, liquid, or gas, and it may be in the form of a pure substance or a mixture.

The key component of FTIR spectroscopy is the interferometer, which splits the infrared beam into two paths. One path passes through the sample, while the other serves as a reference. The two beams are then recombined, creating an interference pattern called an interferogram. The

interferogram contains information about the absorption of infrared light by the sample at different frequencies.

To obtain a spectrum from the interferogram, a mathematical technique called Fourier transformation is applied. This converts the interferogram from the time domain to the frequency domain, resulting in a spectrum that represents the intensity of absorption as a function of wavelength or wave number.

The absorption of radiation at specific wavelengths by covalent bonds in a molecule leads to a change in the vibrational energy within the bond. The nature of the vibration, whether it involves stretching or bending, is determined by the atoms involved in the bond. As different bonds and functional groups absorb distinct frequencies, the resulting transmittance pattern varies among different molecules. Transmittance, which is the opposite of absorbance, refers to the ability of radiation to pass through a substance. To visualize this, a graph is used where the wavenumber (expressed in cm^{-1}), representing the energy of the molecular bond vibration, is plotted on the X-axis, the wavenumber is defined as the reciprocal of wavelength and infrared radiation wavenumbers typically fall within the range of 4000 cm^{-1} to 400 cm^{-1}, while the transmittance is plotted on the Y-axis

The FTIR spectrum provides a fingerprint-like pattern for a given sample, allowing to identify functional groups and chemical bonds present in the sample. By comparing the obtained spectrum with reference spectra in databases, compounds can be identified or characterized. FTIR spectroscopy is widely used in various fields, including chemistry, pharmaceuticals, materials science, forensics, and environmental analysis.

IV.2.4. Structural and morphological properties

IV.2.4.1. X Ray diffractions (XRD)

X Ray diffractions is an analytical technique used to study different aspects of materials, including the phase composition, crystal structure, and orientation of powder, solid, and liquid samples. It provides valuable information about the types of substances present in a material, the arrangement of atoms within its crystal lattice, and the alignment of crystals in different types of samples, whether they are in powdered form, solid objects, or even liquid samples.

X-ray Diffraction is based on the principle that when X-rays interact with a crystalline sample, resulting in constructive interference. The wavelength of the X-rays used is similar to the spacing between atoms in the crystal lattice. As a result, a distinctive diffraction pattern is formed, which can be analyzed using various methods. One widely used approach is the application of Bragg's Law (Eq3), which enables the measurement of crystals and their phases by relating the diffraction angle (θ) to the wavelength (λ) and the lattice spacing (d).

$$n\lambda = 2d_{hkl} \sin\theta \qquad (IV.3)$$

Where:

λ is the x-ray wavelength.

d_{hkl} is the interplanar spacing.

θ is the incident angle (the angle between incident ray and the scatter plane), and n is an integer represents reflection order.

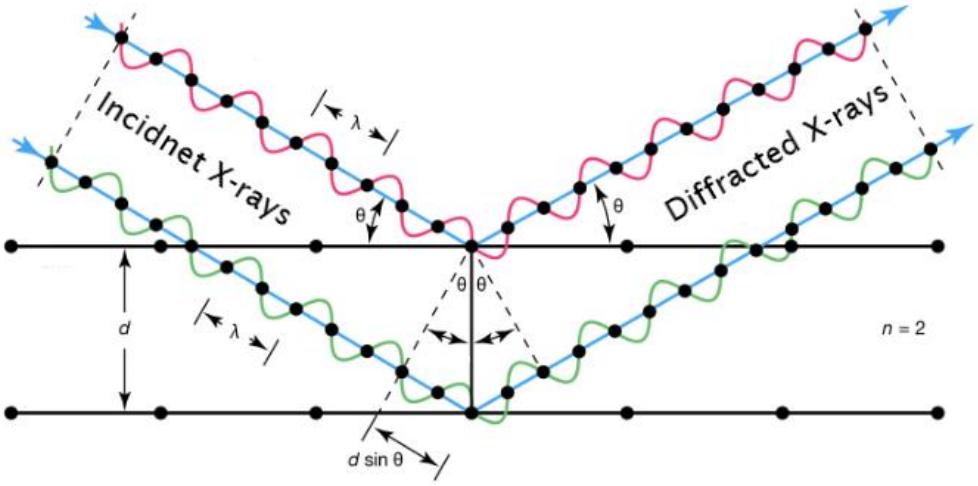

Fig. IV.4 Schematic illustrating the principle of Bragg's law

The XRD technique works through a fascinating process and it is demonstrated bellow:

X-ray Source: An X-ray source, typically a high-energy X-ray tube, emits X-rays with a specific wavelength, usually in the range of 0.01 to 1 nanometer. The most commonly used wavelength is 1.54 angstroms, which corresponds to the characteristic Kα radiation of copper (Cu-Kα).

Sample Preparation: The material of interest, usually in the form of a solid powder or a single crystal, is prepared for analysis. For powders, the sample is typically ground into a fine powder and spread uniformly on a glass slide or loaded into a sample holder. For single crystals, the crystal is aligned in a specific orientation.

Diffraction: The X-rays are directed toward the sample, and the crystalline structure of the material causes the X-rays to diffract. The diffracted X-rays form a pattern of constructive and destructive interference, which depends on the arrangement of atoms in the crystal lattice.

Detector: A detector, such as a scintillation or a solid-state detector, is used to capture the diffracted X-rays. The detector records the intensity and angles of the diffracted X-rays.

Data Analysis: The recorded diffraction pattern is called an X-ray diffraction pattern or X-ray diffraction spectrum. The data obtained from the detector are analyzed using mathematical algorithms to determine the positions and intensities of the diffracted peaks.

Data Interpretation: The diffraction pattern is compared to known reference patterns or databases to identify the crystal structure and phase composition of the material. The positions and intensities of the diffracted peaks provide information about the spacing between atoms in the crystal lattice and the arrangement of atoms within the unit cell.

IV.2.4.1.1. Debye-Scherrer equation

Among various techniques utilized to estimate crystallite size based on X-ray diffraction (XRD) patterns, the Debye-Scherrer equation **(Eq.VI.4)** [163] stands as a fundamental equation employed in XRD analysis for calculating the size of crystallites.

$$D = \frac{K\lambda}{B\cos\theta} \qquad (IV.4)$$

Where:

D is the crystallite size.

K represents the form factor (0.9).

λ is the X-ray wavelength (λ, 1.5418 Å for CuKα).

β is FWHM (the full width at half maximum).

(θ) is the diffraction angle.

This equation establishes a fundamental relationship between the diffraction pattern observed in XRD experiments and the structural characteristics of the crystalline material being analyzed, and the size of the crystalline is estimated by measuring the full width at half maximum (FWHM) of a diffraction peak.

IV.3. Testing protocols

IV.3.1. Photocatalytic activity

IV.3.1.1. Photocatalytic testing of (PPAH/Agx) in the degradation of Rose Bengal dye (R.B)

The catalytic activity of different samples, namely PPAH/Ag1, PPAH/Ag2, PPAH/Ag3, and PPAH/Ag4, was assessed in the context of the photocatalytic degradation of Rose Bengal (R.B) dye utilizing sunlight irradiations. Initially, an aqueous solution of R.B dye with a concentration of 3×10^{-5} M was meticulously prepared using double distilled water. Subsequently, 30 mg of each of the prepared samples was introduced into separate beakers containing 30 ml of the dye solution.

To monitor the progress of the catalytic degradation process, samples (comprising 10 ml of the suspension) were withdrawn from the medium at various time intervals (0, 15, 30, 60, 90, and 120 min). These samples were then subjected to centrifugation at 3000 rpm for 10 minutes to separate the residual catalysts and the resulting supernatant was ultimately analyzed using an ultraviolet-visible (UV-Vis) spectrophotometer at maximum wavelength of the dye (λ_{max} = 543 nm).

The degradation rate (D%) of R.B. dye was calculated using the following equation **(Eq.IV.5)** [164]:

$$D\% = \frac{C_0 - C_t}{C_0} = \frac{A_0 - A_t}{A_0} \qquad (IV.5)$$

In this equation, (Ao - At) represents the difference between the initial and final absorbance of R.B. dye at its maximum wavelength. The initial absorbance (Ao) corresponds to the absorbance of the R.B. dye before the degradation process commences.

It should be noted that the samples PPAH/Ag1, PPAH/Ag2, PPAH/Ag3, and PPAH/Ag4 are denoted as the prepared samples at different concentrations of Ag-loaded PPAH, specifically 2 mM, 5 mM, 10 mM, and 16 mM, respectively. These concentrations serve as indicators of the varying amounts of silver (Ag) incorporated into the PPAH.

IV.3.1.2. Photocatalytic testing of PPAH/Ag@ZnO in the degradation of *o*-toluidine blue (*o*-TB) and 4-bromophenol (4-Bph)

The photocatalytic activity of the prepared (PPAH/Ag@ZnO) sample was investigated by the degradation of *o*-toluidine blue (*o*-TB) and 4-bromophenol (4-Bph) in aqueous solution (7×10^{-5} M, 20 mL) of each dye under sunlight irradiation. To initiate the reaction, a precise quantity of 20 mg of the photocatalyst was introduced into the solutions of dyes contained within glass beakers. Thereafter, 5 mL of the suspensions were removed at regular time intervals, centrifuged at 3000 rpm for 10 min. The absorption spectra of the resulting supernatant were then measured in a SECOMAM Uviline 9600 spectrophotometer. The calculations of the degradation rate (D%) of both dyes were estimated utilizing the equation **(Eq.IV.5)**.

IV.3.1.3 Photocatalytic Kinetics

The photocatalytic degradation of organic pollutants in water generally follows a Langmuir-Hinshelwood mechanism [165], the Langmuir–Hinshelwood (L–H) equation **(Eq.IV.6)** is used to describe photocatalytic kinetics, in which the rate of oxidation is the limiting reaction rate at the maximum coverage of the catalyst [166].

$$r = -\frac{dc}{dt} = k_C \frac{K_{L-H}\, C}{1 + k_{L-H}\, C} \qquad (IV.6)$$

where C is the initial concentration of the organic pollutant to be degraded (mg/L), Kc is the reaction rate constant (mg/L min), and $K_{L\text{-}H}$ is the Langmuir-Hinshelwood adsorption equilibrium constant (L/mg).

In case of low initial concentration of the substance ($C < 5 \times 10^{-3}$ M), the values of ($K_{L\text{-}H}$ $C \ll 1$) and the L–H equation is simplified to a pseudo-first-order kinetic law with respect to C, **(Eq.IV.7)**. At higher initial substance concentrations ($C > 5 \times 10^{-3}$ M), ($K_{L\text{-}H}$ $C \gg 1$) and the reaction rate is of apparent zero order **(Eq.IV.8)**.

$$r = K_C K_{L-H} = K_{app} C \qquad (IV.7)$$

$$r = KC \qquad (IV.8)$$

Where K_{app} is the apparent rate constant of pseudo-first-order

Since the initial concentration of the organic dyes used in this study is low. The integral form *c=f(t)* of the rate equation is:

$$\ln \frac{C}{C_0} = Kt \qquad (IV.9)$$

IV.3.1.4 Reusability performance of PPAH/Ag@ZnO photocatalyst

The reusability test is a complementary investigation to the photocatalytic degradation aimed to evaluate the suitability of the prepared PPAH/Ag@ZnO nanocomposite for industrial applications, considering the crucial factors of sustainability and stability that play a pivotal role in practical implementation. This test was carried out to determine the durability, stability, and long-term viability of the prepared PPAH/Ag@ZnO catalyst for series cycles of use in the degradation of organic dyes, which is considered an important evaluation criterion [167]. In the first cycle, the synthesized photocatalyst sample (20 mg) was added into *o*-TB and 4-Bph dyes solution (7×10^{-5} M, 20 mL), then each solution was subjected to sunlight irradiation for 210 min. Thereafter, the photocatalyst was totally separated from the solutions, washed multiple times with double distilled water, and dried in an oven at 60 °C for several hours to remove the residual moisture. The dried photocatalyst was subsequently used in the next cycle, it is important to mention that the subsequent cycles were carried out under the same experimental conditions as the first cycle. The test was conducted with a total of five cycles.

IV.3.2. Antibacterial test

This test was conducted on the as prepared PPAH/Agx samples, their antibacterial activity was estimated against three types of bacterial strains *Pseudomonas aeruginosa ATCC 27853* (*P. aeruginosa*), *Escherichia coli ATCC 25922* (*E. coli*), and *Staphylococcus aureus ATCC 25923* (*S. aureus*). The agar well diffusion assay (the Kirby-Bauer test) was applied in this test. This method is a very common used method to assess the antibacterial activity of a substance [168]. For this purpose, Frozen bacterial cells of the different strains were cultured overnight in the nutrient medium (composition: agar 15 g, peptone 5 g, sodium chloride (NaCl) 5 g, beef extract 1.5 g, and yeast extract 1.5 g, prepared in 1000 ml distilled water, pH 7.0). Before the cultivation process the nutrient medium was first autoclaved, cooled, poured into petri dishes, and allowed to solidify for 30 minutes. The cultured petri dishes were incubated at 37 ℃ for 24 h to prepare inoculums. Also, sterile Mueller-Hinton agar was poured into sterile petri dishes and allowed to solidify for 30 minutes. Then, four bores with diameter of 6 mm were perfectly cut into Mueller-Hinton agar. Thereafter, Mueller-Hinton agar dishes were inoculated with the tested bacteria strains using a sterile medical swab. Subsequently, the bores of each agar dishes were fully filled with PPAH/Agx samples. Finally, the cultured agar dishes were incubated at 37℃ for 24 h. After incubating, the zones of inhibition were examined. This examination involved measuring the diameter (mm) of the clear zones formed surrounding the bores where the PPAH/Agx samples were placed. This test was repeated three times and along with it, four types of antibiotics particularly gentamicin, ofloxacin, cefixime, and cotrimoxazole were used as positive control. The antibiotics discs were placed in separately agar dishes cultured with the same bacterial strains.

Refences

1. Eid, M., *Gamma radiation synthesis and characterization of starch based polyelectrolyte hydrogels loaded silver nanoparticles.* Journal of Inorganic and Organometallic Polymers and Materials, 2011. **21**: p. 297-305.
2. Mohan, Y.M., et al., *Controlling of silver nanoparticles structure by hydrogel networks.* Journal of Colloid and Interface Science, 2010. **342**(1): p. 73-82.
3. Luo, Q., *Electron microscopy and spectroscopy in the analysis of friction and wear mechanisms.* Lubricants, 2018. **6**(3): p. 58.
4. Mäntele, W. and E. Deniz, *UV–VIS absorption spectroscopy: Lambert-Beer reloaded*. 2017, Elsevier. p. 965-968.
5. Scherrer, P., *Göttinger nachrichten math.* Phys, 1918. **2**: p. 98-100.
6. Khan, M.I., et al., *Green synthesis of magnesium oxide nanoparticles using Dalbergia sissoo extract for photocatalytic activity and antibacterial efficacy.* Applied Nanoscience, 2020. **10**(7): p. 2351-2364.
7. Herrmann, J.-M., et al., *Characterization and photocatalytic activity in aqueous medium of TiO2 and Ag-TiO2 coatings on quartz.* Applied Catalysis B: Environmental, 1997. **13**(3-4): p. 219-228.
8. Molinari, R., et al., *Photocatalytic processes in membrane reactors*, in *Comprehensive Membrane Science and Engineering 2nd Edition*. 2017.
9. Vaiano, V., et al., *Nanostructured N-doped TiO2 coated on glass spheres for the photocatalytic removal of organic dyes under UV or visible light irradiation.* Applied Catalysis B: Environmental, 2015. **170**: p. 153-161.
10. Balouiri, M., M. Sadiki, and S.K. Ibnsouda, *Methods for in vitro evaluating antimicrobial activity: A review.* Journal of pharmaceutical analysis, 2016. **6**(2): p. 71-79.

Chapter V

Results Analysis, and Discussion

Chapter V. Results, Analysis, and Discussion

Preface

This chapter presents a description of the as-prepared NCHs, step by step preparation, the morphological shape and the size of the formed nanoparticles are also described here. How effective are these NCHs in photocatalytic and antibacterial tests are discussed as well. Further findings also were set here

V.1. Synthesis of Ag NPs and Ag@ZnO NPs loaded PPAH

The loading of Ag NPs and Ag@ZnO NPs into PPAH was carried out according to the method described in detail in "Chapter IV" (Section IV.1.2). Briefly, solutions containing the desired metal ions were prepared, and then PPAH was immersed in these solutions to get metal ions loaded PPAH. Subsequently, the swollen PPAH, now containing metal ions, was placed in a $NaBH_4$ solution to enable the in-situ reduction of the metal ions into metal nanoparticles within the PPAH matrix. The choice of sodium borohydride as the reducing agent is based on its efficiency, ease of handling, and relatively mild reaction conditions compared to other reducing agents.

In the presence of sodium borohydride ($NaBH_4$), metal reduction typically takes place through a chemical reaction known as "metal reduction with sodium borohydride." This reaction is frequently utilized in various chemical processes to convert metal compounds into their corresponding metals by employing sodium borohydride as a reducing agent. The general reaction [169] can be represented as follows:

$$M^{m+} + BH^-_4 + H_2O \longrightarrow M^0 + B(OH)_3 + H_2 \qquad \text{(V.1)}$$

Sodium borohydride ($NaBH_4$) has the ability to transfer electrons to other chemical species. When it encounters metal ions the sodium borohydride donates its hydride ions (H^-) to the metal ions, leading to a reduction in the metal's oxidation state. As a result, the metal ions gain electrons and are reduced to their elemental metal form.

This chemical approach is widely used in different fields to achieve controlled reductions of metal compounds, particularly in the synthesis of nanoparticles, and it has been reported in numerous scientific studies [135, 170-172].

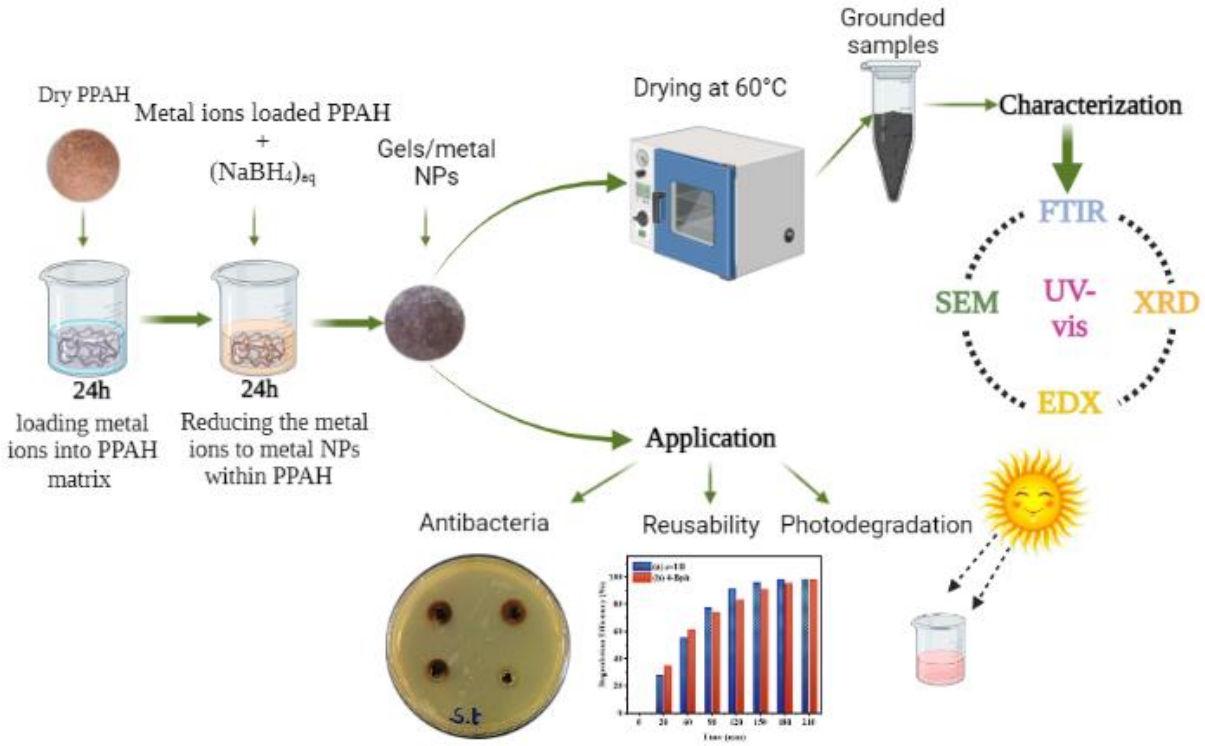

Fig.V.1 Scheme illustrating the synthesis of metal NPs loaded PPAH

V.1.1 Experiment observation

When immersing the granules of PPAH in the $AgNO_3$ and $Zn(NO_3)_2 \cdot 6H_2O$ solutions, a notable transformation occurs, as the PPAH transitions from its dry form to a gel form due to solution absorption. Here, as expected, neither the PPAH gels nor the solutions exhibit any change in color, as depicted in **Fig.V.2 a** and **b**. However, after transferring the gels to $NaBH_4$ solution for the reduction reaction. Instantly, a surprising change took place, the transparent PPAH gels turn into dark brown as seen in **Fig.V.2, c**. This dramatic transformation in color unequivocally signals the successful formation of metal NPs inside the gels. It's like a clear sign that the process worked well.

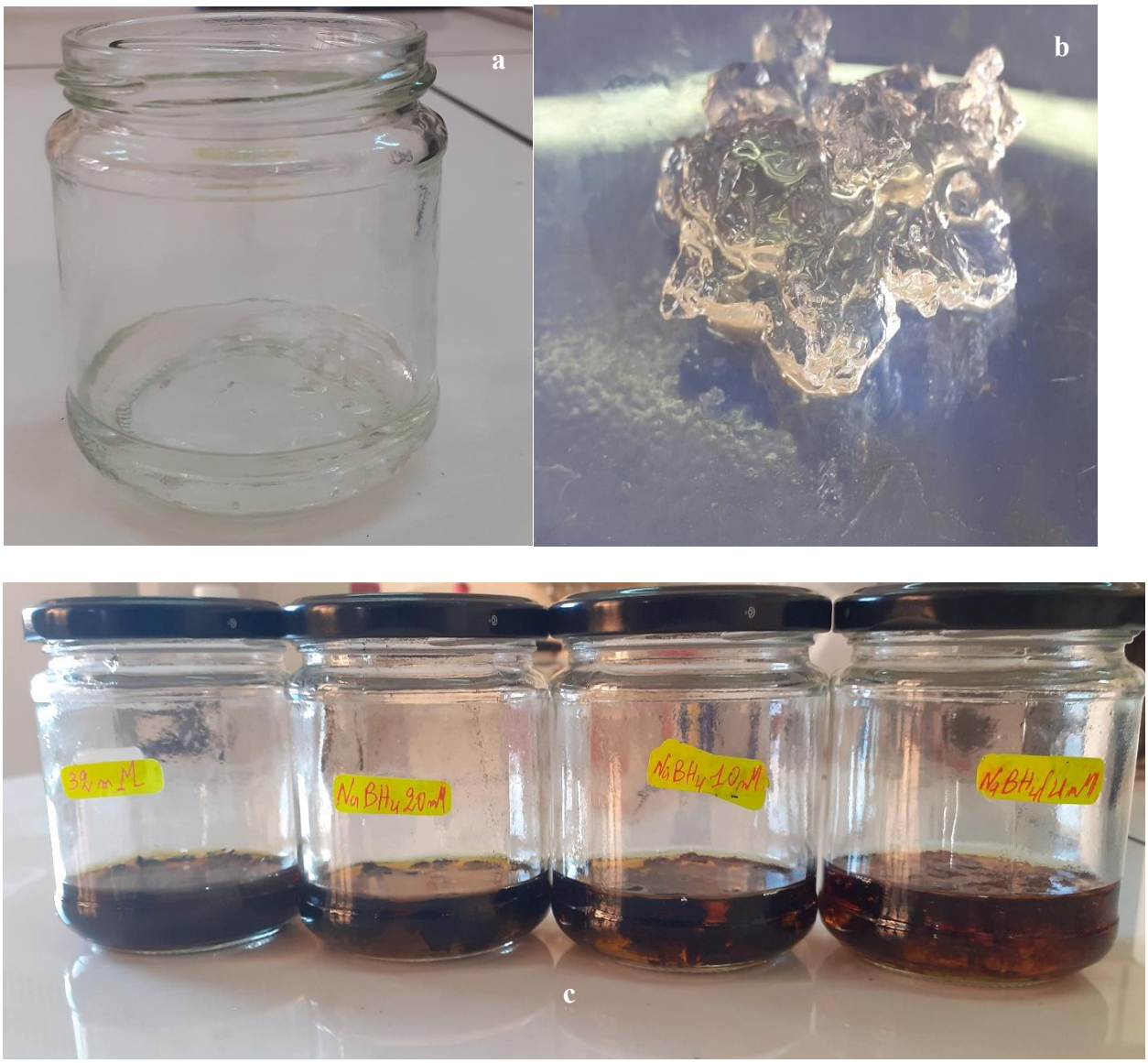

Fig.V.2 Photographs of (a) loading process, (b) PPAH containing metal ions (after 24 h), and (c) PPAH after the reduction reaction

V.2. Characterization of PPAH/Ag NPs and PPAH/Ag@ZnO NPs

V.2.1 UV–Vis spectral analysis

The initial investigation into the incorporation of Ag NPs and Ag@ZnO within the hydrogel matrix commenced with UV-Vis spectroscopy. The UV-Vis spectra and bend gab energy of both samples PPAH/Ag NPs and PPAH/Ag@ZnO are detailed below.

The UV-visible spectra of the prepared samples and the pure PPAH were acquired using a dual-beam UV-Visible spectrophotometer (Shimadzu 1800) across the wavelength range of 200 to 800 nm.

In separate beakers drops of gels containing Ag NPs and Ag@ZnO were immersed in distilled water (10 mg/ml) for a few days. Subsequently, well-dispersed Gles loaded with NPs were obtained, and the mixtures were filtered to separate the gels from the surrounding liquid medium. The resulting medium was then subjected to absorption spectrum measurement, and the distilled water was utilized as the baseline solution.

a/PPAH/Ag

In the UV-Vis spectra of the PPAH containing Ag NPs, a distinct absorption peak emerges at approximately 419 nm **(Fig.V.3, a)**. This resonance peak is a consequence of the surface plasmon resonance attributed to the quantum size of the Ag NPs [173, 174]. Notably, neither the pure hydrogel nor $AgNO_3$ exhibited an absorption peak at this specific wavelength. Furthermore, it is crucial to highlight the absence of absorption peaks at wavelengths of 335 nm and 560 nm as illustrated in **(Fig.V.3, a)**, indicating the absence of Ag NPs aggregation [132]. The dissolution of silver nitrate ($AgNO_3$) in water yields silver ions (Ag^+) and nitrate ions ($NO3^-$). The presence of silver ions (Ag^+) within the solution is accountable for the absorption band observed in the aqueous silver nitrate solution as it seen in **(Fig.V.3, a)**.

In the context of optical properties, an investigation unveiled the indirect optical band gap of Ag NPs, pinpointing it at 2.5 eV **(Fig.V.3, b)**. This revelation unequivocally establishes the PPAH/Ag NCH as an exceptionally promising candidate in the field of photocatalytic degradation.

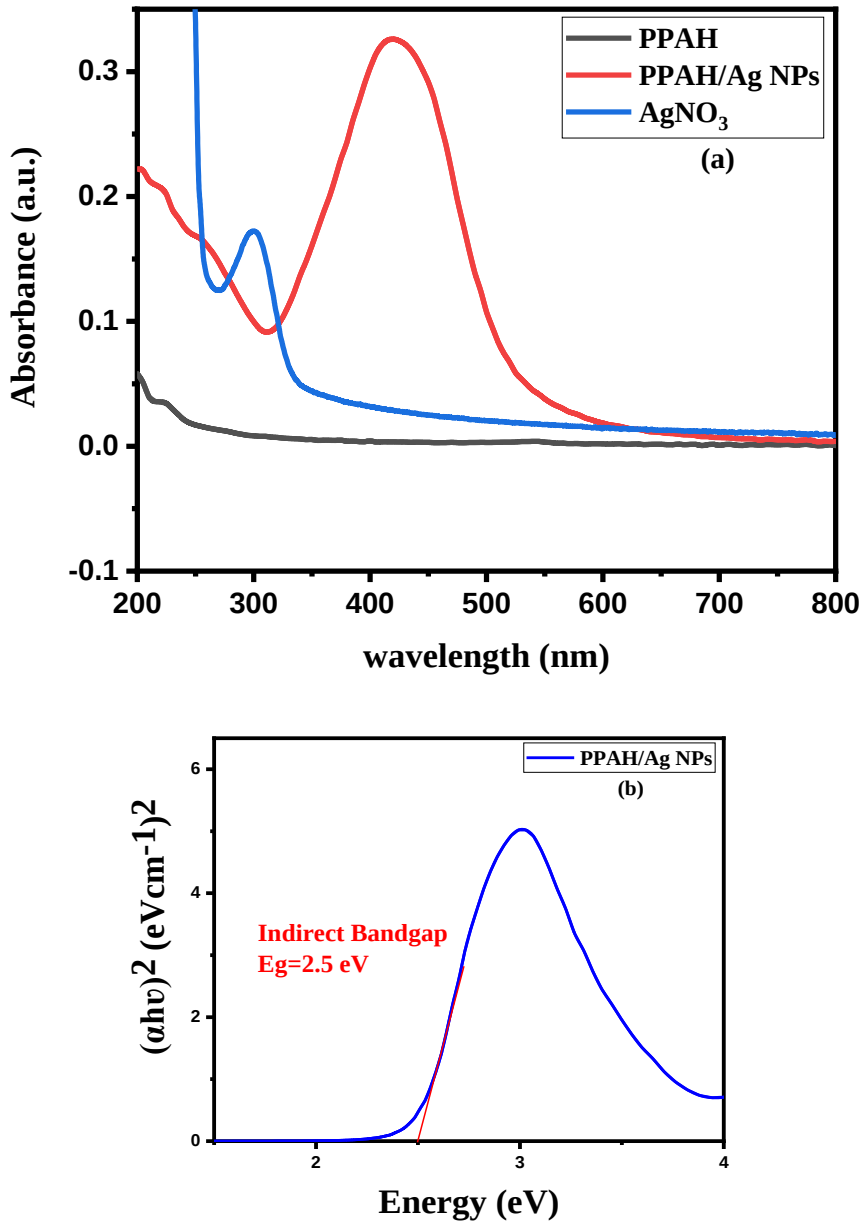

Fig.V.3. UV-vis spectra of (a) pure PPAH and the prepared PPAH/Ag NPs, and (b) Band gap of PPAH/Ag NPs

b/ PPAH/Ag@ZnO

The UV-visible spectra of PPAH/Ag@ZnO demonstrate absorption characteristics spanning from 200 to 800 nm, as depicted in **(Fig.V.4)**. The observed absorption peaks correspond to distinct wavelengths linked to both Ag and Zn elements. These absorption patterns offer valuable insights into the optical properties of the synthesized material. Typically, Ag nanoparticles exhibit absorption within the visible spectrum, commonly ranging from 400 to 500 nm, due to the

surface plasmon resonance (SPR) effect arising from the quantum dimensions of Ag@ZnO NPs [174]. Introducing Ag@ZnO nanoparticles into the PPAH framework leads to heightened light absorption within this particular wavelength range related to Ag. Conversely, ZnO usually displays absorption in the ultraviolet region, typically around 300 to 400 nm. In the case of PPAH/Ag@ZnO, the presence of ZnO plays a pivotal role by contributing significantly to the absorption occurring within the UV range. This interaction between the ZnO component and the composite material leads to the absorption of light at wavelengths falling within the ultraviolet spectrum **(Fig.V.4)**.

The determined indirect band gap energy of 1.75 eV for PPAH/Ag@ZnO points to a narrower band gap when contrasted with pure ZnO (2.7-2.1 eV) [175] and Ag nanoparticles (2.4 eV) [176]. This implies that the incorporation of Ag@ZnO nanoparticles in PPAH has impacted its electronic arrangement, leading to improved light absorption and altered optoelectronic characteristics **(Fig.V.4)**.

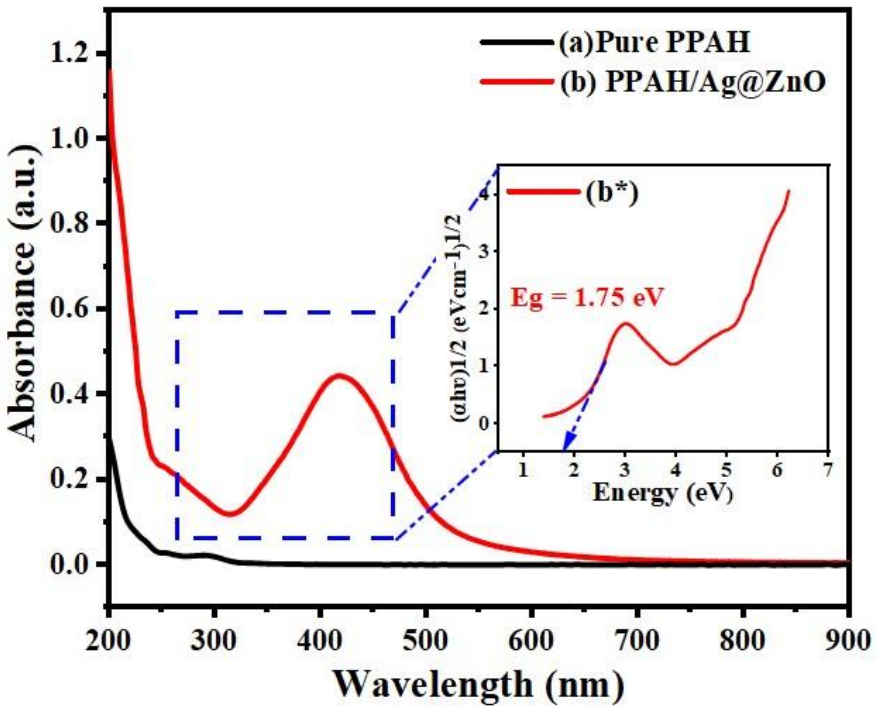

Fig.V.4 Absorbance spectra of (a) pure PPAH, (b) the synthesized PPAH/Ag@ZnO, and (b*) Picture inside represents the Tauc plot of the Kubelka—Munk function (indirect allowed transition) for PPAH/Ag@ZnO.

V.2.2 FTIR spectroscopy

Fourier transform infrared (FTIR) analysis was employed to reveal the molecular bonds, functional groups, and structural attributes of the pure PPAH, and the prepared samples (PPAH/Ag NPs, and PPAH/Ag@ZnO). FTIR analysis was conducted using a Cary 630 FTIR spectrometer. The spectral range spanned from 400 to 4000 cm^{-1}.

(Fig.V.5) depicts the Fourier transform infrared (FTIR) spectra of the samples: the pure PPAH, the PPAH/Ag NPs, and PPAH/Ag@ZnO. The FTIR analysis of the pure PPAH revealed distinct features, including broadened O-H stretching signals at 3376–3235 cm^{-1}, as well as peaks at 2929 cm^{-1} and 1446 cm^{-1} corresponding to C-H asymmetrical/symmetrical stretching and C-H bending, respectively. Additional peaks at 2363 cm^{-1}, 2117 cm^{-1}, and 1654 cm^{-1} were attributed to O=C=O, C≡C, and C=C stretching [177], while the 1401 cm^{-1} peak indicated O-H bending of the carboxylic group. Other observed peaks at 1545 cm^{-1}, 1229 cm^{-1}, and 1319 cm^{-1} were linked to N-H group bending, C-N group stretching [178, 179], and C-O stretching of primary alcohol [180].

When examining the FTIR spectra of the Ag NPs-loaded PPAH, similar peaks were observed compared to the pure PPAH, but with remarkable differences in peaks intensity and frequency. The bending peaks of O-H and N-H showing reduced intensity and obvious shifting from 1401 cm^{-1} to 1395 cm^{-1}, and 1545 cm^{-1} to 1535 cm^{-1}, respectively. The decrease in intensity was correlated with the amount of Ag NPs loaded into PPAH; a higher Ag NPs concentration resulted in lower peak intensity. This weakening maybe attributed to the interaction between silver and oxygen/nitrogen, increasing the overall molecular weight of the compound (PPAH/Ag NPs) and consequently decreasing peak intensity. The shift in O-H and N-H bending to lower frequencies suggested a weakening of intermolecular hydrogen bonds due to the presence of Ag NPs [181].

Moreover, a notable change was the disappearance of the N-H group bending peak at 1229 cm^{-1} in the Ag NPs-loaded PPAH spectra, accompanied by a new peak emerging at 849 cm^{-1}. This new peak indicated the possibility of a newly formed bond between Ag NPs and nitrogen. Additionally, the O-H stretching peak at 3376–3235 cm^{-1} in the pure PPAH showed reduced intensity when loaded with Ag NPs, implying an interaction between oxygen and silver. These

observations collectively provide strong evidence that Ag NPs were effectively incorporated into the PPAH matrices.

In the other part, upon subjecting the PPAH/Ag@ZnO sample to Fourier Transform Infrared (FTIR) analysis, a meticulous examination revealed that the PPAH/Ag@ZnO sample exhibited no noteworthy modifications in comparison to the PPAH/Ag NPs sample. This comprehensive analysis encompassed the vibrational frequencies and spectral patterns of both samples, indicating a remarkable similarity in their chemical composition and structural integrity. The absence of significant alterations further suggests that the incorporation of ZnO nanoparticles into the PPAH/Ag matrix did not induce substantial changes in the overall molecular configuration or bonding characteristics.

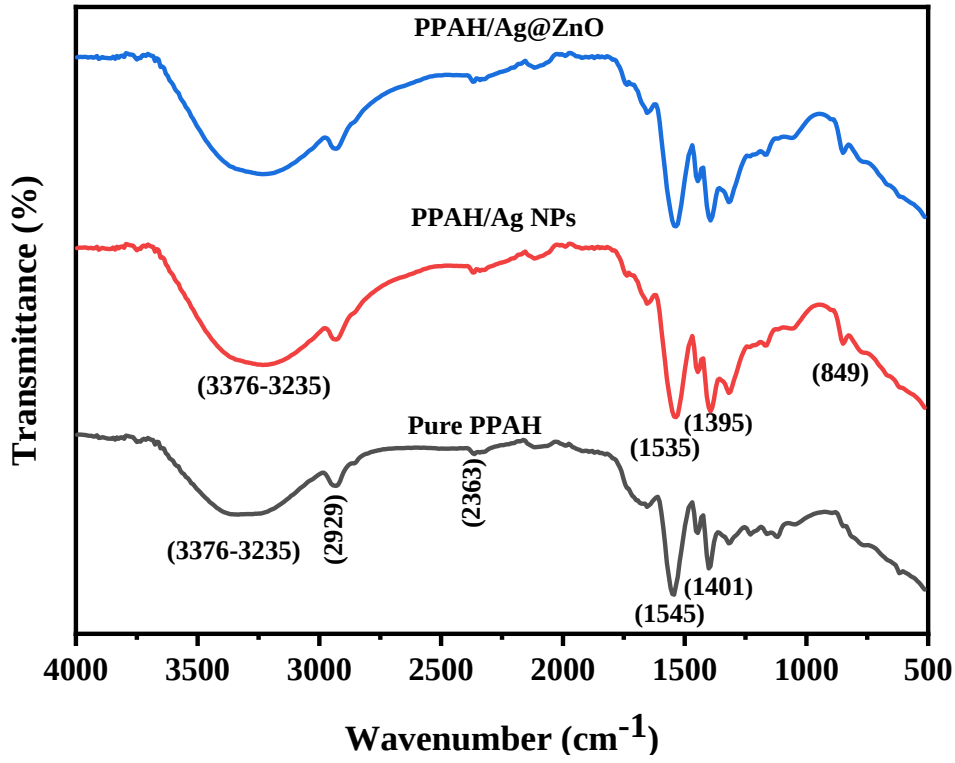

Fig.V.5. FTIR spectra of pure PPAH, PPAH/Ag NPs, and PPAH/Ag@ZnO

V.2.3. X-ray diffraction pattern for the synthesized samples

X-ray Diffraction (XRD) analysis was conducted to investigate the crystalline structure, crystallite size, and phases present in the prepared samples. The XRD patterns were captured using a Rigaku Miniflex 600 X-ray diffractometer, operating within the 2θ range of $10° < 2\theta < 80°$.

Copper Kα radiation (λ= 1.5406 Å) was employed to generate X-rays, utilizing a voltage of 30 kilovolts and a current of 20 mA.

(Fig.V.6) illustrates the X-ray diffraction (XRD) patterns of pure PPAH and the PPAH/Ag NPs sample. In the XRD pattern of pure PPAH, no distinct peaks are observed. However, the XRD pattern of the PPAH/Ag NPs sample clearly displays the crystal phase of Ag NPs. Specifically, four peaks located at 2θ angles of 38.12º, 44.28º, 64.43º, and 77.47º correspond to the diffraction planes (111), (200), (220), and (311) of the face-centered cubic (fcc) structure of the Ag NPs, respectively [182]. These peaks align with the reference data (JCPDS No. 00-004-0783).

In the case of the PPAH/Ag@ZnO NPs sample, its XRD pattern also reveals four peaks associated with Ag NPs. These peaks closely resemble those found in the XRD pattern of PPAH/Ag NPs, although there is a slight reduction in intensity and a minor shift in the peaks at 2θ = 64.43º and 77.47º. Additionally, the XRD pattern displays four additional peaks at 2θ angles of 31.85º, 34.55º, 47.69º, and 66.56º. These peaks are attributed to the diffraction planes (100), (002), (102), and (200) of the hexagonal crystal structure of ZnO NPs [183]. The results obtained from the XRD analysis provide compelling evidence confirming the successful formation and integration of both Ag NPs and Ag@ZnO within the intricate matrix of the hydrogel.

To determine the average crystallite size of the synthesized Ag NPs and Ag@ZnO nanocomposite, the Scherrer formula was applied. The analysis yielded measured sizes of 31.83 nm for Ag NPs in the PPAH/Ag sample. However, after the introduction of ZnO the average nanoparticle size increased to 47 nm in PPAH/Ag@ZnO.

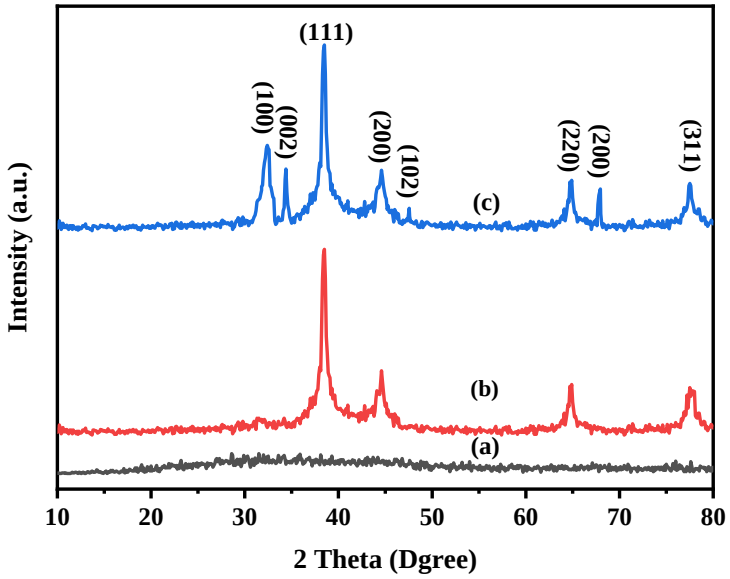

Fig.V.6. XRD patterns of (a) pure PPAH, (b) PPAH/Ag NPs, and (c) PPAH/Ag@ZnO

V.2.4. SEM Analysis of PPAH/Ag NPs and PPAH/Ag@ZnO

The scanning electron microscope instrument used for imaging was the JEOL JSM 840A from Japan. Surface morphology images were acquired for both synthesized samples. To prepare the SEM specimens, a few drops of the samples were deposited onto a silicon wafer and subsequently air-dried.

(Fig.V.7) represents SEM images depicting both the PPAH/Ag NPs and the PPAH/Ag@ZnO. **(Fig.V.7, a)** highlights the evident presence of Ag@ZnO NPs inside the PPAH in the PPAH/Ag@ZnO sample. Furthermore, in PPAH/Ag sample, well distributed Ag NPs throughout the PPAH are distinctly visible in **(Fig.V.7, b)**, assuming the form of small cubic particles. These SEM images serve as compelling evidence, affirming the triumphant synthesis of these metal nanoparticles within the PPAH matrix.

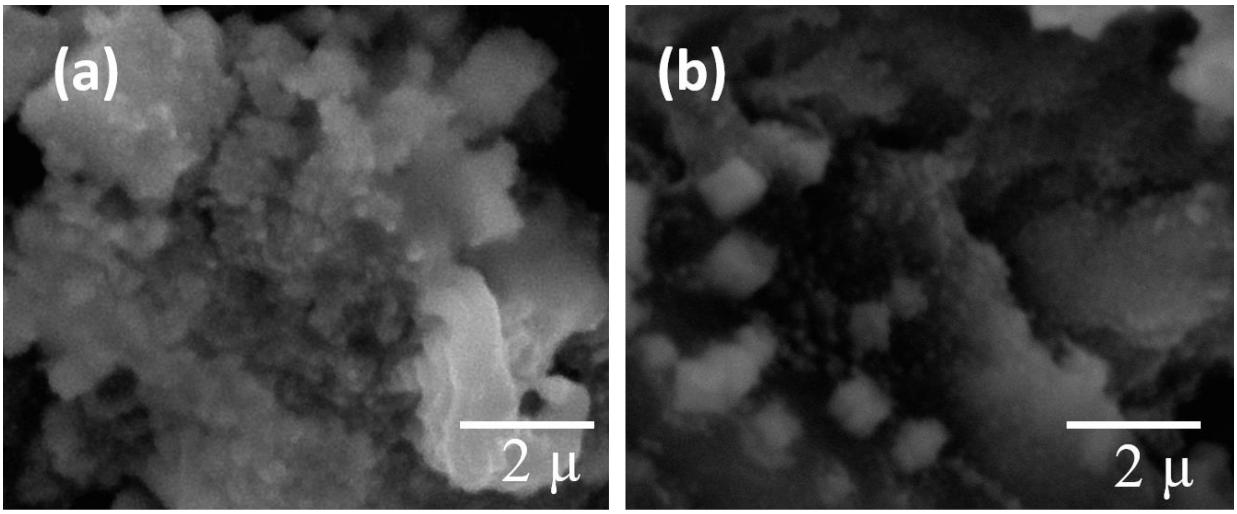

Fig.V.7 SEM images of (a) PPAH/Ag@ZnO, and (b) PPAH/Ag.

V.2.5. EDX analysis of the synthesized PPAH/Ag NPs and PPAH/Ag@ZnO

EDX was utilized to determine the elemental composition of the two samples. **Fig.V.8** illustrates the EDX plot for both samples. The quantitative EDX analysis of PPAH/Ag NPs reveals a composition of 60.48% silver and 34.12% carbon, providing plain confirmation of the integration of Ag NPs into the structural framework of PPAH. Similarly, the EDX analysis of PPAH/Ag@ZnO indicates the composition of 58.77% silver, 28.05% zinc, and 13.18% oxygen. The results regarding the elemental composition provide further evidence or support for the formation of Ag@ZnO NPs within the PPAH matrix.

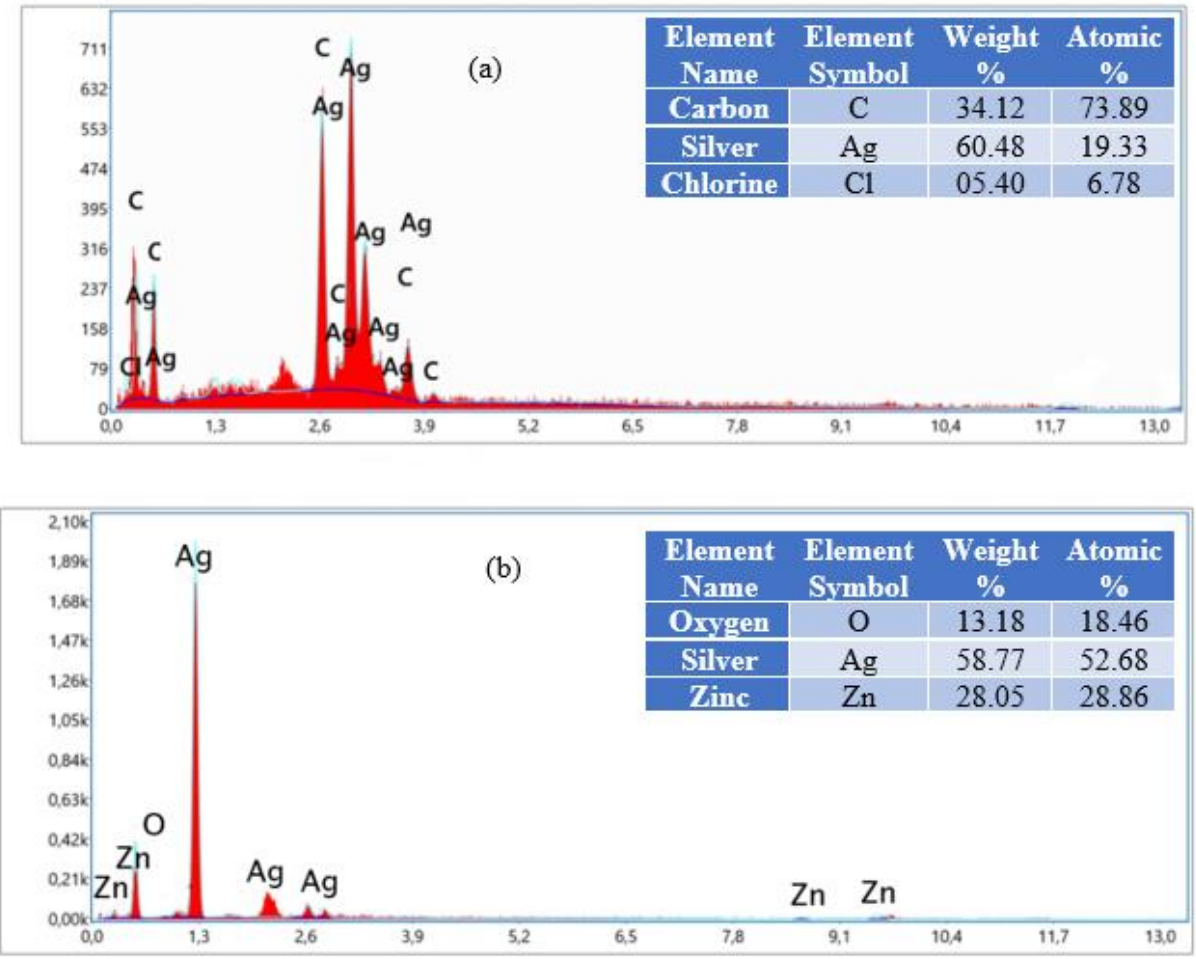

Element Name	Element Symbol	Weight %	Atomic %
Carbon	C	34.12	73.89
Silver	Ag	60.48	19.33
Chlorine	Cl	05.40	6.78

Element Name	Element Symbol	Weight %	Atomic %
Oxygen	O	13.18	18.46
Silver	Ag	58.77	52.68
Zinc	Zn	28.05	28.86

Fig.V.8. EDX analysis results of the synthesized samples (a) PPAH/Ag NPs, and (b) PPAH/Ag@ZnO

V.3. Tests assessment

V.3.1 Photocatalytic activity

Photocatalytic activity is a fascinating phenomenon that emerges when a photocatalyst engages with UV irradiation. This interaction sets in motion a remarkable sequence of events, culminating in the generation of remarkably reactive hydroxyl radicals. These hydroxyl radicals, often hailed as the primary agents driving oxidation [184, 185], possess an intense appetite for electrons, rendering them potent oxidizing entities. In essence, the orchestrated interplay between the photocatalyst and UV light not only initiates a cascade of chemical reactions but also harnesses the power of these hydroxyl radicals to induce transformative oxidation processes.

V.3.1.1. Photocatalytic activity test of PPAH/Ag$_x$ NPs samples

In order to explore the effectiveness of the prepared samples (PPAH/Agx) in degrading anionic dyes. Rose Bengal R.B **(Fig.V.9, a)** was chosen as the representative dye for this study. Rose Bengal R.B, known for its unique characteristics, displays a notable absorption peak at 543 nm, indicating its maximum absorption wavelength. **(Fig.V.9, b)** shows the UV-vis spectra of R.B dye.

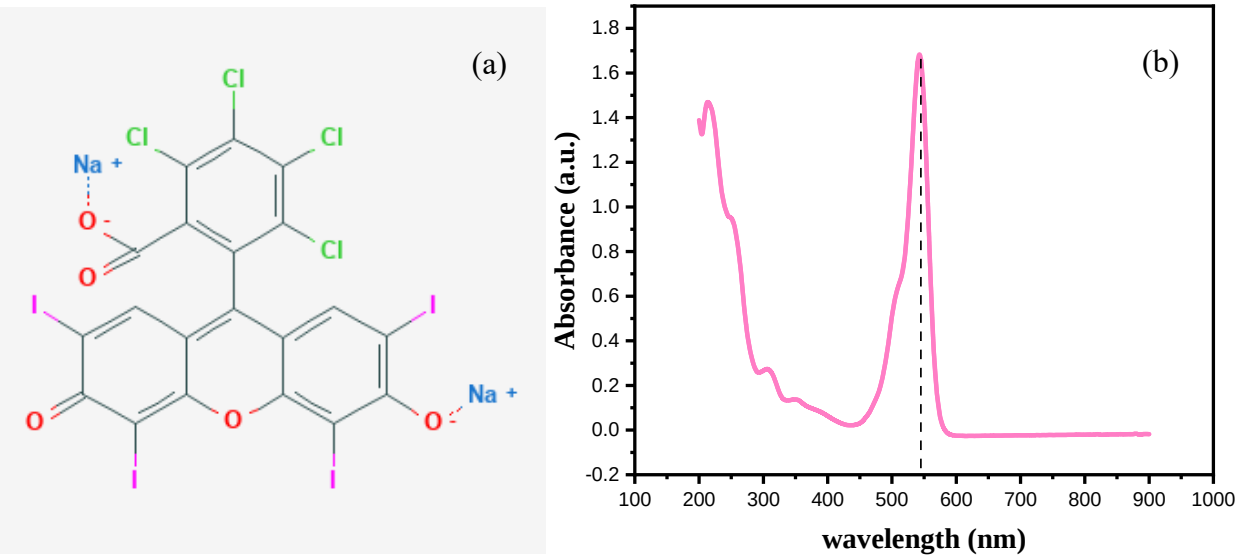

Fig.V.9. (a) Rose Bengal dye structure, and (b) UV-vis spectra of R.B dye

To initiate the degradation reaction, the samples were introduced into beakers containing a solution of R.B (in a 1/1 ratio). In this setup, the samples acted as photocatalysts. The beakers were then exposed to sunlight for varying durations (0, 15, 30, 60, 90, and 120 minutes). Over time, a distinct observation was happened: the color of the Rose Bengal dye degraded gradually, eventually transforming into a colorless state. This phenomenon signifies the presence of the photodegradation process. Furthermore, upon measuring the absorption spectra of R.B solutions, a noteworthy trend emerged: as the exposure time to light irradiation increased, the intensity of the peak at 542 nm decreased significantly until completely disappeared, and no additional peaks were observed, which indicated that R.B dye was fully oxidized, and any intermediate compounds have formed **(Fig.V.10)**. This further confirms the occurrence of the degradation reaction.

The degradation efficiencies were calculated through **(Eq.V.2)**.

$$D\% = \frac{C_0 - C_t}{C_0} = \frac{A_0 - A_t}{A_0} \qquad (V.2)$$

The results displayed nearly identical percentages of degradation across all the prepared photocatalysts. Furthermore, the outcomes indicated that the greatest D% values were attained after 120 min exposure of R.B. dye to sunlight irradiation in the presence of the photocatalysts. The obtained results are tabulated in Table V.1.

V.3.1.1.1. Kinetic study of R.B degradation reaction

The utilization of the pseudo-first-order kinetic equation **(Eq.V.3)** proved to be a valuable approach. It facilitated the thorough investigation of the kinetic parameters governing the degradation reactions of R.B dye under the influence of sunlight irradiation, all while considering the presence of photocatalysts. This analytical method allowed for a detailed exploration of the degradation processes.

$$\ln\frac{C_0}{C} = K_{app}t \qquad (V.3)$$

Where C_0 is the initial concentration of R.B dye and C is the concentration of R.B dye at time (t) of irradiation. Kapp is the apparent pseudo-first-order rate constant (min^{-1}).

(Fig.V.11) shows the plots of $\ln(C_0/C)$ values against irradiation time for the degradation reactions. The values of the rate constant K and the coefficient of determination R^2 are tabulated in Table V.1. The results showed that the photodegradation of R.B dye over PPAH/Ag_3 provided a slightly inferior value of K_{app} compared to the other prepared PPAH/Ag_x catalysts. However, all the prepared catalysts provided considerable values of the rate constant for R.B degradation. Overall, the rate constant values remained almost consistent across diverse catalysts. Moreover, great values of the coefficient of determination R^2 were obtained in this study, which strongly affirms the adherence of the reactions to pseudo-first-order kinetics.

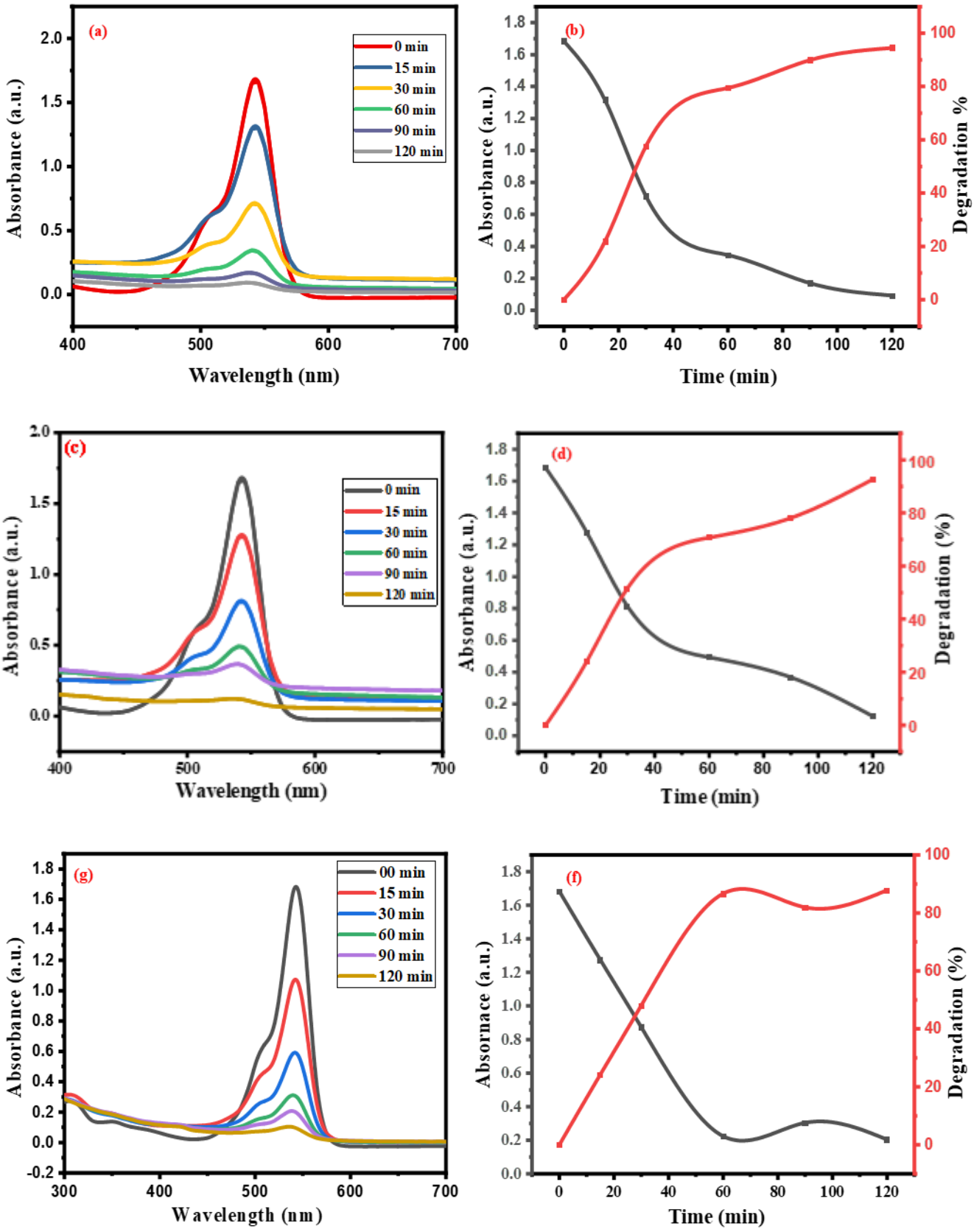
(a)
0 min
15 min
30 min
60 min
90 min
120 min
Absorbance (a.u.)
Wavelength (nm)
(b)
Absorbance (a.u.)
Degradation %
Time (min)
(c)
0 min
15 min
30 min
60 min
90 min
120 min
Absorbance (a.u.)
Wavelength (nm)
(d)
Absorbance (a.u.)
Degradation (%)
Time (min)
(g)
00 min
15 min
30 min
60 min
90 min
120 min
Absorbance (a.u.)
Wavelength (nm)
(f)
Absornace (a.u.)
Degradation (%)
Time (min)

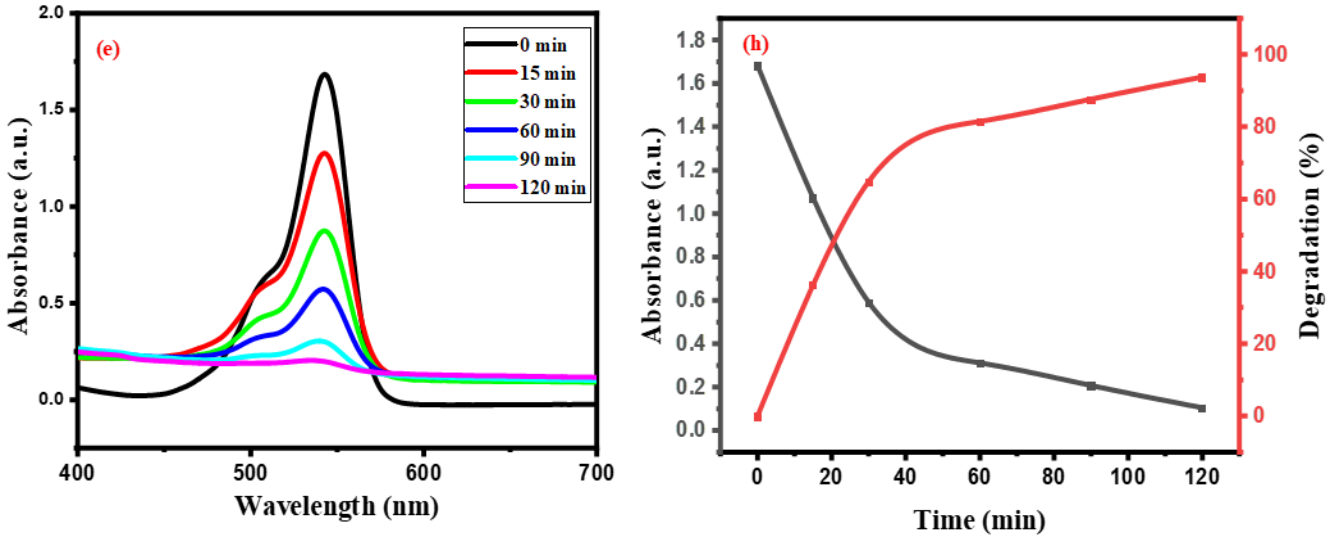

Fig.V.10. UV-Vis spectra of the photodegradation of R.B dye over (a) PPAH/Ag1, (c) PPAH/Ag2, (e) PPAH/Ag3, (g) PPAH/Ag4 and D% in the presence of (b) PPAH/Ag1, (d) PPAH/Ag2, (f) PPAH/Ag3, (h) PPAH/Ag4

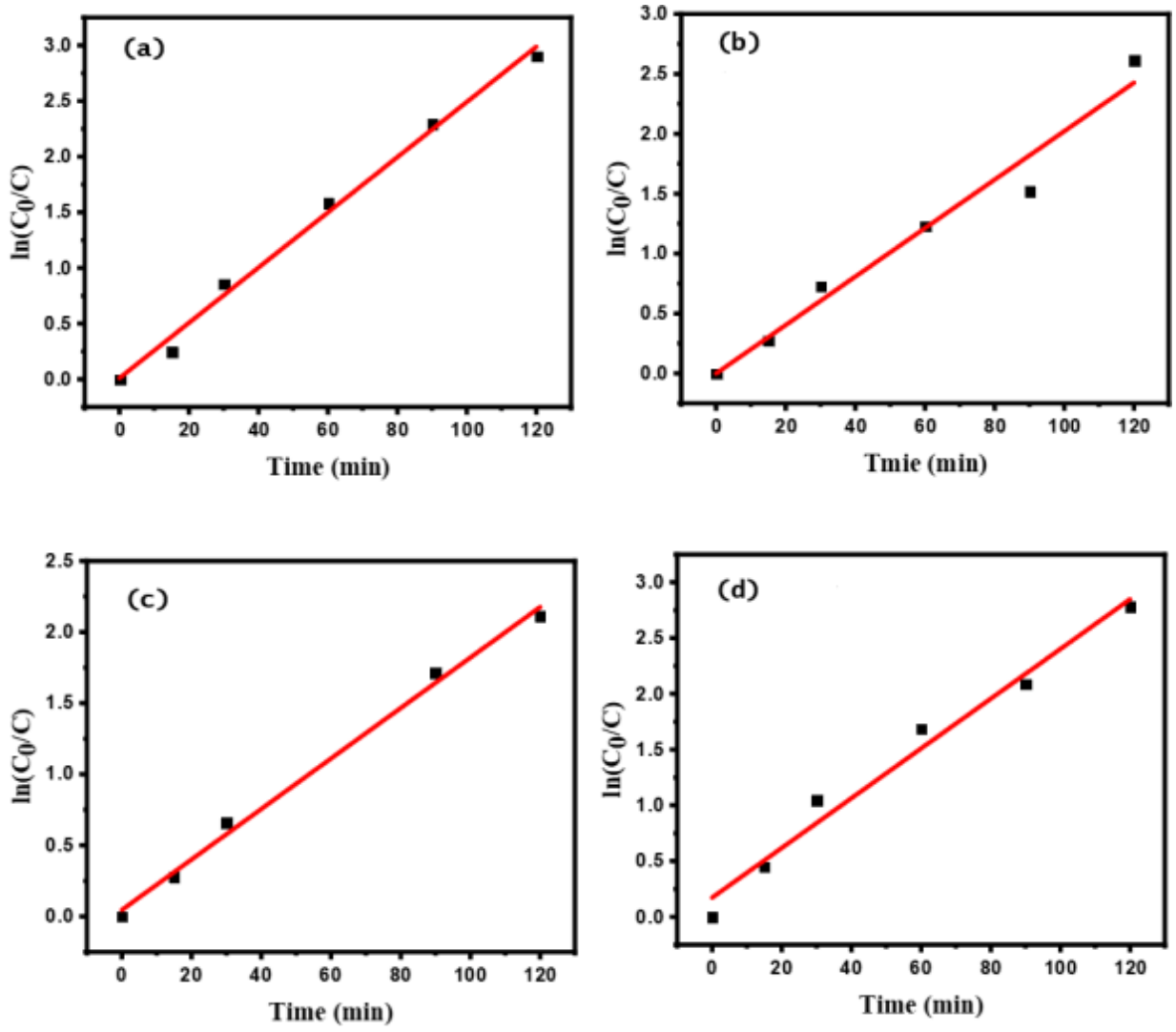

Fig.V.11 Determination of the apparent rate constants for R.B degradation reaction over the prepared catalysts (a) PPAH/Ag1, (b) PPAH/Ag2, (c) PPAH/Ag3, and (d) PPAH/Ag4

Table V.1 values of degradation efficiency, coefficient of determination and rate constant

Catalysts	D (%)	R^2	K_{app} (min^{-1})
PPAH/Ag1	94	0.991	0.025
PPAH/Ag2	93	0.961	0.020
PPAH/Ag3	88	0.992	0.018
PPAH/Ag4	95	0.972	0.022

V.3.1.2. Photocatalytic activity test of PPAH/Ag@ZnO

The photocatalytic efficiency exploration of the prepared PPAH/Ag@ZnO included the degradation of two dyes: *o*-toluidine blue (*o*-TB) and 4-bromophenol (4-Bph), **Fig.V.12** presents the chemical structure of both dyes. The experimental conditions and procedures for this study are previously explained.

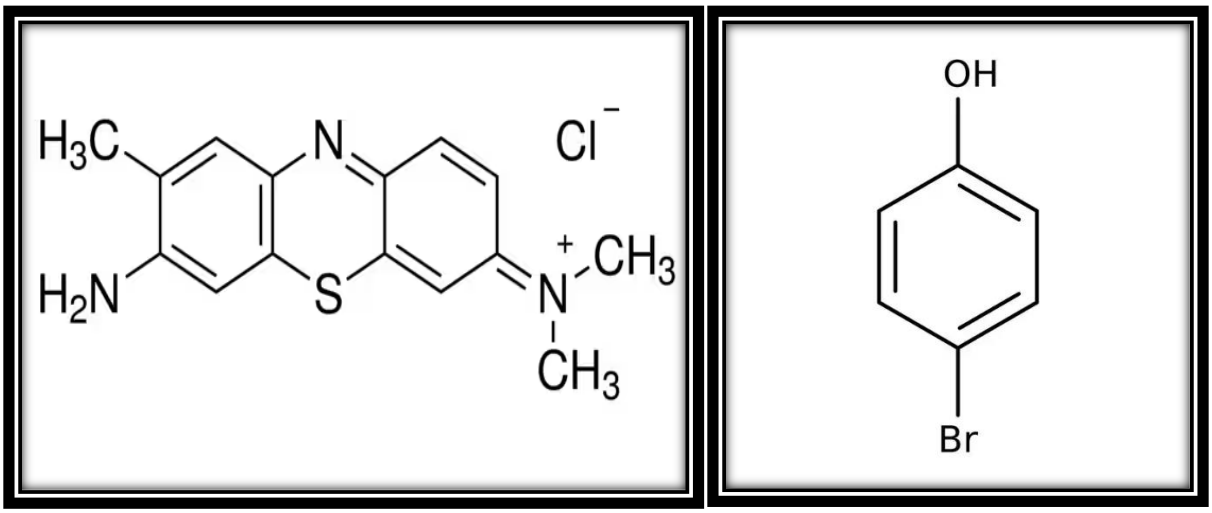

Fig.V.12 The chemical structure of (a) *o*-toluidine blue (*o*-TB), and (b) 4-bromophenol (4-Bph)

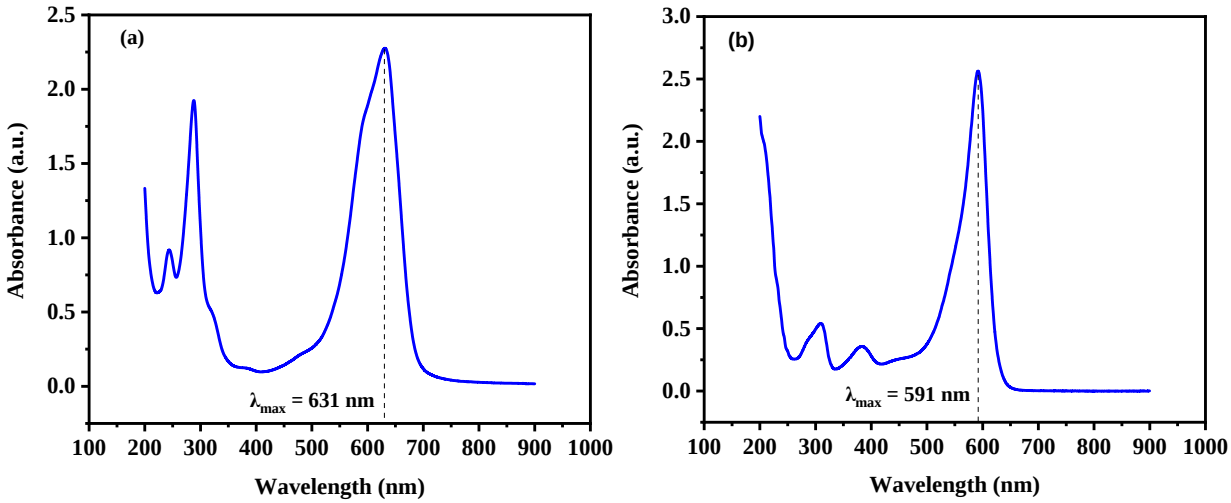

Fig.V.13 UV-vis absorption spectra of (a) *o*-TB, and (b) 4-Bph

The progression of (*o*-TB) degradation was visually monitored through an observable color alteration, transitioning from blue to complete colorless over time. This transformation served as a clear indicator of the ongoing photodegradation process. This visual observation was subsequently substantiated through systematic measurements of absorption spectra at regular time

intervals using SECOMAM Uviline 9600 spectrophotometer. The spectral analyses of (*o*-TB) demonstrated a gradual decrease in absorption intensity at its maximal wavelength, λ_{max} = 631 nm, as the duration of irradiation progressed. These findings are represented in **(Fig.V.14, a).**

Similarly, akin to the degradation patterns of (*o*-TB), the absorption spectra analysis of (4-Bph) in the presence of the prepared PPAH/Ag@ZnO photocatalyst exhibited a strong reduction in absorption intensity at its maximal wavelength, λ_{max} = 591 nm. The results are depicted in **(Fig.V.14, b)**

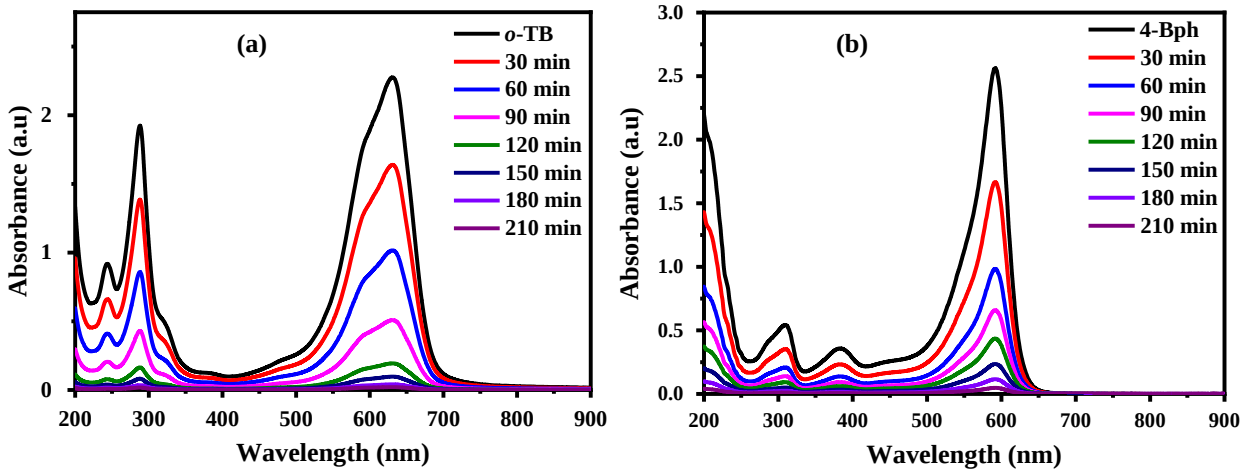

Fig.V.14 The UV-Vis spectra of photodegradation of (a) *o*-TB, and (b) 4-Bph under visible sunlight irradiation at regular irradiation time intervals over PPAH/Ag@ZnO photocatalyst

The prepared PPAH/Ag@ZnO photocatalyst presented a noteworthy photocatalytic activity in degrading the target pollutant dyes. Equation **(Eq.V.2)** was employed to assess the degradation efficiency of the pollutant dyes degradation over PPAH/Ag@ZnO photocatalyst. The outcomes clearly indicate that this photocatalyst exhibited a remarkable performance, as the photocatalytic degradation efficiency was estimated to be 98.77 % and 98.05 % for (o-TB) and (4-Bph), respectively. The results are shown in **(Fig.V.15)**.

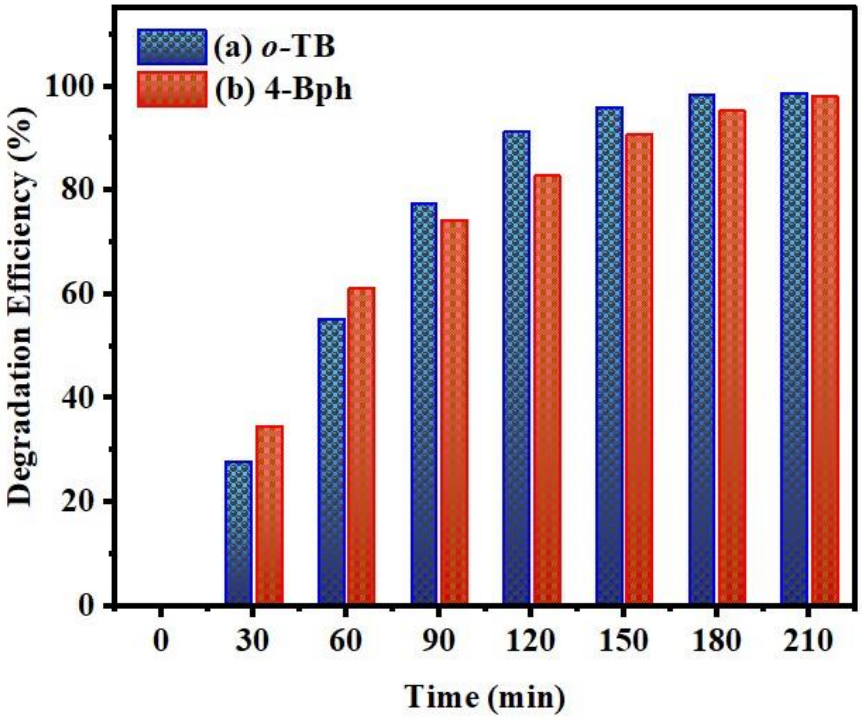

Fig.V.15 The degradation efficiency of the prepared PPAH/Ag@ZnO against (a) *o*-TB and (b) 4-Bph

V.3.1.2.1. Kinetic study o-TB and 4-Bph degradation reactions

The pseudo-first-order kinetic **(Eq.V.3)** was also employed to investigate the kinetic parameters of the pollutant dyes degradation over the PPAH/Ag@ZnO photocatalyst under sunlight irradiation. The apparent rate constants for the photodegradation reactions of *o*-TB and 4-Bph were determined by plotting (C_0/C) against time, as demonstrated in **(Fig.V.16)**. Based on the kinetic findings, the apparent reaction rate constants for the photocatalytic degradation of *o*-TB and 4-Bph over the prepared PPAH/Ag@ZnO photocatalyst were determined to be 0.0229 and 0.018 min^{-1}, respectively.

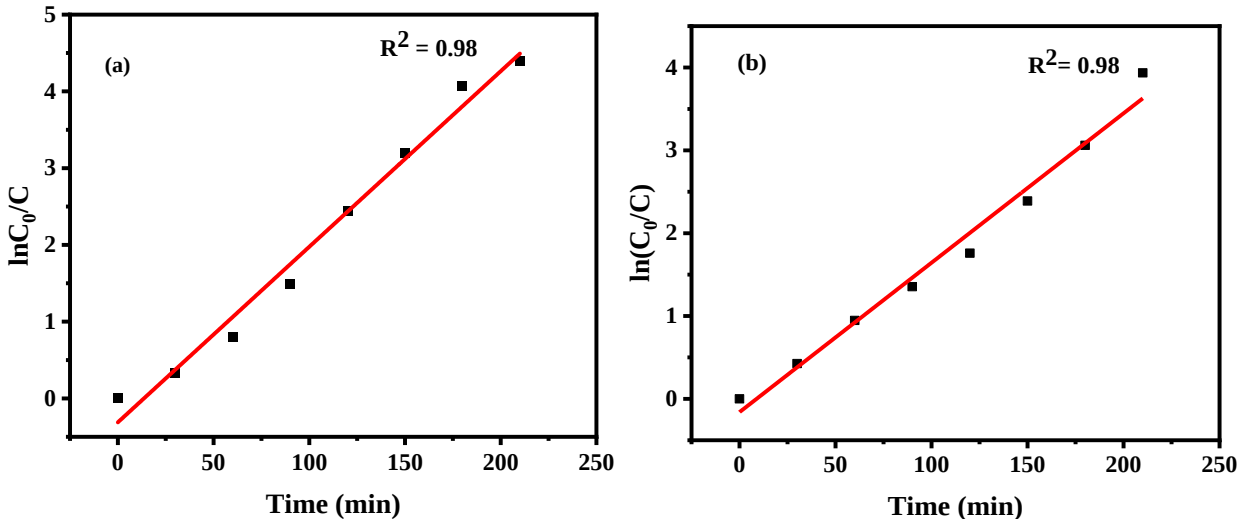

Fig.V.16 Determination of the apparent rate constants for degradation reactions of (a) *o*-TB, and (b) 4-Bph over the prepared PPAH/Ag@ZnO photocatalyst

V.3.1.2.2. Reusability and stability performance of PPAH/Ag@ZnO photocatalyst

For practical applications, along with excellent degradation ability, the photocatalyst needs to be stable and reusable. The synthesized PPAH/Ag@ZnO photocatalyst is expected to demonstrate exceptional recyclability. Hence, it was subjected to a reusability test for the degradation of *o*-TB, and 4-Bph to validate this hypothesis. In each cycle of this test the same conditions (sun light irradiation, 210 min of exposer) of the photodegradation *o*-TB, and 4-Bph were applied. After each photodegrading experiment (cycle), the photocatalyst was separated from the solution, washed, dried, and then reused for the next cycle.

(C/C0 Vs time) and the degradation efficiency was calculated after each cycle **(Fig.V.17)** demonstrates that even after passing through five consecutive recycling runs, PPAH/Ag@ZnO maintains its ability to almost completely degrade the *o*-TB, and 4-Bph dyes. This observation strongly suggests that PPAH/Ag@ZnO possesses exceptional photocatalytic stability when it comes to removing these dyes.

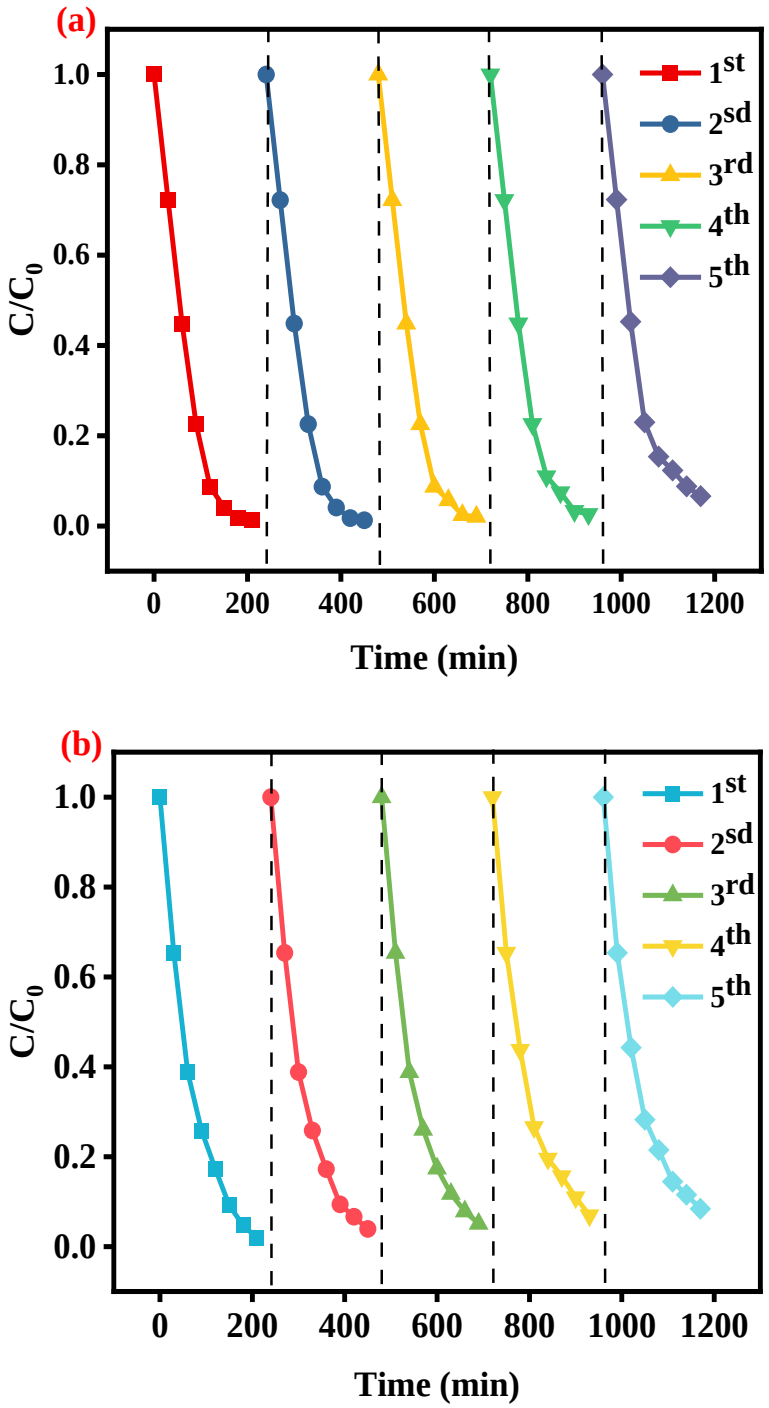

Fig.V.17 Cycling tests (C/C_0 vs. time) for the degradation of (a) *o*-TB, and (b) 4-Bph over the synthesized PPAH/Ag@ZnO photocatalyst.

Moreover, the repeated utilization of the synthesized PPAH/Ag@ZnO photocatalyst did not result in any significant degradation efficiency decline. As evident from **(Fig.V.18)**, the degradation efficiency of the photocatalyst decreased slightly from 98.77% to 93.41% and from

98.04% to 91.60% in the degradation of *o*-TB, and 4-Bph, respectively. The slight decrease in photodegradation efficiency can be attributed to the adsorption of dye molecules obstructing active sites on the catalytic surface and the potential loss of Ag@ZnO nanoparticles from the PPAH surface during the washing procedure [186]. The obtained results show that the synthesized PPAH/Ag@ZnO photocatalyst stays stable even after multiple uses.

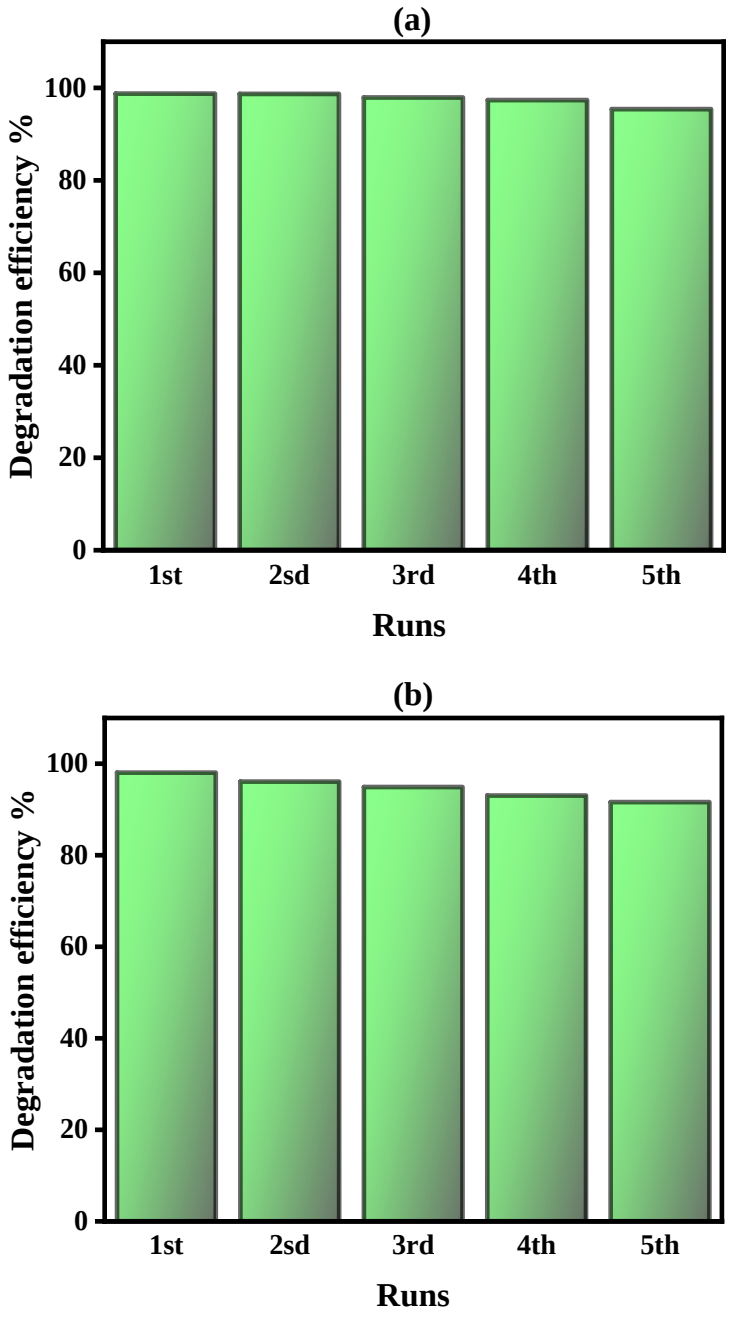

Fig.V.18 Cycling tests (degradation efficiency vs. number of cycles) for the degradation of (a) *o*-TB, and (b) 4-Bph over the synthesized PPAH/Ag@ZnO photocatalyst

V.3.1.3. Degradation mechanism

Basically, the Photocatalytic degradation of organic dyes over metal nanoparticles involves a process in which light energy is used to activate the metal nanoparticles, which then facilitate the degradation of the target organic dyes. This process primarily relies on the properties of metal nanoparticles to absorb light energy from light sources (e.g., sunlight, UV radiation) and generate reactive species that can degrade the dye molecules.

In this study, silver nanoparticles (Ag NPs), and zinc oxide (ZnO), have the ability to absorb photons from solar light. This absorption of photons leads to the generation of electron-hole pairs (h_{vB^+} and e_{CB^-}). These pairs are generated when the absorbed photon energy (hv) equals or surpasses the band gap of the Ag and ZnO nanoparticles. The sufficient absorbed energy allows for the promotion of an electron (e_{CB^-}) from the valence band (VB) to the conduction band (CB) of the synthesized photocatalysts, leaving behind a positively charged hole (h_{vB^+})in the (VB) **(Eq.V.4)**. These electron-hole pairs are highly reactive and serve as crucial intermediates in the photocatalytic process [20]. The electrons in the conduction band (e_{CB^-}) can reduce molecular oxygen (O_2) to form superoxide radicals ($O_2^{\bullet-}$, $HOO^{\bullet}$) **(Eq.V.5)** or hydroxyl radicals ($OH^{\bullet}$) **(Eq.V.10)**. Meanwhile, the holes in the valence band can ultimately trapped with OH^- ions or with H_2O on the Ag/ZnO NPs surface to generate hydroxyl radicals ($OH^{\bullet}$) **(Eq.V.11-12)**. or directly react with organic dye molecules.

The holes in the valence band and the generated reactive species, including hydroxyl radicals $OH^{\bullet}$ and superoxide radicals ($O_2^{\bullet-}$, $HOO^{\bullet}$), are highly oxidizing agents and can attack the organic dye molecules adsorbed on the surface of the Ag/ZnO photocatalysts or in the surrounding solution **(Eq.V.13)**. These radicals break down the dye molecules into smaller, less harmful compounds, such as carbon dioxide (CO_2) and water (H_2O) [187]. The highly reactive superoxide radicals ($O_2^{\bullet}$, $HOO^{\bullet}$), and hydroxyl radicals ($OH^{\bullet}$) generated over Ag/ZnO NPs could potentially interact with the pollutant dyes molecules, leading to their rapid degradation into less harmful compounds [188].

$$\text{Ag/ZnO NPs} + hv \rightarrow h_{VB}^{+} + e_{CB}^{-} \qquad (V.4)$$

$$e_{CB}^{-} + O_2 \rightarrow O_2^{\bullet-} \qquad (V.5)$$

$$O_2^{\bullet-} + H^{+} \rightarrow HOO^{\bullet} \qquad (V.6)$$

$$HOO^{\bullet} + e_{CB}^{-} \rightarrow HO_2^{-} \quad (V.7)$$

$$HO_2^{-} + H^{+} \rightarrow H_2O_2 \quad (V.8)$$

$$H_2O_2 + O_2^{\bullet -} \rightarrow OH^{\bullet} + OH^{-} + O_2 \quad (V.9)$$

$$H_2O_2 + e_{CB}^{-} \rightarrow OH^{\bullet} + OH^{-} \quad (V.10)$$

$$h_{VB}^{+} + H_2O \rightarrow H^{+} + OH^{\bullet} \quad (V.11)$$

$$h_{VB}^{+} + OH^{-} \rightarrow OH^{\bullet} \quad (V.12)$$

$$(O_2^{\bullet -}, HOO^{\bullet}, OH^{\bullet}, h_{VB}^{+}) + OD \rightarrow DP \quad (V.13)$$

Where,

OD: Organic dyes

DP: Degraded pollutants

The photocatalytic process is cyclic, as the Ag/ZnO NPs can continuously absorb light and generate electron-hole pairs as long as they are exposed to the light source. This allows for the continuous degradation of dyes molecules in the presence of light. In addition to the generation of reactive species, Ag/ZnO NPs also provide a surface for the adsorption of dye molecules. This enhances the contact between the dyes' molecules and the reactive species, further promoting the degradation process. The above explained photocatalytic mechanism is represented in **(Fig.V.19)**

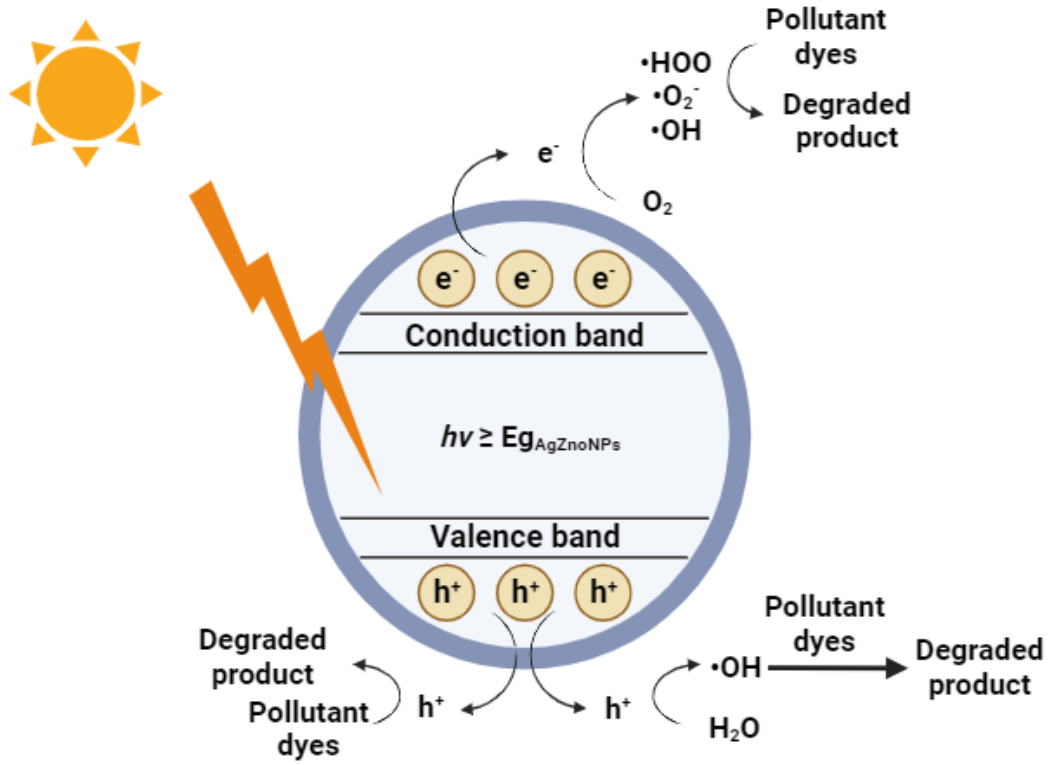

Fig.V.19 Schematic represents the proposed photocatalytic mechanism of Ag/ZnO NPs

V.3.2. Antibacterial test

The pure PPAH and all the prepared variations of hydrogel containing Ag NPs (PPAH/Ag1, PPAH/Ag2, PPAH/Ag3, and PPAH/Ag4) were tested against three distinct types of microorganisms: *Pseudomonas aeruginosa*, *Escherichia coli*, and *Staphylococcus aureus*, all the bacteria strains were obtained from Pasteur Institute, Algeria, the test was conducted in triplicate. As indicated in **Table V.2**, all PPAH/Agx samples exhibited significant antibacterial effect against the various microorganisms, while the pure hydrogel demonstrated no effect, as visualized in **(Fig.V.20)**. Notably, PPAH/Ag1 displayed a remarkable inhibition zone against both *P. aeruginosa* and *E. coli* **(Fig.V.20)**.

Additionally, as indicated in **(Table V.2)**, PPAH/Ag1 sample showed better effect when it is compared with the other prepared samples. Particularly, PPAH/Ag1 displayed inhibition zones that were relatively comparable to those of Ofloxacin against *E. coli* and *P. aeruginosa* bacterial strains **(Table V.2)**, and notably larger inhibition zones compared to the other antibiotics used in

the experiment. Furthermore, PPAH/Ag2, PPAH/Ag3, and PPAH/Ag4 exhibited superior antibacterial effects compared to Cefixime against *S. aureus* **(Table V.2)**.

These findings suggest that the primary mechanisms underlying the antimicrobial action of these materials may involve the release of Ag NPs from PPAH, their attachment to microbial cells, penetration into these cells, and subsequent disruption of both the respiratory chain and cell division by interacting with phosphorus and sulfur-containing compounds within bacterial cells, ultimately resulting in bacterial cell death.

Table V.2 Inhibition zones of PPAH/Agx samples (mm) ±2 in antibacterial activity test

Samples	P. aeruginosa	E. Coli	S. aureus
PPA/Ag1	18.5	21	11
PPA/Ag2	13	12	13
PPA/Ag3	14	12	15
PPA/Ag4	14	13	12.5

Table V.3 Inhibition zones of antibiotics (mm) ±1 in antibacterial activity test

Antibiotics	P. aeruginosa	E. Coli	S. aureus
Cefixime	6	9	13
Ofloxacin	21	21	23
Cotrimoxazole	nil	nil	17
Gentamicin	/	16	/

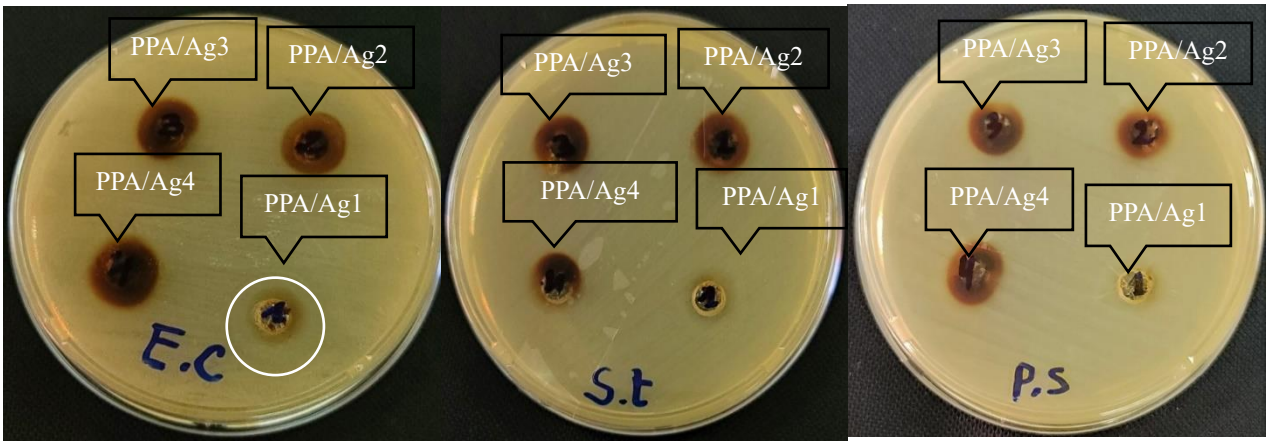

Fig.V.20 Images of antibacterial activity effect of the prepared samples against the different strains

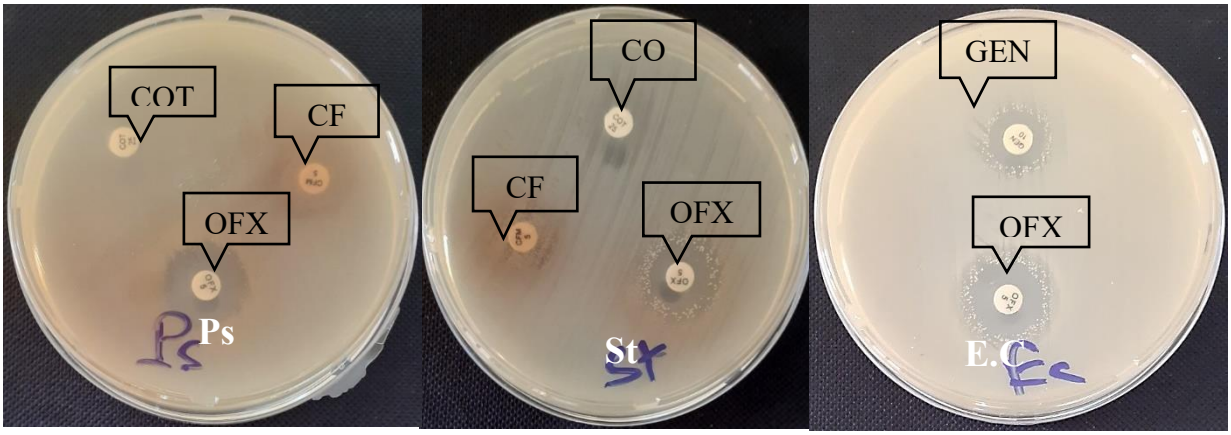

Fig.V.21 Images of antibacterial activity effect of the antibiotics against the different strains

Summary

The employed method for synthesizing metal nanoparticle-loaded hydrogel simplifies the production of PPAH/Ag_x and PPAH/Ag@ZnO samples. The presence of silver and zinc oxide nanoparticles within the hydrogel matrices was confirmed through a range of analytical techniques, including UV-Vis spectrophotometry, FTIR spectroscopy, XRD, and SEM.

Furthermore, the prepared PPAH/Ag_x samples and PPAH/Ag@ZnO demonstrated remarkable efficacy in the photocatalytic degradation of various organic dyes, achieving exceptionally high degradation efficiencies of up to 95% and 98%, respectively. Moreover, these PPAH/Agx samples exhibited wide zones of inhibition when tested against *E. coli*, *P. aeruginosa*, and *S. aureus* strains, underscoring their potent antimicrobial properties.

Based on the obtained results, these PPAH/Ag_x and PPAH/Ag@ZnO nanocomposites hold great promise for applications in wastewater treatment as efficient catalysts and in medical fields, where they can serve as drug carriers and contribute to wound healing processes. Their versatility and demonstrated effectiveness make them valuable candidates for addressing critical environmental and healthcare challenges.

References

1. Nasrollahzadeh, M., et al., *An introduction to nanotechnology*, in *Interface science and technology*. 2019, Elsevier. p. 1-27.
2. Omran, B.A. and B.A. Omran, *Fundamentals of nanotechnology and nanobiotechnology.* Nanobiotechnology: A Multidisciplinary Field of Science, 2020: p. 1-36.
3. Barber, D.J. and I.C. Freestone, *An investigation of the origin of the colour of the Lycurgus Cup by analytical transmission electron microscopy.* Archaeometry, 1990. **32**(1): p. 33-45.
4. Kaniewska, K., M. Karbarz, and E. Katz, *Nanocomposite hydrogel films and coatings–Features and applications.* Applied Materials Today, 2020. **20**: p. 100776.
5. Aguilar, Z., *Nanomaterials for medical applications*. 2012: Newnes.
6. Poizot, P., et al., *Nano-sized transition-metal oxides as negative-electrode materials for lithium-ion batteries.* Nature, 2000. **407**(6803): p. 496-499.
7. Ohde, H., et al., *Hydrogenation of olefins in supercritical CO2 catalyzed by palladium nanoparticles in a water-in-CO2 microemulsion.* Journal of the American Chemical Society, 2002. **124**(17): p. 4540-4541.
8. Zohra, R., et al., *Biosynthesis and Characterization of MnO2 and Zn/Mn2O4 NPs Using Ziziphus Spina-Christi Aqueous Leaves Extract: Effect of Decoration on Photodegradation Activity against various organic Dyes.* Inorganic Chemistry Communications, 2023: p. 111304.
9. Terea, H., et al., *Preparation and characterization of cellulose/ZnO nanoparticles extracted from peanut shells: Effects on antibacterial and antifungal activities.* Biomass Conversion and Biorefinery, 2023: p. 1-12.
10. Ali, F., et al., *Bactericidal and catalytic performance of green nanocomposite based-on chitosan/carbon black fiber supported monometallic and bimetallic nanoparticles.* Chemosphere, 2017. **188**: p. 588-598.
11. Dannert, C., B.T. Stokke, and R.S. Dias, *Nanoparticle-hydrogel composites: from molecular interactions to macroscopic behavior.* Polymers, 2019. **11**(2): p. 275.
12. Piantanida, E., et al., *Design of nanocomposite injectable hydrogels for minimally invasive surgery.* Accounts of chemical research, 2019. **52**(8): p. 2101-2112.
13. Sershen, S. and J. West, *Implantable, polymeric systems for modulated drug delivery.* Advanced drug delivery reviews, 2002. **54**(9): p. 1225-1235.
14. van der Linden, H., et al., *Development of stimulus-sensitive hydrogels suitable for actuators and sensors in microanalytical devices.* Sens. Mater, 2002. **14**(3): p. 129-139.
15. You, H., et al., *Synthesis of colloidal metal and metal alloy nanoparticles for electrochemical energy applications.* Chemical Society Reviews, 2013. **42**(7): p. 2880-2904.
16. Hasan, S., *A review on nanoparticles: their synthesis and types.* Res. J. Recent Sci, 2015. **2277**: p. 2502.
17. Ealia, S.A.M. and M.P. Saravanakumar. *A review on the classification, characterisation, synthesis of nanoparticles and their application*. in *IOP conference series: materials science and engineering*. 2017. IOP Publishing.
18. Shomura, R., et al., *Gold nanoparticles with cyclic phenylazomethines: one-pot synthesis and metal ion sensing.* Langmuir, 2011. **27**(13): p. 7972-7975.
19. Hazarika, P., S.M. Jickells, and D.A. Russell, *Rapid detection of drug metabolites in latent fingermarks.* Analyst, 2009. **134**(1): p. 93-96.

20. Bouafia, A., et al., *Removal of hydrocarbons and heavy metals from petroleum water by modern green nanotechnology methods.* Scientific Reports, 2023. **13**(1): p. 5637.
21. Kim, G.H., et al., *Inverted colloidal quantum dot solar cells.* Advanced Materials, 2014. **26**(20): p. 3321-3327.
22. Pichaandi, J. and F.C. van Veggel, *Near-infrared emitting quantum dots: Recent progress on their synthesis and characterization.* Coordination Chemistry Reviews, 2014. **263**: p. 138-150.
23. Noske, A.B. and B.J. Marsh, *Mapping the ß-Cell in 3D at the nanoscale using novel cellular electron tomography and computational approaches.* BetaSys: Systems Biology of Regulated Exocytosis in Pancreatic ß-Cells, 2011: p. 147-183.
24. Bogart, L.K., et al., *Nanoparticles for imaging, sensing, and therapeutic intervention.* ACS nano, 2014. **8**(4): p. 3107-3122.
25. Hasan, G.G., et al., *Synergistic effect of novel biosynthesis SnO2@ Fe3O4 nanocomposite: A comprehensive study of its photocatalytic of Dyes & antibiotics, antibacterial, and antimutagenic activities.* Journal of Photochemistry and Photobiology A: Chemistry, 2023. **443**: p. 114874.
26. Zohra, R., et al., *Enhanced photocatalytic degradation of dyes and antibiotics with biosynthesized FeMn2O4 nanocomposite under sunlight irradiation: isotherm and kinetic study.* Biomass Conversion and Biorefinery, 2023: p. 1-12.
27. Terris, B. and T. Thomson, *Nanofabricated and self-assembled magnetic structures as data storage media.* Journal of physics D: Applied physics, 2005. **38**(12): p. R199.
28. Bouafia, A., et al., *The recent progress on silver nanoparticles: Synthesis and electronic applications.* Nanomaterials, 2021. **11**(9): p. 2318.
29. Ahmad, S., et al., *Development of conductive fabrics by using silver nanoparticles for electronic applications.* Journal of Electronic Materials, 2020. **49**: p. 1330-1337.
30. Cho, E.J., et al., *Nanoparticle characterization: state of the art, challenges, and emerging technologies.* Molecular pharmaceutics, 2013. **10**(6): p. 2093-2110.
31. Machado, S., et al., *Characterization of green zero-valent iron nanoparticles produced with tree leaf extracts.* Science of the total environment, 2015. **533**: p. 76-81.
32. Tiwari, D.K., J. Behari, and P. Sen, *Application of nanoparticles in waste water treatment.* World Appl Sci J, 2008. **3**(3): p. 417-433.
33. Lee, P. and D. Meisel, *Adsorption and surface-enhanced Raman of dyes on silver and gold sols.* The Journal of Physical Chemistry, 1982. **86**(17): p. 3391-3395.
34. Klasen, H., *Historical review of the use of silver in the treatment of burns. I. Early uses.* Burns, 2000. **26**(2): p. 117-130.
35. Lea, M.C., *Allotropic forms of silver.* American Journal of science, 1889. **3**(222): p. 476-491.
36. Frens, G. and J.T.G. Overbeek, *Carey Lea's colloidal silver.* Kolloid-Zeitschrift und Zeitschrift für Polymere, 1969. **233**: p. 922-929.
37. Yu, S.-j., Y.-g. Yin, and J.-f. Liu, *Silver nanoparticles in the environment.* Environmental Science: Processes & Impacts, 2013. **15**(1): p. 78-92.
38. Bogdanchikova, N., et al., *Activity of colloidal silver preparations towards smallpox virus.* Pharmaceutical Chemistry Journal, 1992. **26**(9-10): p. 778-779.
39. Bechhold, H., *Die Gallertfiltration.* Zeitschrift für Chemie und Industrie der Kolloide, 1907. **2**(1): p. 3-9.

40. Henglein, A., *Small-particle research: physicochemical properties of extremely small colloidal metal and semiconductor particles.* Chemical reviews, 1989. **89**(8): p. 1861-1873.
41. Hahn, H., *Unique features and properties of nanostructured materials.* Nanomaterials by Severe Plastic Deformation, 2004: p. 2-17.
42. Kim, M., et al., *Spontaneous formation of silver nanoparticles on polymeric supports.* Materials Research Bulletin, 2009. **44**(2): p. 334-338.
43. Khan, Z., et al., *Preparation and characterization of silver nanoparticles by chemical reduction method.* Colloids and Surfaces B: Biointerfaces, 2011. **82**(2): p. 513-517.
44. Qurbat, Z., et al., *A mini review on the synthesis of ag-nanoparticles by chemical reduction method and their biomedical applications.* 2016.
45. Tessier, P.M., et al., *Assembly of gold nanostructured films templated by colloidal crystals and use in surface-enhanced Raman spectroscopy.* Journal of the American Chemical Society, 2000. **122**(39): p. 9554-9555.
46. Rosi, N.L. and C.A. Mirkin, *Nanostructures in biodiagnostics.* Chemical reviews, 2005. **105**(4): p. 1547-1562.
47. Steinigeweg, D. and S. Schluecker, *Monodispersity and size control in the synthesis of 20–100 nm quasi-spherical silver nanoparticles by citrate and ascorbic acid reduction in glycerol–water mixtures.* Chemical Communications, 2012. **48**(69): p. 8682-8684.
48. Abdulrahaman, M. and H.Z. Hussein, *Antifungal effect of silver nanoparticles (AgNPs) against Aspergillus flavus.* EC Microbiol, 2017. **6**: p. 63-66.
49. Widatalla, H.A., et al., *Green synthesis of silver nanoparticles using green tea leaf extract, characterization and evaluation of antimicrobial activity.* Nanoscale Advances, 2022. **4**(3): p. 911-915.
50. Kotakadi, V.S., et al., *New generation of bactericidal silver nanoparticles against different antibiotic resistant Escherichia coli strains.* Applied Nanoscience, 2015. **5**: p. 847-855.
51. Wang, J., et al., *Silver nanoparticles coated poly (L-lactide) electrospun membrane for implant associated infections prevention.* Frontiers in Pharmacology, 2020. **11**: p. 431.
52. Senthamarai Kannan, M., et al., *Fabrication of anti-bacterial cotton bandage using biologically synthesized nanoparticles for medical applications.* Progress in Biomaterials, 2022. **11**(2): p. 229-241.
53. Vigneswari, S., et al., *Transformation of biowaste for medical applications: incorporation of biologically derived silver nanoparticles as antimicrobial coating.* Antibiotics, 2021. **10**(3): p. 229.
54. Kithiyon, M., et al., *Efficacy of mycosynthesised AgNPs from Earliella scabrosa as an in vitro antibacterial and wound healing agent.* IET nanobiotechnology, 2019. **13**(3): p. 339-344.
55. Hebeish, A., et al., *Antimicrobial wound dressing and anti-inflammatory efficacy of silver nanoparticles.* International journal of biological macromolecules, 2014. **65**: p. 509-515.
56. KJ, P., *Multi-functional silver nanoparticles for drug delivery: A review.* Int. J. Curr. Pharm. Rev. Res, 2017. **9**: p. 1-5.
57. Van Cleve, T., E. Gibara, and S. Linic, *Electrochemical oxygen reduction reaction on Ag nanoparticles of different shapes.* ChemCatChem, 2016. **8**(1): p. 256-261.
58. Mughal, S.S., *Role of silver nanoparticles in colorimetric detection of biomolecules.* Authorea Preprints, 2022.

59. Wahab, M.A., et al., *Silver nanoparticle-based nanocomposites for combating infectious pathogens: Recent advances and future prospects.* Nanomaterials, 2021. **11**(3): p. 581.
60. Qian, X.-M. and S.M. Nie, *Single-molecule and single-nanoparticle SERS: from fundamental mechanisms to biomedical applications.* Chemical Society Reviews, 2008. **37**(5): p. 912-920.
61. Li, Y., Y. Wu, and B.S. Ong, *Facile synthesis of silver nanoparticles useful for fabrication of high-conductivity elements for printed electronics.* Journal of the American Chemical Society, 2005. **127**(10): p. 3266-3267.
62. Tate, J., et al., *Anodization and microcontact printing on electroless silver: Solution-based fabrication procedures for low-voltage electronic systems with organic active components.* Langmuir, 2000. **16**(14): p. 6054-6060.
63. Tolaymat, T.M., et al., *An evidence-based environmental perspective of manufactured silver nanoparticle in syntheses and applications: a systematic review and critical appraisal of peer-reviewed scientific papers.* Science of the total environment, 2010. **408**(5): p. 999-1006.
64. Jin, H., et al., *Selective and sensitive electrochemical sensing of gastrodin based on nickel foam modified with reduced graphene oxide/silver nanoparticles complex-encapsulated molecularly imprinted polymers.* Sensors and Actuators B: Chemical, 2018. **277**: p. 14-21.
65. Wang, N., et al., *A novel surface plasmon resonance biosensor based on the PDA-AgNPs-PDA-Au film sensing platform for horse IgG detection.* Spectrochimica Acta Part A: Molecular and Biomolecular Spectroscopy, 2018. **191**: p. 290-295.
66. Brubaker, D. and M. Fuller, *The electrical charging of electron diffraction specimens.* Journal of Applied Physics, 1945. **16**(3): p. 128-130.
67. Gomez, J.L. and O. Tigli, *Zinc oxide nanostructures: from growth to application.* Journal of Materials Science, 2013. **48**: p. 612-624.
68. Jay Chithra, M., M. Sathya, and K. Pushpanathan, *Effect of pH on crystal size and photoluminescence property of ZnO nanoparticles prepared by chemical precipitation method.* Acta Metallurgica Sinica (English Letters), 2015. **28**: p. 394-404.
69. Maruthupandy, M., et al., *Synthesis of metal oxide nanoparticles (CuO and ZnO NPs) via biological template and their optical sensor applications.* Applied Surface Science, 2017. **397**: p. 167-174.
70. Narayana, A., et al., *Green and low-cost synthesis of zinc oxide nanoparticles and their application in transistor-based carbon monoxide sensing.* RSC advances, 2020. **10**(23): p. 13532-13542.
71. Son, D.I., et al., *Emissive ZnO–graphene quantum dots for white-light-emitting diodes.* Nature nanotechnology, 2012. **7**(7): p. 465-471.
72. Sun, Y., et al., *The applications of morphology controlled ZnO in catalysis.* Catalysts, 2016. **6**(12): p. 188.
73. Franco, M.A., et al., *A review on chemiresistive ZnO gas sensors.* Sensors and Actuators Reports, 2022. **4**: p. 100100.
74. Nigam, A. and S. Pawar, *Synthesis and characterization of ZnO nanoparticles to optimize drug loading and release profile for drug delivery applications.* Materials Today: Proceedings, 2020. **26**: p. 2625-2628.
75. Vaseem, M., A. Umar, and Y.-B. Hahn, *ZnO nanoparticles: growth, properties, and applications.* Metal oxide nanostructures and their applications, 2010. **5**(1): p. 10-20.

76. Han, J., et al., *ZnO nanotube-based dye-sensitized solar cell and its application in self-powered devices.* Nanotechnology, 2010. **21**(40): p. 405203.
77. Burkert, S., et al., *Cross-linking of poly (N-vinyl pyrrolidone) films by electron beam irradiation.* Radiation Physics and Chemistry, 2007. **76**(8-9): p. 1324-1328.
78. Zhao, W., et al., *Degradable natural polymer hydrogels for articular cartilage tissue engineering.* Journal of Chemical Technology & Biotechnology, 2013. **88**(3): p. 327-339.
79. Sennakesavan, G., et al., *Acrylic acid/acrylamide based hydrogels and its properties-A review.* Polymer Degradation and Stability, 2020. **180**: p. 109308.
80. Peppas, N.A., et al., *Hydrogels in pharmaceutical formulations.* European journal of pharmaceutics and biopharmaceutics, 2000. **50**(1): p. 27-46.
81. Davis, K.A. and K.S. Anseth, *Controlled release from crosslinked degradable networks.* Critical Reviews™ in Therapeutic Drug Carrier Systems, 2002. **19**(4-5).
82. Lin, C.-C. and A.T. Metters, *Hydrogels in controlled release formulations: network design and mathematical modeling.* Advanced drug delivery reviews, 2006. **58**(12-13): p. 1379-1408.
83. Iizawa, T., et al., *Synthesis of porous poly (N-isopropylacrylamide) gel beads by sedimentation polymerization and their morphology.* Journal of applied polymer science, 2007. **104**(2): p. 842-850.
84. Yang, L., J.S. Chu, and J.A. Fix, *Colon-specific drug delivery: new approaches and in vitro/in vivo evaluation.* International journal of pharmaceutics, 2002. **235**(1-2): p. 1-15.
85. Ahmed, E.M., *Hydrogel: Preparation, characterization, and applications: A review.* Journal of advanced research, 2015. **6**(2): p. 105-121.
86. Wichterle, O. and D. Lim, *Hydrophilic gels for biological use.* Nature, 1960. **185**(4706): p. 117-118.
87. Abdullah, J.A.A., et al., *Biopolymer-Based Films Reinforced with FexOy-Nanoparticles.* Polymers, 2022. **14**(21): p. 4487.
88. Tavakoli, J. and Y. Tang, *Hydrogel based sensors for biomedical applications: An updated review.* Polymers, 2017. **9**(8): p. 364.
89. Tavakoli, S. and A.S. Klar, *Advanced hydrogels as wound dressings.* Biomolecules, 2020. **10**(8): p. 1169.
90. Kopecek, J., *Hydrogels: From soft contact lenses and implants to self-assembled nanomaterials.* Journal of Polymer Science Part A: Polymer Chemistry, 2009. **47**(22): p. 5929-5946.
91. Sun, Y., et al., *Recent advances of injectable hydrogels for drug delivery and tissue engineering applications.* Polymer Testing, 2020. **81**: p. 106283.
92. Jeong, K.-H., D. Park, and Y.-C. Lee, *Polymer-based hydrogel scaffolds for skin tissue engineering applications: a mini-review.* Journal of Polymer Research, 2017. **24**(7): p. 112.
93. Ahmadi, F., et al., *Chitosan based hydrogels: characteristics and pharmaceutical applications.* Research in pharmaceutical sciences, 2015. **10**(1): p. 1.
94. Parhi, R., *Cross-linked hydrogel for pharmaceutical applications: A review.* Advanced pharmaceutical bulletin, 2017. **7**(4): p. 515-530.
95. Ramli, R.A., *Slow release fertilizer hydrogels: a review.* Polymer Chemistry, 2019. **10**(45): p. 6073-6090.
96. Azeem, M.K., et al., *Eco-friendly three-dimensional hydrogels for sustainable agricultural applications: Current and future scenarios.* Polymers for Advanced Technologies, 2023. **34**(9): p. 3046-3062.

97. Zhang, Z., et al., *Hydrogel materials for sustainable water resources harvesting & treatment: Synthesis, mechanism and applications.* Chemical Engineering Journal, 2022. **439**: p. 135756.
98. Bachra, Y., et al., *Synthesis, characterization, and swelling properties of a new highly absorbent hydrogel based on carboxymethyl guar gum reinforced with bentonite and Silica particles for disposable hygiene products.* ACS omega, 2022. **7**(43): p. 39002-39018.
99. Shewan, H.M. and J.R. Stokes, *Review of techniques to manufacture micro-hydrogel particles for the food industry and their applications.* Journal of Food Engineering, 2013. **119**(4): p. 781-792.
100. Zhang, J., et al., *Flexible and wearable strain sensors based on conductive hydrogels.* Journal of Polymer Science, 2022. **60**(18): p. 2663-2678.
101. Guo, X., et al., *Application of conductive polymer hydrogels in flexible electronics.* Journal of Polymer Science, 2022. **60**(18): p. 2635-2662.
102. Tabata, Y., *Biomaterial technology for tissue engineering applications.* Journal of the Royal Society interface, 2009. **6**(suppl_3): p. S311-S324.
103. Shantha, K. and D. Harding, *Synthesis and evaluation of sucrose-containing polymeric hydrogels for oral drug delivery.* Journal of applied polymer science, 2002. **84**(14): p. 2597-2604.
104. Mane, S., S. Ponrathnam, and N. Chavan, *Effect of chemical cross-linking on properties of polymer microbeads: A review.* Can Chem Trans, 2015. **3**(4): p. 473-485.
105. Wang, H. and S.C. Heilshorn, *Adaptable hydrogel networks with reversible linkages for tissue engineering.* Advanced Materials, 2015. **27**(25): p. 3717-3736.
106. Kenawy, E.-R., et al., *Physically crosslinked poly (vinyl alcohol)-hydroxyethyl starch blend hydrogel membranes: Synthesis and characterization for biomedical applications.* Arabian Journal of Chemistry, 2014. **7**(3): p. 372-380.
107. de Santa Maria, L.C., et al., *Synthesis of crosslinked resin based on methacrylamide, styrene and divinylbenzene obtained from polymerization in aqueous suspension.* European polymer journal, 2003. **39**(2): p. 291-296.
108. Kiatkamjornwong, S., *Superabsorbent polymers and superabsorbent polymer composites.* ScienceAsia, 2007. **33**(1): p. 39-43.
109. Qunyi, T. and Z. Ganwei, *Rapid synthesis of a superabsorbent from a saponified starch and acrylonitrile/AMPS graft copolymers.* Carbohydrate polymers, 2005. **62**(1): p. 74-79.
110. Karadağ, E., D. Saraydın, and O. Güven, *Radiation induced superabsorbent hydrogels. Acrylamide/itaconic acid copolymers.* Macromolecular Materials and Engineering, 2001. **286**(1): p. 34-42.
111. Ajji, Z., et al., *Use of electron beam for the production of hydrogel dressings.* Radiation Physics and Chemistry, 2008. **77**(2): p. 200-202.
112. Pal, K. and I. Banerjee, *Polymeric gels: characterization, properties and biomedical applications*. 2018: Woodhead Publishing.
113. Ganji, F., F.S. Vasheghani, and F.E. Vasheghani, *Theoretical description of hydrogel swelling: a review.* 2010.
114. Lowman, A.M., *Smart pharmaceuticals.* Journal, 2008.
115. Dorkoosh, F., et al., *Intestinal absorption of human insulin in pigs using delivery systems based on superporous hydrogel polymers.* International journal of pharmaceutics, 2002. **247**(1-2): p. 47-55.

116. Mutar, M.A. and R.K. Kmal, *Preparation of copolymer of acrylamide and acrylic acid and its application for slow release sodium nitrate fertilizer.* Al-Qadisiyah Journal of Pure Science, 2012. **17**(4): p. 71-83.
117. Mun, G., et al., *Superabsorbent hydrogels.* Biomedical applications of hydrogels handbook, 2010: p. 375-391.
118. Yang, T., *Mechanical and swelling properties of hydrogels*. 2012, KTH Royal Institute of Technology.
119. Mohammed Mohammed, H.A., et al., *A novel biosynthesis of MgO/PEG nanocomposite for organic pollutant removal from aqueous solutions under sunlight irradiation.* Environmental Science and Pollution Research, 2023. **30**(19): p. 57076-57085.
120. Salmi, C., et al., *Biosynthesis of Mn3O4/PVP nanocomposite for enhanced photocatalytic degradation of organic dyes under sunlight irradiation.* Journal of Cluster Science, 2023: p. 1-15.
121. Mbhele, Z., et al., *Fabrication and characterization of silver− polyvinyl alcohol nanocomposites.* Chemistry of Materials, 2003. **15**(26): p. 5019-5024.
122. Xu, S., et al., *From hybrid microgels to photonic crystals.* Advanced functional materials, 2003. **13**(6): p. 468-472.
123. Thomas, V., et al., *Review on polymer, hydrogel and microgel metal nanocomposites: A facile nanotechnological approach.* Journal of Macromolecular Science, Part A: Pure and Applied Chemistry, 2007. **45**(1): p. 107-119.
124. Kamal, T., et al., *Silver nanoparticles embedded in gelatin biopolymer hydrogel as catalyst for reductive degradation of pollutants.* Journal of Polymers and the Environment, 2020. **28**: p. 399-410.
125. Eid, M., *Gamma radiation synthesis and characterization of starch based polyelectrolyte hydrogels loaded silver nanoparticles.* Journal of Inorganic and Organometallic Polymers and Materials, 2011. **21**: p. 297-305.
126. Nguyen, N.T.-P., et al., *Stabilization of silver nanoparticles in chitosan and gelatin hydrogel and its applications.* Materials Letters, 2019. **248**: p. 241-245.
127. Mohan, Y.M., et al., *Fabrication of silver nanoparticles in hydrogel networks.* Macromolecular Rapid Communications, 2006. **27**(16): p. 1346-1354.
128. Loo, S.-L., et al., *Effect of synthesis routes on the properties and bactericidal activity of cryogels incorporated with silver nanoparticles.* RSC Advances, 2015. **5**(55): p. 44626-44635.
129. Thoniyot, P., et al., *Nanoparticle–hydrogel composites: Concept, design, and applications of these promising, multi-functional materials.* Advanced Science, 2015. **2**(1-2): p. 1400010.
130. Sershen, S., et al., *Independent optically addressable nanoparticle-polymer optomechanical composites.* Applied Physics Letters, 2002. **80**(24): p. 4609-4611.
131. Weissman, J.M., et al., *Thermally switchable periodicities and diffraction from mesoscopically ordered materials.* Science, 1996. **274**(5289): p. 959-963.
132. Mohan, Y.M., et al., *Controlling of silver nanoparticles structure by hydrogel networks.* Journal of Colloid and Interface Science, 2010. **342**(1): p. 73-82.
133. Saxena, S. and S. Bajpai, *Is a Cationic-Resin-Loaded Polymeric Gel a Better Antibacterial Material than a Nanosilver-Loaded Gel?* Designed Monomers and Polymers, 2010. **13**(2): p. 157-165.

134. Varaprasad, K., et al., *Development of microbial resistant Carbopol nanocomposite hydrogels via a green process.* Biomaterials science, 2014. **2**(2): p. 257-263.
135. Wang, C., N.T. Flynn, and R. Langer, *Controlled structure and properties of thermoresponsive nanoparticle–hydrogel composites.* Advanced Materials, 2004. **16**(13): p. 1074-1079.
136. Lavrador, P., et al., *Stimuli-responsive nanocomposite hydrogels for biomedical applications.* Advanced Functional Materials, 2021. **31**(8): p. 2005941.
137. Souza, G.R., et al., *Networks of gold nanoparticles and bacteriophage as biological sensors and cell-targeting agents.* Proceedings of the National Academy of Sciences, 2006. **103**(5): p. 1215-1220.
138. Zhang, K., et al., *Nanocomposite hydrogels stabilized by self-assembled multivalent bisphosphonate-magnesium nanoparticles mediate sustained release of magnesium ion and promote in-situ bone regeneration.* Acta biomaterialia, 2017. **64**: p. 389-400.
139. Wu, H., et al., *Stable Li-ion battery anodes by in-situ polymerization of conducting hydrogel to conformally coat silicon nanoparticles.* Nature communications, 2013. **4**(1): p. 1943.
140. Sharma, G., et al., *Applications of nanocomposite hydrogels for biomedical engineering and environmental protection.* Environmental chemistry letters, 2018. **16**: p. 113-146.
141. Haraguchi, K., K. Uyama, and H. Tanimoto, *Self-healing in nanocomposite hydrogels.* Macromolecular rapid communications, 2011. **32**(16): p. 1253-1258.
142. Zhang, J., Q. Wang, and A. Wang, *In situ generation of sodium alginate/hydroxyapatite nanocomposite beads as drug-controlled release matrices.* Acta Biomaterialia, 2010. **6**(2): p. 445-454.
143. Satarkar, N.S. and J.Z. Hilt, *Hydrogel nanocomposites as remote-controlled biomaterials.* Acta biomaterialia, 2008. **4**(1): p. 11-16.
144. Sinha, A., et al., *Poly (vinyl alcohol)–hydroxyapatite biomimetic scaffold for tissue regeneration.* Materials Science and Engineering: C, 2007. **27**(1): p. 70-74.
145. Baskovich, B., et al., *Wound dressing components degrade proteins detrimental to wound healing.* International wound journal, 2008. **5**(4): p. 543-551.
146. Hebeish, A. and S. Sharaf, *Novel nanocomposite hydrogel for wound dressing and other medical applications.* RSC advances, 2015. **5**(125): p. 103036-103046.
147. Varshney, L., *Role of natural polysaccharides in radiation formation of PVA–hydrogel wound dressing.* Nuclear Instruments and Methods in Physics Research Section B: Beam Interactions with Materials and Atoms, 2007. **255**(2): p. 343-349.
148. Chaturvedi, A., et al., *Evaluation of poly (vinyl alcohol) based cryogel–zinc oxide nanocomposites for possible applications as wound dressing materials.* Materials Science and Engineering: C, 2016. **65**: p. 408-418.
149. Mohandas, A., et al., *Chitosan based metallic nanocomposite scaffolds as antimicrobial wound dressings.* Bioactive materials, 2018. **3**(3): p. 267-277.
150. Yadollahi, M., et al., *Synthesis and characterization of antibacterial carboxymethyl cellulose/ZnO nanocomposite hydrogels.* International journal of biological macromolecules, 2015. **74**: p. 136-141.
151. Porter, G.C., et al., *AgNP/Alginate Nanocomposite hydrogel for antimicrobial and antibiofilm applications.* Carbohydrate Polymers, 2021. **251**: p. 117017.

152. Pathania, D., et al., *Photocatalytic degradation of highly toxic dyes using chitosan-g-poly (acrylamide)/ZnS in presence of solar irradiation.* Journal of Photochemistry and Photobiology A: Chemistry, 2016. **329**: p. 61-68.
153. Thomas, M., et al., *Effective photocatalytic degradation of Congo red dye using alginate/carboxymethyl cellulose/TiO2 nanocomposite hydrogel under direct sunlight irradiation.* Journal of Photochemistry and Photobiology A: Chemistry, 2016. **327**: p. 33-43.
154. Sharma, G., et al., *Fabrication and characterization of a nanocomposite hydrogel for combined photocatalytic degradation of a mixture of malachite green and fast green dye.* Nanotechnology for Environmental Engineering, 2017. **2**: p. 1-7.
155. Naushad, M., et al., *Efficient removal of toxic phosphate anions from aqueous environment using pectin based quaternary amino anion exchanger.* International Journal of Biological Macromolecules, 2018. **106**: p. 1-10.
156. Sharma, G., et al., *Fabrication, characterization and antimicrobial activity of polyaniline Th (IV) tungstomolybdophosphate nanocomposite material: efficient removal of toxic metal ions from water.* Chemical Engineering Journal, 2014. **251**: p. 413-421.
157. Sharma, G., et al., *Polyacrylamide@ Zr (IV) vanadophosphate nanocomposite: ion exchange properties, antibacterial activity, and photocatalytic behavior.* Journal of Industrial and Engineering Chemistry, 2016. **33**: p. 201-208.
158. Sharma, G., et al., *A multifunctional nanocomposite pectin thorium (IV) tungstomolybdate for heavy metal separation and photoremediation of malachite green.* Desalination and Water Treatment, 2016. **57**(41): p. 19443-19455.
159. Sayed, A., et al., *Radiation synthesis of green nanoarchitectonics of guar gum-pectin/polyacrylamide/zinc oxide superabsorbent hydrogel for sustainable agriculture.* Journal of Inorganic and Organometallic Polymers and Materials, 2022. **32**(12): p. 4589-4600.
160. Shang, H., et al., *Copper oxide nanoparticle-embedded hydrogels enhance nutrient supply and growth of lettuce (Lactuca sativa) infected with Fusarium oxysporum f. sp. lactucae.* Environmental science & technology, 2021. **55**(20): p. 13432-13442.
161. Luo, Q., *Electron microscopy and spectroscopy in the analysis of friction and wear mechanisms.* Lubricants, 2018. **6**(3): p. 58.
162. Mäntele, W. and E. Deniz, *UV–VIS absorption spectroscopy: Lambert-Beer reloaded*. 2017, Elsevier. p. 965-968.
163. Scherrer, P., *Göttinger nachrichten math.* Phys, 1918. **2**: p. 98-100.
164. Khan, M.I., et al., *Green synthesis of magnesium oxide nanoparticles using Dalbergia sissoo extract for photocatalytic activity and antibacterial efficacy.* Applied Nanoscience, 2020. **10**(7): p. 2351-2364.
165. Herrmann, J.-M., et al., *Characterization and photocatalytic activity in aqueous medium of TiO2 and Ag-TiO2 coatings on quartz.* Applied Catalysis B: Environmental, 1997. **13**(3-4): p. 219-228.
166. Molinari, R., et al., *Photocatalytic processes in membrane reactors*, in *Comprehensive Membrane Science and Engineering 2nd Edition*. 2017.
167. Vaiano, V., et al., *Nanostructured N-doped TiO2 coated on glass spheres for the photocatalytic removal of organic dyes under UV or visible light irradiation.* Applied Catalysis B: Environmental, 2015. **170**: p. 153-161.

168. Balouiri, M., M. Sadiki, and S.K. Ibnsouda, *Methods for in vitro evaluating antimicrobial activity: A review.* Journal of pharmaceutical analysis, 2016. **6**(2): p. 71-79.
169. Chen, J.P. and L. Lim, *Key factors in chemical reduction by hydrazine for recovery of precious metals.* Chemosphere, 2002. **49**(4): p. 363-370.
170. Ajmal, M., et al., *Poly (acrylic acid) hydrogel microparticles fabricated with silver nanoparticles: synthesis, characterization, and catalytic applications.* Polymer Engineering & Science, 2020. **60**(11): p. 2918-2929.
171. Agnihotri, S., S. Mukherji, and S. Mukherji, *Antimicrobial chitosan–PVA hydrogel as a nanoreactor and immobilizing matrix for silver nanoparticles.* Applied Nanoscience, 2012. **2**: p. 179-188.
172. Sahiner, N., *In situ metal particle preparation in cross-linked poly (2-acrylamido-2-methyl-1-propansulfonic acid) hydrogel networks.* Colloid and Polymer Science, 2006. **285**: p. 283-292.
173. Zhang, J., S. Xu, and E. Kumacheva, *Polymer microgels: reactors for semiconductor, metal, and magnetic nanoparticles.* Journal of the American Chemical Society, 2004. **126**(25): p. 7908-7914.
174. Filippo, E., A. Serra, and D. Manno, *Poly (vinyl alcohol) capped silver nanoparticles as localized surface plasmon resonance-based hydrogen peroxide sensor.* Sensors and Actuators B: Chemical, 2009. **138**(2): p. 625-630.
175. Gherbi, B., et al., *Effect of pH value on the bandgap energy and particles size for biosynthesis of ZnO nanoparticles: Efficiency for photocatalytic adsorption of methyl orange.* Sustainability, 2022. **14**(18): p. 11300.
176. Mistry, H., et al., *Biogenically proficient synthesis and characterization of silver nanoparticles employing marine procured fungi Aspergillus brunneoviolaceus along with their antibacterial and antioxidative potency.* Biotechnology Letters, 2021. **43**: p. 307-316.
177. Coates, J., *Interpretation of infrared spectra, a practical approach*. 2000.
178. Abdullah, J.A.A., et al., *Effect of Calcination Temperature and Time on the Synthesis of Iron Oxide Nanoparticles: Green vs. Chemical Method.* Materials, 2023. **16**(5): p. 1798.
179. Abdullah, J.A.A., et al., *Gelatin-based biofilms with FexOy-NPs incorporated for antioxidant and antimicrobial applications.* Materials, 2022. **15**(5): p. 1966.
180. Liu, Y., et al., *Silver nanoparticle-embedded hydrogel as a photothermal platform for combating bacterial infections.* Chemical Engineering Journal, 2020. **382**: p. 122990.
181. Porchezhiyan, V. and S. Noorjahan, *Fabrication of a versatile chitosan nanocomposite hydrogel impregnated with biosynthesized silver nanoparticles using Sapindus mukorossi: characterization and applications.* RSC advances, 2016. **6**(98): p. 95564-95573.
182. Gloria, E.C., et al. *Synthesis of silver nanoparticles (AgNPs) with antibacterial activity*. in *Journal of Physics: Conference Series*. 2017. IOP Publishing.
183. Abdullah, J.A.A., et al., *Eco-friendly synthesis of ZnO-nanoparticles using Phoenix dactylifera L., polyphenols: physicochemical, microstructural, and functional assessment.* New Journal of Chemistry, 2023. **47**(9): p. 4409-4417.
184. Kumar, R., et al., *Ce-doped ZnO nanoparticles for efficient photocatalytic degradation of direct red-23 dye.* Ceramics International, 2015. **41**(6): p. 7773-7782.
185. Bhatia, S. and N. Verma, *Photocatalytic activity of ZnO nanoparticles with optimization of defects.* Materials Research Bulletin, 2017. **95**: p. 468-476.

186. Zhu, J., et al., *Preparation of PdNPs doped chitosan-based composite hydrogels as highly efficient catalysts for reduction of 4-nitrophenol.* Colloids and Surfaces A: Physicochemical and Engineering Aspects, 2021. **611**: p. 125889.
187. Ayon, S.A., et al., *Enhanced photocatalytic activity of Ho3+ doped ZnO NPs synthesized by modified sol-gel method: an experimental and theoretical investigation.* Journal of Alloys and Compounds, 2021. **856**: p. 158217.
188. Liqiang, J., et al., *Review of photoluminescence performance of nano-sized semiconductor materials and its relationships with photocatalytic activity.* Solar Energy Materials and Solar Cells, 2006. **90**(12): p. 1773-1787.

Conclusions and Future Recommendations

Conclusions and Future Recommendations

Conclusions

Nanocomposite hydrogels represent a vibrant and distinct domain within the realm of nanotechnology, nanocomposite hydrogels have gained considerable interest in the last two decades, due to their unique properties. In particular, stimuli responsive properties and controlled swelling behavior, make them suitable materials for a wide range of different applications.

In this thesis, the incorporation of (Ag NPs) and (Ag@ZnO NPs) into potassium polyacrylate hydrogel (PPAH) was carried out through a facile and efficient technique. Namely, the *in-situ* reduction technique. Basically, this technique consists of two steps: i) loading metal ions within the hydrogel matrix, and ii) in-situ reduction of metal ions to metal NPs using a reductant. various instrumental analysis techniques including UV-Vis spectroscopy, Fourier-transform infrared (FT-IR) spectroscopy, X-ray diffraction (XRD), and scanning electron microscopy (SEM), were used to confirm and identify the resulting nanocomposite hydrogel samples, denoted as PPAH/Agx NPs and PPAH/Ag@ZnO NPs.

From UV-Vis spectra, a distinct absorption peak was observed at 419 nm indicating the presence of Ag NPs. Additionally, the obtained findings from FT-IR analysis describe the modifications that occurred in the structure of the PPAH. Also, the peaks in the XRD pattern refer to the existence of Ag NPs and Ag@ZnO NPs in the synthesized PPAH/Ag NPs and PPAH/Ag@ZnO NPs, respectively. SEM imaging further elucidated the morphology, revealing well distribution of the formed nanoparticles within the hydrogel.

The photocatalytic efficiency of the samples was investigated in the photodegradation of kinds of organic dyes under sunlight irradiation. All the tested NCH samples present significant catalytic activity and the outcomes highlight their potential use as an effective photocatalyst for the degradation of organic pollutants in wastewater purification. Moreover, PPAH/Ag@ZnO NCH exhibited high performance in the reusability test up to five cycles.

Furthermore, the examination of PPAH/Agx NPs antibacterial activity was performed by testing them against three different bacteria strains. Notably, *Pseudomonas aeruginosa*, *Escherichia coli*, and *Staphylococcus aureus* using agar well diffusion assay. From this study, all the tested samples were observed to have strong antimicrobial potential. When the results were

compared with the effect of different antibiotics like Cefixime, Ofloxacin, Cotrimoxazole, and Gentamicin, the PPAH/Agx samples were found more potent than majority if these antibiotics. These findings serve PPAH/Agx NCHs as promising candidates for applications in the biomedical field.

Future recommendations

Future recommendations are highlighted in the following points:

- ✓ Investigate the adoption of environmentally friendly reducing agents to drive the reduction of metal precursors in the in-situ reduction method to achieve sustainable material synthesis.
- ✓ To extend the range of potential applications, conduct thorough assessments encompassing antifungal, antiviral, and anticancer tests on these materials should be considered.
- ✓ The synthesis of these materials should be transferred from laboratory scale toward industrial, also extending their application into real-world scenarios instead of laboratory experiments is still a challenge.
- ✓ Prior to considering their application in the biomedical field, embark on an exhaustive, extended-term evaluation of these materials. This examination should encompass their compatibility with living organisms and their propensity for biodegradation, ensuring their safety and effectiveness in the biomedical domain.